

# NAVAL POSTGRADUATE SCHOOL MONTEREY, CALIFORNIA



## THESIS

**MODELING STUDIES OF THE EFFECTS OF  
SEASONAL WIND FORCING AND  
THERMOHALINE GRADIENTS ON THE  
LEEUVIN CURRENT SYSTEM**

by

Anthony W. Cox

December 1998

Thesis Advisor:

Mary L. Batteen

**Approved for public release; distribution is unlimited.**

19990115 012

REPORT DOCUMENTATION PAGE			Form Approved OMB No. 0704-0188	
Public reporting burden for this collection of information is estimated to average 1 hour per response, including the time for reviewing instruction, searching existing data sources, gathering and maintaining the data needed, and completing and reviewing the collection of information. Send comments regarding this burden estimate or any other aspect of this collection of information, including suggestions for reducing this burden, to Washington Headquarters Services, Directorate for Information Operations and Reports, 1215 Jefferson Davis Highway, Suite 1204, Arlington, VA 22202-4302, and to the Office of Management and Budget, Paperwork Reduction Project (0704-0188) Washington DC 20503.				
1. AGENCY USE ONLY (Leave blank)	2. REPORT DATE December 1998	3. REPORT TYPE AND DATES COVERED Master's Thesis		
4. TITLE AND SUBTITLE MODELING STUDIES OF THE EFFECTS OF SEASONAL WIND FORCING AND THERMOHALINE GRADIENTS ON THE LEEUWIN CURRENT SYSTEM		5. FUNDING NUMBERS		
6. AUTHOR(S) Anthony W. Cox in conjunction with Mary L. Batteen				
7. PERFORMING ORGANIZATION NAME(S) AND ADDRESS(ES) Naval Postgraduate School Monterey, CA 93943-5000		8. PERFORMING ORGANIZATION REPORT NUMBER		
9. SPONSORING/MONITORING AGENCY NAME(S) AND ADDRESS(ES)		10. SPONSORING/MONITORING AGENCY REPORT NUMBER		
11. SUPPLEMENTARY NOTES The views expressed in this thesis are those of the author and do not reflect the official policy or position of the Department of Defense or the U.S. Government.				
12a. DISTRIBUTION/AVAILABILITY STATEMENT Approved for public release; distribution is unlimited.		12b. DISTRIBUTION CODE		
13. ABSTRACT (maximum 200 words) A high-resolution, multi-level, primitive equation ocean model is used to investigate the effects of seasonal thermohaline gradients and wind forcing in the generation of currents and eddies off the western and southwestern coasts of Australia. Additionally, an investigation of the generation mechanisms for undercurrents in the region is conducted. Model results demonstrate the roles of seasonal thermohaline gradients, wind forcing, and North West Shelf waters in the Leeuwin Current System. While the basic flow is poleward and eastward off the western and southern coasts, due to strong thermohaline gradients, there is significant variability in the flow from the seasonal nature of the wind forcing and the onset of the North West Shelf waters. Model results also indicate that an equatorward (westward) undercurrent off the western (southwestern) coast of Australia is generated and maintained due to the conservation of mass continuity in response to an alongshore thermohaline gradient at deeper levels.				
14. SUBJECT TERMS Primitive equation model, Leeuwin Current System, currents, meanders, eddies, filaments		15. NUMBER OF PAGES 141		
		16. PRICE CODE		
17. SECURITY CLASSIFICATION OF REPORT Unclassified	18. SECURITY CLASSIFICATION OF THIS PAGE Unclassified	19. SECURITY CLASSIFICATION OF ABSTRACT Unclassified	20. LIMITATION OF ABSTRACT UL	



Approved for public release; distribution is unlimited.

**MODELING STUDIES OF THE EFFECTS OF SEASONAL WIND  
FORCING AND THERMOHALINE GRADIENTS ON THE LEEUWIN  
CURRENT SYSTEM**

Anthony W. Cox  
Lieutenant, United States Navy  
B.S., United States Naval Academy, 1992

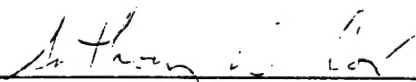
Submitted in partial fulfillment  
of the requirements for the degree of

**MASTER OF SCIENCE IN  
METEOROLOGY AND PHYSICAL OCEANOGRAPHY**

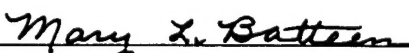
from the

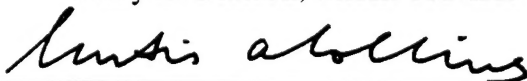
**NAVAL POSTGRADUATE SCHOOL  
December 1998**


Author:

  
\_\_\_\_\_  
Anthony W. Cox

Approved by:

  
\_\_\_\_\_  
Mary L. Batteen, Thesis Advisor

  
\_\_\_\_\_  
Curtis A. Collins, Second Reader

  
\_\_\_\_\_  
Roland W. Garwood Jr., Chairman  
Department of Oceanography





## ABSTRACT

A high-resolution, multi-level, primitive equation ocean model is used to investigate the effects of seasonal thermohaline gradients and wind forcing in the generation of currents and eddies off the western and southwestern coasts of Australia. Additionally, an investigation of the generation mechanisms for undercurrents in the region is conducted.

Model results demonstrate the roles of seasonal thermohaline gradients, wind forcing, and North West Shelf waters in the Leeuwin Current System. While the basic flow is poleward and eastward off the western and southern coast, due to strong thermohaline gradients, there is significant variability in the flow from the seasonal nature of the wind forcing and the onset of the North West Shelf waters. Model results also indicate that an equatorward (westward) undercurrent off the western (southwestern) coast of Australia is generated and maintained due to the conservation of mass continuity in response to an alongshore thermohaline gradient at deeper levels.



## TABLE OF CONTENTS

I.	INTRODUCTION .....	1
II.	MODEL DESCRIPTION .....	5
	A. MODEL EQUATIONS AND METHOD OF SOLUTION .....	5
	B. FORCING CONDITIONS AND EXPERIMENTAL DESIGN.....	8
	C. ENERGY ANALYSIS TECHNIQUE .....	11
III.	RESULTS OF THE BASIC EXPERIMENTS.....	13
	A. EXPERIMENT 1 .....	13
	B. EXPERIMENT 2.....	17
	C. EXPERIMENT 3.....	20
	D. EXPERIMENT 4.....	22
	E. EXPERIMENT 5.....	26
IV.	ANALYSIS OF UNDERCURRENT GENERATION MECHANISMS.....	31
V.	SUMMARY AND RECOMMENDATIONS .....	35
	LIST OF REFERENCES .....	119
	INITIAL DISTRIBUTION LIST .....	123



## LIST OF FIGURES

1. Annual cycle of net forcing for the Leeuwin Current between 22°S and 32°: Dashed line is observed pressure gradient forcing; dotted line is observed wind stress; solid line is net forcing. Positive is southward (from Godfrey and Ridgway)..... 39
2. Model domain, coastline and geographic locations of the western and southwestern coasts of Australia. The area of study is bounded by 22.5° S to 40° S, 107.5° E to 122.5° E..... 40
3. Time series plots of monthly temperature fields used as seasonal forcing in the basic simulation. The '\*' symbol represents data at 22.5° S, 107.5° E, while the '+' symbol represents data at 40° S, 107.5° E for (a) 10 m and (b) 30 m depth..... 41
4. Climatological winds over the Leeuwin Current System used to force the model. The climatological (1980-1989) ECMWF winds are shown here for (a) February, (b) May, (c) July, and (d) November. .... 43
5. Temperature contours and velocity vectors at 10 m depth at days (a) 3, (b) 18, (c) 30, (d) 60, (e) 180, and (f) 360 in Experiment 1. The contour interval is 1°C. To avoid clutter, the velocity vectors are plotted every third grid point in the east-west direction and every fourth grid point in the north-south direction. Maximum velocity is 50 cm/s in (a) and 100 cm/s in (b) through (f)..... 47
6. Cross-shore section of meridional velocity ( $v$ ) at ~ 32° S (near Freemantle) on day 60 of Experiment 1. The contour interval is 5.0 cm/s. Poleward flow is negative (dashed line) and equatorward flow is positive (solid line). .... 53
7. Mean temperature and velocity vectors at 10 m depth averaged for days 90 to 270 of Experiment 1. Contour interval is 0.1°C with colder waters in the southern end of model domain; maximum velocity vector is 50 cm/s. .... 54
8. Horizontal maps at 10 m depth of (a) mean kinetic energy (MKE) and (b) eddy kinetic energy (EKE) averaged for days 90 to 270 of Experiment 1. Contour interval is 250 cm<sup>2</sup>/s<sup>2</sup>..... 55
9. Temperature contours and velocity vectors at 10 m depth at days (a) 90, (b) 180, and (c) 360 of Experiment 2. Contour interval is 1°C; maximum velocity vector is 100 cm/s. .... 57
10. Cross-shore section of meridional velocity ( $v$ ) at ~ 32° S (near Freemantle) on days (a) 90, (b) 180, and (c) 360 of Experiment 2. The contour interval is 1.0 cm/s for poleward (dashed line) flow and 2.0 cm/s for equatorward (solid line) flow. .... 60
11. Cross-shore sections of temperature at ~ 32°S (near Freemantle) at days (a) 90, (b) 180, (c) 360 of Experiment 2. Contour interval is 1°C ..... 63

12. Cross-shore section of mean zonal velocity ( $u$ ) at $\sim 117^\circ$ E averaged for days 90 to 270 of Experiment 2. Contour interval is 1.0 cm/s for eastward (solid line) flow and 2.0 cm/s for westward (dashed line) flow .....	66
13. Mean temperature and velocity vectors at 10 m depth averaged for days 90 to 270 of Experiment 2. Contour interval is $0.1^\circ\text{C}$ with colder waters in the coastal region of model domain; maximum velocity vector is 50 cm/s .....	67
14. Horizontal maps at 10 m depth of (a) mean kinetic energy (MKE) and (b) eddy kinetic energy (EKE) averaged for days 90 to 270 of Experiment 2. Contour interval is $100\text{ cm}^2/\text{s}^2$ in (a) and $25\text{ cm}^2/\text{s}^2$ in (b). .....	68
15. Temperature contours and velocity vectors at 10 m depth at days (a) 45, (b) 180, and (c) 360 of Experiment 3. Contour interval is $1^\circ\text{C}$ ; maximum velocity vector is 100 cm/s. ....	70
16. Cross-shore section of meridional velocity ( $v$ ) at $34^\circ$ S (off Cape Leeuwin), for day 180 of Experiment 3. The contour interval is 5.0 cm/s for poleward (dashed line) flow and 2.0 cm/s for equatorward (solid line) flow. ....	73
17. Mean temperature and velocity vectors at 10 m depth averaged for days 90 to 270 of Experiment 3. Contour interval is $1^\circ\text{C}$ ; maximum velocity vector is 50 cm/s .....	74
18. Horizontal maps at 10 m depth of (a) mean kinetic energy (MKE) and (b) eddy kinetic energy (EKE) averaged for days 90 to 270 of Experiment 3. Contour interval is $50\text{ cm}^2/\text{s}^2$ in (a) and $100\text{ cm}^2/\text{s}^2$ in (b). ....	75
19. Temperature contours and velocity vectors at 10 m depth at days (a) 15, (b) 30, (c) 90, (d) 180, and (e) 345 of Experiment 4. The contour interval is $1^\circ\text{C}$ ; maximum velocity vector is 50 cm/s in (a) and 100 cm/c in (b)–(e). ....	77
20. Cross-shore section of meridional velocity ( $v$ ) at $\sim 32^\circ$ S (near Freemantle) for days (a) 30 and (b) 90, and at $34^\circ$ S (off Cape Leeuwin) for days (c) 180 and (d) 345 of Experiment 3. The contour interval is 5.0 cm/s for poleward (dashed line) flow and 2.0 cm/s in (a), (b) and 1.0 cm/s in (c), (d) for equatorward (solid line) flow. ....	82
21. Cross-shore section of zonal velocity ( $u$ ) at $\sim 117^\circ$ E for days (a) 30, (b) 90, (c) 180, and (d) 345 of Experiment 4. Contour interval is 5.0 cm/s in (a)–(c) and 2.0 cm/s for eastward (solid line) flow and 5.0 cm/s for westward (dashed line) flow in (d). ....	86
22. Mean temperature and velocity vectors at 10 m depth averaged for days 90 to 270 of Experiment 4. Contour interval is $0.1^\circ\text{C}$ with colder waters in the south end of the model domain; maximum velocity vector is 50 cm/s .....	90
23. Horizontal maps at 10 m depth of (a) mean kinetic energy (MKE) and (b) eddy kinetic energy (EKE) averaged for days 90 to 270 of Experiment 4. Contour interval is $100\text{ cm}^2/\text{s}^2$ .....	91
24. Temperature contours and velocity vectors at 10 m depth at days (a) 78, (b) 90, (c) 180, and (d) 345 of Experiment 5. The contour interval is $1^\circ\text{C}$ ; maximum velocity vector is 100 cm/s. ....	93

25. Cross-shore section of meridional velocity ( $v$ ) at $28^\circ$ S (near Shark Bay), on day 90 of Experiment 5. The contour interval is 5.0 cm/s for poleward (dashed line) and equatorward (solid line) flow. ....	97
26. Mean temperature and velocity vectors at 10 m depth averaged for days 90 to 270 of Experiment 5. Contour interval is $0.1^\circ\text{C}$ with colder waters in the south end of the model domain; maximum velocity vector is 50 cm/s. ....	98
27. Horizontal maps at 10 m depth of (a) mean kinetic energy (MKE) and (b) eddy kinetic energy (EKE) averaged for days 90 to 270 of Experiment 5. Contour interval is $100\text{ cm}^2/\text{s}^2$ in (a) and $250\text{ cm}^2/\text{s}^2$ in (b). ....	99
28. Mean temperature and velocity vectors at 600 m depth averaged for days 90 to 270 of (a) Experiment 1, (b) Experiment 2, (c) Experiment 3, (d) Experiment 4, and (e) Experiment 5. Contour interval is $1^\circ\text{C}$ ; maximum velocity vector is 20 cm/s .....	101
29. Cross-shore section of meridional velocity ( $v$ ) for day 3 at (a) $\sim 26^\circ$ S, and (b) $32^\circ$ S of Experiment 6. The contour interval is 5.0 cm/s for poleward (dashed line) flow and 2.0 cm/s for equatorward (solid line) flow. ....	106
30. Cross-shore section of meridional velocity ( $v$ ) for day 9 at (a) $\sim 26^\circ$ S, and (b) $32^\circ$ S of Experiment 6. The contour interval is 5.0 cm/s for poleward (dashed line) flow and 2.0 cm/s for equatorward (solid line) flow. ....	108
31. Cross-shore section of zonal velocity ( $u$ ) at $\sim 117^\circ$ E for days (a) 3, (b) 9, and (c) 15 of Experiment 1. Contour interval is 1.0 cm/s in (a),(b) and 5.0 cm/s in (c) for eastward (solid line) flow and 1.0 cm/s for westward (dashed line) flow.....	110
32. Cross-shore section of zonal velocity ( $u$ ) at $\sim 117^\circ$ E for days (a) 3, (b) 9, and (c) 15 of Experiment 6. Contour interval is 1.0 cm/s in (a),(b) and 5.0 cm/s in (c) for eastward (solid line) flow and 1.0 cm/s for westward (dashed line) flow.....	113





## LIST OF TABLES

1. Values of Constants Used in the Model .....	116
2. Temperature Profile: North West Shelf Waters .....	117
3. Summary of Specific Experiments and Forcing Mechanisms.....	118



## **ACKNOWLEDGEMENT**

I would like to thank my advisor, Dr. Mary Batteen for her exceptional professional advice and guidance, which has made this study possible. The constructive advice provided by Dr. Curtis Collins, as second reader, was greatly appreciated. The computer assistance from Mike Cook and Pete Braccio was invaluable.

I cannot overlook the overwhelming support of my wife, Suzanne, whose patience and understanding have allowed me to pursue my career and education goals. I hope that I can support her equally as well as she pursues her goal of graduate education.

Thank you!



## I. INTRODUCTION

The Leeuwin Current is a thermally driven, anomalous, surface eastern boundary current. It flows poleward along the western Australian coast, down to Cape Leeuwin, and then eastward into the Great Australian Bight (e.g., Cresswell and Golding, 1980). There is general agreement (e.g., Godfrey and Ridgway, 1985) that the Leeuwin Current is generated by a meridional pressure gradient, which overwhelms the equatorward wind stress. The source for the Leeuwin Current is predominantly geostrophic inflow from the west (e.g., McCreary *et al.*, 1986; Thompson, 1987) and is augmented by a source from the North West Shelf (e.g., Gentilli, 1972), possibly having its origin in the Pacific Ocean.

Godfrey and Ridgway (1985) have examined the observed seasonal signals of the forcing mechanisms between 22° S and 32° S. They discuss for this region, the relative strengths of the equatorward wind forcing and the opposing pressure gradient (Figure 1), noting that the individual seasonal cycle of one forcing mechanism reinforces the seasonal trends of the other. Specifically, the pressure gradient term, which experiences a larger seasonal amplitude than wind forcing, reaches its strongest poleward forcing when the opposing wind stress reaches its weakest equatorward forcing. This combination of the two forces with similar phases and opposing directions could explain the observed seasonal trends in the Leeuwin Current System (LCS). Added to this seasonal forcing is a surge of warm, less saline water which flows poleward from the North West Shelf (NWS) region during the austral autumn (i.e. March through May) (Smith *et al.*, 1991). This

surge of warmer water occurs during the same period in which Godfrey and Ridgway (1985) found the strongest poleward pressure gradient forcing and weakest equatorward wind stress, resulting in a strong poleward driving function.

Below the Leeuwin Current, there is an anomalous equatorward undercurrent off western Australia (e.g., Church *et al.*, 1989). This undercurrent is centered near 450 m depth and can attain speeds comparable to the surface flow, exceeding on average 10 cm/s (Smith *et al.*, 1991). Although there is evidence of a westward flow of  $\sim 20$  cm/s centered between  $\sim 400$  m and 700 m depth at Clifty Head off the southern coast of Australia (Cresswell and Peterson, 1993), no studies to date have clearly resolved whether there is a westward undercurrent in this region.

Previous numerical modeling studies by Batteen *et al.* (1992) investigated the effects of annual climatological wind forcing and initialized thermohaline gradients on the LCS, but the study was limited to the coast of Western Australia, during the period when the LCS is observed to be strongest. Batteen and Butler (1998) examined the effects of continuously forced annual Indian Ocean thermohaline gradients on the LCS off both the western and southwestern coasts of Australia.

This study extends prior efforts through the addition of seasonal (rather than annual) wind forcing and thermohaline gradients, permitting a more representative forcing of the highly seasonal LCS. In particular, a full primitive equation (PE) ocean model is used to investigate the individual and combined roles of seasonal wind stress and thermohaline gradients, including NWS forcing, in the generation of currents and eddies off the western and southern coasts of Australia. One particular focus of this study

will be to examine the development and variation of the equatorward undercurrent along the western coast of Australia. Additionally, the nature of the subsurface flow off the southwestern coast of Australia will be investigated, with particular focus on whether there is a westward undercurrent.

The organization of the study is as follows: the PE model, thermohaline gradients, wind forcing conditions and experiment design are described in chapter II. The results and energy analyses of the model experiments are presented in chapter III. Analysis of undercurrent development is presented in chapter IV. A summary is presented in chapter V.





## II. MODEL DESCRIPTION

### A. MODEL EQUATIONS AND METHOD OF SOLUTION

The PE model in this study was originally a coarse resolution model used in closed basin studies by Haney (1974). It has recently been adapted by Batteen (1997) for eddy-resolving, limited eastern boundary current (EBC) regions with open boundaries to the north, south, and west and by Batteen and Butler (1998) to include an additional open boundary to the east. The model is multi-level, non-adiabatic, and uses the beta-plane approximation. It has both baroclinic and barotropic velocity components and uses the hydrostatic and Boussinesq approximations as well as a rigid lid. The governing equations are as follows:

$$\frac{du}{dt} = \frac{-1}{\rho_0} \frac{\partial p}{\partial x} + fv - A_M \nabla^4 u + K_M \frac{\partial^2 u}{\partial z^2} \quad (1)$$

$$\frac{dv}{dt} = \frac{-1}{\rho_0} \frac{\partial p}{\partial y} - fu - A_M \nabla^4 v + K_M \frac{\partial^2 v}{\partial z^2} \quad (2)$$

$$\frac{\partial u}{\partial x} + \frac{\partial v}{\partial y} + \frac{\partial w}{\partial z} = 0 \quad (3)$$

$$\frac{\partial p}{\partial z} = -\rho g \quad (4)$$

$$\rho = \rho_0 [1 - \alpha(T - T_0) + \beta(S - S_0)] \quad (5)$$

$$\frac{dT}{dt} = -A_H \nabla^4 T + K_H \frac{\partial^2 T}{\partial z^2} \quad (6)$$

$$\frac{dS}{dt} = -A_H \nabla^4 S + K_H \frac{\partial^2 S}{\partial z^2} \quad (7)$$

In the above equations,  $t$  is time and  $(x,y,z)$  is a right-handed Cartesian coordinate system with  $x$  pointing toward shore,  $y$  alongshore, and  $z$  upward. The corresponding velocity components are  $(u,v,w)$ .  $T$ ,  $S$ , and  $p$  are temperature, salinity and pressure, respectively, and  $\rho$  is density. Table 1 provides a list of other symbols found in the model equations, as well as values of constants used throughout the study.

A space-staggered B-scheme (Arakawa and Lamb, 1977) is used for the horizontal finite differencing. This scheme has been shown by Batteen and Han (1981) to be appropriate when the grid spacing is approximately the same order as, or less than, the Rossby radius of deformation. The horizontal grid spacing is 11 km in the east-west direction and 14 km in the north-south direction, while the internal Rossby radius of deformation is  $\sim 30$  km.

The model uses ten vertical layers, with constant  $z$ -levels, at depths of 10, 30, 75, 150, 250, 400, 600, 1226, 2283, and 3656 m. This vertical scheme is designed to concentrate more layers above the thermocline in the dynamically active portion of the ocean.

The model domain (Figure 2) encompasses the western and southwestern coasts of Australia, from  $22.5^\circ$  S to  $40^\circ$  S (1792 km alongshore), and from  $107.5^\circ$  E to  $122.5^\circ$  E offshore (1408 km cross-shore). The coastal boundaries of the model domain are closed, and have both tangential and normal velocity components set to zero. To isolate the roles of wind and thermohaline forcing mechanisms from the possible coupled effect of forcing

mechanisms and topography (which will be considered in a separate study), bottom topography has been omitted and the coastal boundary is modeled as a vertical wall. The constant depth used in the model is 4500 m. A modified version of the radiation boundary conditions of Camerlengo and O'Brien (1980) is used for the open boundaries to the north, south, east, and west with some spatial smoothing applied in the vicinity of these boundaries (Batteen, 1997).

Biharmonic lateral heat and momentum diffusion is used in the model with the same choice of coefficients (i.e.,  $2.0 \times 10^{17} \text{ cm}^4/\text{s}$ ) as in Batteen (1997). Holland (1978) showed that biharmonic diffusion acts predominantly on submesoscales, while Holland and Batteen (1986) found that baroclinic mesoscale processes can be damped by Laplacian lateral heat diffusion. As a result, the use of biharmonic lateral diffusion should allow mesoscale eddy generation via barotropic (horizontal shear) and/or baroclinic (vertical shear) instability mechanisms. As in Batteen (1997), weak ( $0.5 \text{ cm}^2/\text{s}$ ) vertical eddy viscosities and conductivities are used and bottom stress is parameterized by a simplified quadratic drag law (Weatherly, 1972).

The method of solution is straightforward with the rigid lid and flat bottom assumptions because the vertically integrated horizontal velocity is subsequently nondivergent. The vertical mean flow can be described by a streamfunction which can be predicted from the vorticity equation, while the vertical shear currents can be predicted after the mean vertical flow is subtracted from the original equations. The other variables, i.e. temperature, salinity, vertical velocity, and pressure, can be explicitly obtained from the thermodynamic energy equation (6), salinity equation (7), continuity equation (3), and

hydrostatic equation (4) respectively (for more complete details on the method of solution see Batteen, 1997).

## **B. FORCING CONDITIONS AND EXPERIMENTAL DESIGN**

The effects of thermohaline gradients on the Leeuwin Current are included using monthly temperature and salinity climatology from Levitus *et al.* (1994) and Levitus and Boyer (1994) to initialize the model and force the model at the western boundary (107.5° E) every third day (see Figure 5a, for example). Temperature forcing occurs over the upper seven levels, and salinity forcing occurs over the upper five levels, which are initially assumed to be zonally homogeneous. Since the lower three levels of temperature and the lower five levels of salinity do not exhibit significant horizontal variation, constants are assumed for each level. Temperature values used for levels 8 (1226 m), 9 (2283 m), and 10 (3656 m) are 3.88°C, 2.20°C, and 2.00°C, respectively, while the salinity constant used for the lower five levels is 34.7. Only the upper layer (e.g., 10 m and 30 m) temperature forcing conditions show significant seasonal variability with a temperature maximum in late summer to early fall and minimum in late winter to early spring throughout the region (e.g., Figures 3a and 3b). Below these depths, both the seasonal temperature fluctuations and temperature gradient weaken. Conversely, salinity forcing conditions at all five levels have no significant seasonal cycle.

To investigate the role of seasonal wind forcing, the model is forced from rest with climatological wind fields from a  $2.5^\circ$  by  $2.5^\circ$  grid of the European Centre for Medium Range Weather Forecasts (ECMWF) near-surface wind analyses (Trenberth *et al.*, 1990). The monthly mean stresses, based on twice daily wind analyses from 1980-1989, have been interpolated spatially to the 11 by 14 km model resolution and temporally to daily wind values.

Sample wind fields used in the basic study are shown in Figure 4, which depicts the seasonal influence and migration of flow around the Southern Indian Ocean Subtropical High over the area encompassed by the model domain. In February (Figure 4a), the winds circulate anticyclonically around the Subtropical High positioned to the southwest of Cape Leeuwin. This flow produces upwelling favorable winds along both the western and southern coasts of Australia. By May (Figure 4b), the Subtropical High has migrated equatorward and is now positioned at  $\sim 30^\circ$  S. The equatorward component of flow has weakened off western Australia and the wind has shifted to downwelling favorable westerlies off the southern coast of Australia. The Subtropical High reaches its maximum equatorward location by July (Figure 4c), resulting in weaker equatorward flow off Western Australia. South of Cape Leeuwin, strong westerlies and northwesterlies dominate. By November (Figure 4d), the Subtropical High has migrated poleward, producing upwelling favorable winds with a strong equatorward component along the western coast of Australia. The winds off southern Australia have shifted from downwelling favorable westerlies to weak upwelling favorable easterlies.

The NWS waters provide a significant influx of warm, low salinity tropical water to the Leeuwin Current and are used as an additional thermal forcing source. The climatology of Levitus and Boyer (1994) provides a representative temperature profile for the NWS waters, which is used in this study (Table 2). The NWS waters are modeled as a horizontal homogeneous raft of warm water simulating a “dam breaking” applied to the northeastern ocean boundary of the model domain once during a model year (see Figure 24a, for example). This model approach is consistent with the hypothesis of flow reversals as a function of monsoonal winds isolating water on the NWS, which subsequently flow poleward (Gentili, 1972).

To address the objectives discussed in chapter 1, five basic experiments and one sensitivity experiment (see Table 3) have been designed. Experiment 1 investigates the effects of seasonal thermohaline gradients on the generation of the Leeuwin Current. With the use of a numerical model, we examine in an idealized way, the development of flow from rest when the temperatures are initially assigned the offshore alongshore gradient. The system is then forced every third day at the western boundary (107.5°E) with seasonally-varying climatological temperature and salinity fields from Levitus and Boyer (1994). Experiment 2 examines the role of seasonal wind forcing in the absence of thermohaline gradients. The model is initialized using a horizontally homogeneous temperature field and a constant salinity of 34.7 psu. The model is then forced daily with the seasonal ECMWF winds (see Figure 4). Experiment 3 investigates the combined effects of an initial thermohaline gradient and seasonal wind forcing. The model is initialized with the January 1 alongshore thermohaline gradients, and then forced daily

using only the seasonal ECMWF winds. Experiment 4 examines the full combined effects of seasonal wind forcing and thermohaline gradients. The model is initialized as in Experiment 3 and then forced with seasonal ECMWF winds and the seasonal temperature and salinity fields from Levitus and Boyer (1994). Finally, Experiment 5 investigates the additional impact of the NWS waters (Table 2), along with seasonal wind forcing and thermohaline gradients. The model is run as in Experiment 4 with the release of NWS waters at model day 75 (which corresponds to mid-March, the timing of which is based on observations by Cresswell and Peterson, 1993). Experiment 6, a sensitivity experiment, will be discussed in section IV.

### C. ENERGY ANALYSIS TECHNIQUE

The energy analysis technique used is the same as that used and described by Batteen *et al.* (1992) and is based on that of Han (1975) and Semtner and Mintz (1977). This analysis is done to gain a better understanding of the types of energy transfer during unstable flow in the LCS. A brief summary of the method follows.

Kinetic energy is calculated for the horizontal components. After a quasi-steady state is reached where the total kinetic energy is nearly constant, mean kinetic energy (MKE) and eddy kinetic energy (EKE) are calculated using the sum of squared mean and horizontal fields, respectively. Next, the available potential energy is calculated and used to determine when a quasi-steady state is reached and when statistics should be collected. Then both mean and eddy available energies are computed. The baroclinic and barotropic



energy transfers, defined by Batteen *et al.* (1992), are used to argue for the type of instability mechanism (e.g., baroclinic, barotropic, or mixed) leading to the initial eddy generation. Specifically, the baroclinic (vertical shear) transfer is the transfer between eddy available potential energy and the eddy kinetic energy. The barotropic (horizontal shear) transfer is the transfer between time-averaged mean kinetic energy and the eddy kinetic energy.

### III. RESULTS OF THE BASIC EXPERIMENTS

#### A. EXPERIMENT 1

Due to the initial alongshore temperature field, the resulting pressure gradient establishes an onshore geostrophic inflow from the interior of the ocean. The onshore flow varies between  $\sim 2$  and  $10$  cm/s. As the flow approaches the coast, it turns and forms a narrow poleward boundary current, which subsequently enters the Great Australian Bight (Figure 5a). Additional onshore flow augments the coastal current causing the magnitude of the current to increase in both the poleward and eastward directions (e.g., day 18, Figure 5b). By day 30 (Figure 5c), maximum velocities of the order of  $\sim 90$  cm/s are observed off Western Australia near Cape Leeuwin (see Figure 2 for geographical locations), and maximum velocities of  $\sim 70$  cm/s are observed off southern Australia. After day 30, the onshore geostrophic flow slightly weakens and is maintained at  $\sim 2$  to  $5$  cm/s.

Along the south coast of Australia, the current "jets" around the Cape Leeuwin meander and accelerates, advecting anticyclonic vorticity downstream and intensifying the undulations and offshoots upstream of Esperance. The current reaches a maximum velocity of  $\sim 90$  cm/s (Figure 5c). The eastward current is greatest near the coast and decreases offshore.

The initial temperature field changes, as warm water is advected poleward and eastward throughout the domain. By day 30 (Figure 5c),  $19^{\circ}\text{C}$  water has been advected

around Cape Leeuwin and reached the Great Australian Bight. Additionally, 20°C water extends to the coast of Clifly Head, 21°C water extends to Cape Naturaliste, and 22°C water has been advected to Freemantle.

A cross-section of meridional velocity (Figure 6) shows the typical structure of the poleward Leeuwin Current and the equatorward undercurrent off the west coast of Australia. The Leeuwin Current jet axis is within ~ 50 km of the coast and extends to ~300 m depth. Core velocities range from ~ 40 to 95 cm/s. A weaker undercurrent with a core velocity of ~ 20 cm/s is also seen. The offshore extent of the undercurrent core is confined to ~ 50 km of the coast, while the average core depth is found ~ 600 m.

Studies by Batteen and Butler (1998) demonstrated that an irregular coastline and the Indian Ocean climatological thermohaline gradients resulted in significant instability at preferred locations. Consistent with their results, large current offshoots, evident by model day 18 (Figure 5b), occur along the west coast and around Cape Leeuwin where the current changes direction. Anticyclonic meanders are established south of Shark Bay, between Freemantle and Dongara, off Cape Naturaliste, Cape Leeuwin, and Clifly Head. The growth of these meanders affects the current characteristics both upstream and downstream.

The mesoscale features in the current intensify and grow. By day 60 (Figure 5d), the Shark Bay, Freemantle, and Cape Naturaliste warm, anticyclonic meanders have developed into eddies that are propagating westward at speeds of ~ 5 to 10 km/day, consistent with Rossby wave propagation speeds. Eddy pairs are also discernible in the

coastal region (see, for example, the eddy pair off Freemantle at  $\sim 32^\circ$  S). Cold, cyclonic eddies form from the anticyclonic limb of the established warm core eddies, resulting in the development of two counter-rotating cells. As the eddies begin their westward propagation, the poleward Leeuwin Current intensifies as nonlinear effects result in a "jet" between the eddies and the coast. These effects translate downstream to augment the current velocities off Southern Australia. In time, the anticyclonic eddies detach and propagate northwestward, and new anticyclonic meanders and eddies form near the same preferred locations.

Figure 5e at day 180 illustrates the propagation of eddies and meandering of the Leeuwin Current. A large anticyclonic eddy has detached off Dongara and is propagating westward. The poleward Leeuwin Current follows the coast around Shark Bay and then meanders offshore at Dongara. It then flows offshore of an anticyclonic meander near Cape Leeuwin. Offshore velocities of the Leeuwin Current reach a maximum of  $\sim 95$  cm/s.

The formation of eddies contributes to a significant amount of advection of warm water offshore (e.g., Figure 5e). For example, the warm core eddy off Dongara propagates northwestward, bringing  $23^\circ\text{C}$  water into the interior ocean. West of Cape Leeuwin, a warm core eddy of  $21^\circ\text{C}$  water, and a cold core eddy of  $18^\circ\text{C}$  water establish a sharp temperature front in the peripheral of the eddy pair. By day 360 (Figure 5f), a significant number of eddies can be seen, advecting warmer waters to the interior ocean.

The Leeuwin Current continues to “jet” around Cape Leeuwin, advecting anticyclonic vorticity and augmenting the flow off the southern coast.

The results (Figure 7) of averaging the temperature and velocity fields for the period when the Leeuwin Current is strongest (i.e., days 90 through 270) shows that the seasonal thermohaline gradient produces a poleward and eastward surface current off the western and southern coasts of Australia, respectively. Large current offshoots are discernible at Dongara, Cape Leeuwin and Clifffy Head.

Horizontal maps of the upper layer mean kinetic energy (MKE) and eddy kinetic energy (EKE), averaged over the time period the Leeuwin Current is strongest (days 90 to 270), are shown in Figures 8a and 8b. Maps of MKE and EKE are suggestive of where mean and eddy energy sources are to be found (Holland *et al.*, 1983).

A comparison of MKE (Figure 8a) with the mean temperature and velocity field (Figure 7; Plate1) shows that high values of MKE are found along the axis of the meandering poleward and eastward current. High values also occur in coastal regions where the coastal current is strongest, and in regions of anticyclonic eddy generation, specifically at Shark Bay (~ 28° S), Dongara (~ 29.5° S), Freemantle (~ 32° S), Cape Leeuwin (~ 34° S), the area between Clifffy Head and Albany (117° E), and near Esperance (120° E).

A comparison of EKE (Figure 8b) with the mean velocity field (Figure 7) shows that high values of EKE correspond to locations where eddies are likely to be generated and in the offshore region where eddies propagate. The maximum values of EKE are

located at the specific eddy generation locations mentioned above, with diminishing values at increasing distances offshore.

Maximum values of both MKE and EKE occur along the Leeuwin Current jet axis, with MKE generally higher than EKE. Analysis of Figure 6 reveals that there is significant horizontal (barotropic) and vertical (baroclinic) shear in the region near the coast. As a result, eddies can be generated from instabilities of the mean Leeuwin Current and the undercurrent via baroclinic and/or barotropic instability processes.

## **B. EXPERIMENT 2**

As expected, the initially strong upwelling favorable wind stress results in an equatorward surface current off western Australia and a westward surface current off southern Australia (e.g., Figure 9a). Additionally, during the period of strong equatorward winds, offshore Ekman transport has resulted in coastal upwelling off the western coast. The weak easterlies off the southern coast have also produced colder water consistent with upwelling along with a westward current, which attains a maximum velocity of  $\sim 50$  cm/s near Albany. Cyclonic meanders in the flow are discernible around Clifty Head, Cape Leeuwin and Shark Bay, while a cold, cyclonic eddy is discernible at Dongara. A cross-section of meridional velocity at  $32^\circ$  S (Figure 10a) shows the relatively shallow ( $< 200$  m) surface equatorward current with a speed of  $\sim 25$  cm/s overlying a weaker poleward undercurrent with an average core depth of 500 m and a speed of  $\sim 3$  cm/s. A cross-section of temperature at Fremantle (Figure 11a) depicts the

strong upward bending of isotherms at the coast. Cooler, subsurface water has been brought to the surface in response to the offshore Ekman transport.

By day 180 (Figure 9b), during the period of weakest winds off western Australia, the equatorward flow has weakened significantly. The westward surface current off the southern coast weakens slightly, although the onshore Ekman transport produced by the stronger westerlies in that region (see Figure 4c, for example), augments the westward flow, extending the current west of Cape Leeuwin. A large (~ 300 km) cyclonic eddy has formed off Cape Leeuwin and the surface flow “jets” westward and equatorward around this feature. A cross-shore section of meridional velocity off Freemantle (Figure 10b) shows the equatorward surface current to be much weaker (~ 10 cm/s) than during the stronger equatorward wind period. A cross-section of isotherms (Figure 11b) indicates that little, if any, coastal upwelling is present.

By the end of the year (day 360, Figure 9c), due to the return of strong equatorward winds, significant upwelling and a strong equatorward surface current with a speed of ~ 30 cm/s off western Australia are discernible. There is a large cyclonic meander off Cape Leeuwin, extending well into the interior ocean. Smaller meanders occur at preferred locations equatorward (i.e., south of Dongara and near Shark Bay). An anticyclonic eddy off Dongara and a cyclonic eddy off the coast at 28° S are also present. A cross-section of meridional velocity at Freemantle (Figure 10c) depicts the broad and shallow nature of the equatorward surface current. Below this, a poleward undercurrent has strengthened to ~ 6 cm/s. A cross-section of temperature (Figure 11c) depicts the

upward bending of isotherms and the upwelling of 17° C water to the surface. The return of easterly winds off the southern coast strengthens the westward surface flow and produces stronger upwelling near Albany (Figure 9c). The surface velocities near Albany reach a maximum of ~ 1.5 m/s.

During the same period, in the equatorward end of the domain, off the western coast of Australia, cold cyclonic eddies propagate westward, advecting cooler, upwelled waters from the coast into the interior ocean. For example, at day 360 (Figure 9c), a cold, cyclonic eddy south of Shark Bay has transported 18°C water offshore. Further north, another cyclonic eddy of 18°C water is propagating westward.

It is interesting to note that no subsurface current above ~ 1000 m depth develops off the southern coast. For example, the mean subsurface flow is found below the westward surface current of ~ 35 cm/s at ~ 1200 m depth and is relatively weak, with a typical eastward speed of ~ 4 cm/s (e.g., Figure 12). The equatorward flow below the deep surface current of ~ 35 cm/s only attains a maximum speed of ~ 4 cm/s (e.g., Figure 12).

Figure 13 shows the average of the temperature and velocity fields for the period that the Leeuwin current is strongest (i.e., days 90 to 270). The results show that the combination of seasonal wind forcing and an initialized horizontally homogeneous thermohaline field produce a westward surface current which flows west past Cape Leeuwin and then turns equatorward, meandering along the coast. Strong upwelling



regions occur north of Dongara ( $\sim 29.5^\circ$  S), while off the southern coast, weaker upwelling occurs.

Horizontal maps of the upper layer MKE and EKE, averaged over the time period when the Leeuwin Current is strongest (days 90 to 270), are shown in Figures 14a and 14b. High values of MKE are found mainly off the southern coast of Australia near Albany, while regions of relatively high EKE values occur off the western coast. A comparison of MKE and EKE values (Figures 14a and 14b) with the mean velocity field (Figure 13) shows that high values of MKE are located along the axis of the eastward flow and specifically at regions where the current is strongest, e.g., near Albany. Relatively high values of EKE are found off the western coast in regions of meanders and offshore in the region of eddy propagation.

### **C. EXPERIMENT 3**

The addition of an initialized Indian Ocean thermohaline gradient to the seasonal wind forcing used in Experiment 2 is expected to lead to the following scenario: Initially, the strong alongshore thermohaline gradient is expected to be the dominant forcing mechanism. As the model year progresses, the continual implementation of wind forcing is expected to overcome the initial forcing of the thermohaline gradient and subsequently become the dominant forcing mechanism.

As expected, the initial thermohaline gradient establishes a poleward (eastward) surface current inshore near the western (southern) coast of Australia. Offshore to the

west, the equatorward wind stress drives an offshore Ekman transport. By day 45 (Figure 15a), the poleward surface current has strengthened, with a maximum velocity of  $\sim 50$  cm/s. Along the coast, the equatorward winds have produced regions of shallow upwelling at Shark Bay, Dongara, Freemantle, and Cape Naturaliste. There are anticyclonic meanders south of Shark Bay, between Dongara and Freemantle, and around Cape Leeuwin. An anticyclonic eddy has formed off Freemantle and has begun a westward propagation.

By day 180 (Figure 15b), the poleward flow has weakened and is barely discernible. A meridional cross-section of velocity near Cape Leeuwin (Figure 16) indicates that the surface flow has weakened to  $\sim 25$  cm/s and is now confined to the upper 200 m depth. Off the southern coast, the strong westerly winds drive onshore Ekman transport and augment the eastward surface flow, which attains a maximum velocity of  $\sim 60$  cm/s (Figure 15b).

By day 360 (Figure 15c), when the Indian Ocean Subtropical High has migrated to its farthest poleward location, the strong equatorward winds off the western coast produce a strong offshore Ekman transport that overcomes the imposed initial thermohaline gradient and an equatorward surface current develops. Off the southern coast, where the winds have become upwelling favorable, a westward surface current develops.

The results (Figure 17) of averaging the temperature and velocity fields for the period the Leeuwin Current is strongest (days 90 to 270) indicate that there is a poleward surface current along the western coast and a stronger eastward surface current off the southern coast. A cyclonic eddy is discernible west of Cape Leeuwin, while a cyclone-

anticyclone eddy pair is visible off Dongara. Near Albany, there is a large current offshoot and an anticyclonic eddy.

Horizontal maps of upper layer MKE and EKE, averaged over days 90 to 270, are shown in Figures 18a and 18b. High values of MKE occur along the entire southern coast of the model domain, and off Cape Leeuwin and Freemantle along the western coast. High values of EKE occur off the southern coast between Albany and Esperance and along the western coast near Cape Leeuwin and Freemantle. A comparison of MKE and EKE (Figures 18a and 18b) with the average temperature and velocity fields (Figure 17), shows that high values of MKE occur along the eastward current jet axis off the southern coast, particularly near Albany. Along the western coast, high values of MKE occur in regions where the coastal current is strongest, specifically Cape Leeuwin and Freemantle. High values of EKE occur in coastal regions corresponding to preferred eddy generation locations and offshore in the regions of eddy propagation.

#### **D. EXPERIMENT 4**

In previous experiments, the presence of seasonal thermohaline gradients only caused geostrophic inflow to dominate throughout the domain. The presence of wind forcing only, due to the seasonally varying alongshore and cross-shore components of wind velocity (Figure 4), produces a more complex flow regime. In particular, at the equatorward end of the model domain, since the winds have offshore and equatorward components, Ekman theory predicts poleward and offshore transport of mass,

respectively. At the poleward end of the model domain off Western Australia, since the winds have onshore and equatorward components, there should be equatorward and offshore transport, respectively. Off the southern coast, the change from upwelling favorable to downwelling favorable winds as the seasons change should produce offshore and then onshore mass transport.

The combination of seasonal Indian Ocean temperature and salinity forcing at the western boundary with seasonal wind forcing is expected to produce results similar to actual observations. Based on the results of the previous experiments, it is speculated that the seasonally-varying strengths of the thermohaline gradients and wind forcing mechanisms (see Figure 1) will result in an unstable poleward flow that adjusts to the seasonal variations.

As expected, the initial thermohaline gradient, with temperature decreasing poleward, establishes a predominantly onshore geostrophic inflow in the interior ocean. On approaching the coast, the onshore flow turns and forms a poleward boundary current (e.g., Figure 19a), which advects warmer water from the equatorward end of the model domain. Offshore to the west, the equatorward wind stress dominates and drives offshore flow. To the south, the poleward surface current rounds Cape Leeuwin and flows eastward towards the Great Australian Bight. The upwelling favorable winds near the coast of Esperance (see Figure 4a), dominate initially and drive an offshore flow, while the westerlies poleward of  $36^{\circ}$  S drive an onshore flow.

By day 30 (Figure 19b), the poleward flow is well established and anticyclonic meanders appear near Shark Bay, Freemantle, and in the vicinity of Cape Naturaliste and

Cape Leeuwin. The current “jets” around Clifffy Head, accelerating toward the Great Australian Bight region. Warm ( $19^{\circ}\text{C}$ ) water has been advected around Cape Leeuwin and reached the coast of Albany. A cross-shore section of meridional velocity off Freemantle (Figure 20a), depicts the relatively narrow structure of the poleward current extending to  $\sim 300$  m depth with a surface velocity of  $\sim 50$  cm/s. There is also a weaker ( $\sim 18$  cm/s) equatorward undercurrent centered at  $\sim 600$  m depth. Figure 20a also shows that there is considerable horizontal and vertical shear above 300 m depth which could contribute to the instability of the Leeuwin Current. A cross-shore section off the southern coast (Figure 21a) depicts an eastward surface current, which has a core velocity of  $\sim 35$  cm/s. Below this, a westward undercurrent with a velocity of  $\sim 20$  cm/s is also present, consistent with subsurface observations off Clifffy Head by Cresswell and Peterson (1993).

By day 90, the season of strongest equatorward wind stress transitions to a weaker atmospheric flow regime. Figure 19c show that the boundary current is still poleward, although it has slowed considerably. A westward propagating anticyclonic-cyclonic eddy pair has formed near Freemantle. Off the southern coast, the flow is no longer rapidly advecting warmer waters into the Great Australian Bight. A meridional velocity cross-section at Freemantle (Figure 20b) shows that the Leeuwin Current has moved  $\sim 50$  km offshore with a velocity of  $\sim 35$  cm/s. Inshore, the equatorward undercurrent has shoaled and weakened. A cross-shore velocity section (Figure 21b) shows only a westward surface present, which has surface speeds of  $\sim 5$  cm/s westward (Figure 19c)

By day 180 (Figure 19d), during the period when the Leeuwin Current is observed to be the strongest, the poleward flow is maintained at  $\sim 35$  cm/s off the western coast. Off southern Australia, the strong westerlies compliment the thermohaline gradients and drive an eastward surface flow, attaining speeds of  $\sim 50$  cm/s near Albany. Cross-shore velocity sections at Cape Leeuwin (Figure 20c) and off Albany (Figure 21c) indicate the typical nature of the Leeuwin Current. A shallow poleward and eastward surface current ( $< 300$ m) is confined to within 50 km of the coast, with a weaker equatorward and westward undercurrent with a speed of  $\sim 4$ -5 cm/s at  $\sim 600$  m depth.

Near the end of the model year (day 345, Figure 19e), when the winds have become strongly equatorward off the western coast and easterly off the southern coast, the Leeuwin Current slows. The barely discernible poleward flow along the western coast has moved offshore in response to the offshore Ekman wind stress. To the south, an eastward surface current with velocities on the order of  $\sim 5$  cm/s is present between Cliffy Head and Albany. Near Esperance, an anticyclonic eddy dominates the flow. A cross-shore velocity section at Cape Leeuwin (Figure 20d) shows a poleward surface current with a core velocity of  $\sim 25$  cm/s overlying an equatorward undercurrent, with a core velocity of  $\sim 4$  cm/s between  $\sim 400$  and 600 m depth. A meridional velocity cross-section near Albany (Figure 21d) depicts a relatively weak eastward surface current inshore of an anticyclonic eddy.

The result of averaging the temperature and velocity fields (Figure 22) for days 90 to 270, shows that an unstable poleward surface current off the western coast of Australia has developed from geostrophic inflow. The current "jets" around Cape Leeuwin and

accelerates into the Great Australian Bight, attaining a maximum velocity of  $\sim 50$  cm/s. A large cyclonic eddy is discernible off Cape Leeuwin, while smaller anticyclonic eddies have developed near Dongara and Freemantle.

Horizontal maps of MKE and EKE (Figures 23a and 23b) are compared to the average temperature and velocity fields (Figure 22) to find the locations of mean and eddy energy sources. High values of MKE are located along the poleward surface current axis near Cape Leeuwin and along the eastward surface current axis off the southern coast of Australia. The highest values of MKE are located between Clifty Head and Albany, where the current is strongest. High values of EKE are located near Freemantle, Clifty Head and between Albany and Esperance.

## **E. EXPERIMENT 5**

The addition of NWS waters to the combination of wind forcing and thermohaline gradients is expected to generate the most realistic results. The release of the NWS waters during mid March of the model year is expected to introduce baroclinicity into the Leeuwin Current (e.g., Batteen *et al.*, 1992), although the effects should diminish away from the source region. Batteen and Butler (1998) demonstrated that the addition of warmer NWS waters could intensify the current velocity and temperature fronts, and act to produce a more unstable flow regime.

The flow initially develops as in Experiment 4, with onshore geostrophic flow driving a poleward surface current along the western coast. Off southern Australia, the

current "jets" around Cape Leeuwin and flows into the Great Australian Bight. By day 75 (not shown), anticyclonic meanders and instabilities have developed at coastal promontories, anticyclonic eddies have propagated westward advecting warm water to offshore regions, and the flow around the southern coast has weakened in response to easterly winds.

The release of the NWS waters in the coastal region north of Shark Bay at day 78 (Figure 24a) introduces a strong thermal front in the region and augments the poleward flow. By day 90 (Figure 24b), the "raft" of NWS water has been advected poleward and has reached Dongara. A cross-shore section of velocity at Shark Bay (Figure 25a) depicts the well-developed surface current with speeds of  $\sim 50$  cm/s above a 15 cm/s undercurrent centered at  $\sim 500$  m depth. An anticyclonic meander has developed south of Shark Bay. Off Freemantle, an anticyclonic-cyclonic eddy pair is well developed. The flow around Cape Leeuwin has become stronger, attaining a speed of  $\sim 60$  cm/s, consistent with the increased thermohaline forcing and the weakening winds during this time. A comparison of Figure 24b with day 90 of Experiment 4 (Figure 19c) indicates that the NWS waters have had little effect on the circulation off the southern coast.

The effects of the NWS waters have reached their furthest extent by day 180 (Figure 24c). The warm surge of NWS water is contained close to the coast with  $22^{\circ}\text{C}$  water reaching Clifty Head. Off Dongara, an anticyclonic eddy advects  $26^{\circ}\text{C}$  water westward. The NWS waters augment the geostrophic inflow along the western coast,



such that the poleward flow is relatively strong along the western and southern coasts with large current offshoots at Cape Leeuwin, Clifly Head and Albany.

By day 345 (Figure 24d), when the opposing wind forcing (see Figure 4) has strengthened, the effects of the NWS waters have diminished and the poleward surface current off the western coast is no longer discernible. The region offshore is filled with warm anticyclonic eddies and eddy pairs. The opposing wind off the southern coast has resulted in a weakening of the eastward surface current. Large anticyclonic eddies persist offshore of Albany and Esperance, advecting warmer waters away from the coast.

The results (Figure 26) of averaging the temperature and velocity fields for the period when the Leeuwin Current is strongest (i.e., days 90 to 270), show that the poleward and eastward surface current are relatively strong and confined to the coast. The warmest waters of  $27^{\circ}\text{C}$  are confined north of Dongara. The surface currents are strongest near Shark Bay, Cape Naturaliste, and between Clifly Head and Albany. Off Dongara, there is a large anticyclonic meander of  $23^{\circ}\text{C}$  water.

A comparison of mean temperature and velocity fields (Figure 26) with horizontal maps of MKE (Figure 27a) and EKE (Figure 27b) shows that high values of MKE and EKE occur along the jet axis of the surface current off the western and southern coasts of Australia. The highest values of MKE are located near Shark Bay, Dongara, Freemantle, Cape Leeuwin and Albany. The highest values of EKE are collocated with the MKE in the regions of eddy generation, as well as offshore where eddies propagate. The NWS

waters have added baroclinic and barotropic energy to the equatorward region of the model domain.



#### IV. ANALYSIS OF UNDERCURRENT GENERATION MECHANISMS

Previous modeling studies (Weaver and Middleton, 1988; Batteen *et al.*, 1992; Batteen and Butler, 1998) have generated an equatorward undercurrent off the western coast of Australia, consistent with observations of LUCIE (Boland *et al.*, 1988). Although Cresswell and Peterson (1993) found evidence of a westward flow at Cliffy Head between 400 and 700 m depth with a speed of  $\sim 20$  cm/s, a lack of observations off the southern coast of Australia, east of Cliffy Head, leaves some question as to the nature of the subsurface flow in that region, including its generation mechanism if present.

It is not clear what the mechanism for the generation of undercurrents would be in the LCS. One possible mechanism for the development of the undercurrent could be the pressure gradient forcing at depth. The Indian Ocean seasonal thermohaline gradients experience a reversal between 400 m and 700 m depth, such that warmer waters are present in the poleward end of the model domain and cooler waters in the equatorward end.

Another possible mechanism for the generation of the undercurrent is conservation of mass continuity. When the system is in equilibrium, the strong flow of the surface current generates alongshore temperature gradients at deeper levels, with warm waters at the poleward end of the model domain off Cape Leeuwin. These "headwaters" are sufficient to feed the equatorward undercurrent and maintain it. For our idealized Experiment 2, the offshore Ekman transport at the surface could produce divergent upwelling below, which could then be balanced by an onshore Ekman transport

at levels near  $\sim 500$  m depth. This onshore Ekman transport could be sufficient to drive a poleward undercurrent.

We examine first, the subsurface flow off the western coast of Australia. All experiments develop an undercurrent in the opposite direction of the surface current in this region. The time-averaged velocity fields for days 90 to 270 at 600 m depth are shown in Figure 28. Experiments 1,3,4, and 5 all developed an equatorward undercurrent off the western coast of Australia between  $\sim 400$  and 700 m depth, while Experiment 2 developed a weak poleward undercurrent near  $\sim 500$  depth.

Of the two proposed mechanisms, the alongshore pressure gradient at depth cannot explain the equatorward undercurrent. The geostrophic velocity in response to the pressure gradient at depth would be in the offshore direction rather than onshore. Therefore we hypothesize that the second proposed mechanism, the generation of deeper alongshore thermohaline gradients by the surface flow, may explain the equatorward undercurrent.

To examine this further, we conducted a special experiment (Experiment 6 in Table 3) that removes the thermohaline gradient below 400 m depth. The model is initialized as in Experiment 1; however, the thermohaline forcing is only applied at the upper five levels. Level 6 (400 m) is given a constant temperature of  $10.7^{\circ}\text{C}$ , while level 7 (600 m) is given the constant temperature of  $8.6^{\circ}\text{C}$ .

Figure 29 shows cross-shore velocity sections for this experiment at  $\sim 26^{\circ}$  S and at  $\sim 32^{\circ}$  S for model day 3. At this time, the shallowest equatorward undercurrent with a

core depth of  $\sim 600$  m has developed near  $\sim 26^\circ$  S. The undercurrent continues to develop poleward so that by day 9 (Figure 30), equatorward undercurrents are well developed at both latitudes. The core of the deepest and strongest undercurrent (Figure 30b), however, is located near the poleward end of the model domain. The progression of development of this undercurrent in the absence of an initial pressure gradient, with the deepest and strongest current in the poleward region of the model domain, is consistent with our second proposed mechanism. In particular, the strengthening poleward surface flow generates alongshore temperature gradients at deeper levels, creating a “headwaters” region near Cape Leeuwin that feeds the equatorward undercurrent.

We now examine the nature of the subsurface flow off the southern coast of Australia. Analysis of Figure 28 shows that in all experiments, with the exception of Experiment 2, an undercurrent develops in the opposite direction of the surface flow. There again are two possible mechanisms for driving an undercurrent off the southern coast. Unlike the western coast of Australia, the Indian Ocean thermohaline gradient at deeper levels could drive an alongshore geostrophic current in the westward direction that may be sufficient to maintain an undercurrent.

The second proposed mechanism is once again the argument of mass continuity. The strong surface flow could advect warm waters and transport mass towards the Great Australian Bight region. There is a large current offshoot near Albany, that could provide a “headwaters” source region to feed the undercurrent.

To examine the flow development further, we compare cross-shore velocity sections at model days 3, 9, and 15 at  $\sim 117^\circ$  E in Experiment 1 (Figure 31) and Experiment 6 (Figure 32). In Experiment 1, a westward undercurrent centered at  $\sim 600$  m depth has developed by day 9 (Figure 31b). In Experiment 6 a westward undercurrent also develops by day 9 (Figure 32b), but it develops at a much deeper level of  $\sim 1200$  m depth. This would suggest that the system is developing an undercurrent in the opposite direction as the surface current to achieve balance. In Experiment 6, even with the absence of a deep thermohaline gradient, an undercurrent in response to the surface current still develops.

These results suggest that a combination of mechanisms is likely responsible for the development of a westward undercurrent off the southern coast of Australia. Initially, the thermohaline gradients at deeper levels are sufficient to drive an alongshore flow and set up an undercurrent below  $\sim 400$  m depth. This undercurrent can then be maintained by mass continuity, as the system moves towards equilibrium. Specifically, the undercurrent is maintained by a balance of mass, in response to the thermohaline gradients at depth.

## V. SUMMARY AND RECOMMENDATIONS

The objective of this study was to investigate the effect of seasonal thermohaline gradients and wind forcing on the LCS. Toward this end, a high resolution, multi-level, PE model was forced from rest in several experiments using either thermohaline gradients only, wind forcing only, or a combination of both. Additionally, the seasonal effects of the NWS waters were included in another experiment, yielding insight into the importance of this secondary forcing mechanism. A final goal of this research was to investigate the development of undercurrents along the western and southern coast of Australia.

The results of Experiment 1 revealed how seasonal thermohaline gradients generate and maintain a poleward and eastward surface current overlying a westward and equatorward undercurrent with a core depth of  $\sim 600$  m. The opposing nature of the surface current and undercurrent resulted in both horizontal (barotropic instability) and vertical (baroclinic instability) shear. Horizontal maps of MKE and EKE showed that high values of both occurred in coastal regions near Shark Bay, Dongara, Freemantle, Cape Leeuwin, and between Clifty Head and Albany. High values of EKE were also found offshore in regions of westward eddy propagation.

In Experiment 2, the application of seasonal wind forcing in the absence of ocean thermohaline gradients demonstrated the importance of this spatially and temporally varying forcing mechanism in the seasonal nature of the LCS. The strong equatorward winds of the austral spring and summer generated significant upwelling along the entire



coastline, particularly in the equatorward region of the model domain. This upwelling became weak and somewhat suppressed with the weaker winds of the austral fall and winter, which corresponds to the period when the Leeuwin Current is observed to be the strongest. Maps of MKE and EKE showed that high values of MKE were found off the southern coast, while relatively high values of EKE were found off the western coast in regions of eddy development.

Experiment 3 investigated the relative strengths of an initial thermohaline gradient and seasonal wind forcing. The thermohaline gradient established a poleward (eastward) surface current overlying a westward (equatorward) undercurrent off the western (southern) coast of Australia. As the effects of the initial thermohaline gradient diminished with time, the seasonally varying wind forcing produced localized upwelling at Shark Bay, Dongara, Freemantle, and Cape Naturaliste, as well as a strengthening of the eastward surface current along the southern coast. During the austral fall and early spring (i.e., September to December), the upwelling favorable winds along the western (southern) coasts resulted in a weak equatorward (westward) surface current. Maps of MKE and EKE showed that high values of MKE were located along the eastward surface current axis near Albany and off the western coast near Cape Leeuwin. High values of EKE occurred in coastal regions where eddies were likely to be generated and in offshore regions of westward eddy propagation.

The results of Experiment 4 explored the combined role of seasonal thermohaline gradients and wind forcing in the LCS. The relative strength of the combined forcing mechanism varied with the seasonal fluctuations of thermohaline gradients and wind

forcing. The poleward and eastward Leeuwin Current strengthened and weakened in response to these seasonal variations. Maps of MKE and EKE showed high values of both along the current axis off the western and southern coasts of Australia. Maximum values of both MKE and EKE, occurred in regions of eddy generation.

The added contribution of NWS waters in Experiment 5 augmented the onshore geostrophic inflow, strengthening the poleward flow and advecting warmer waters along the coastal region. The warmer waters along the coast resulted in advection of warmer waters offshore by anticyclonic eddies. The steadily increasing forcing from stronger thermohaline gradients and the poleward surge of NWS waters combined to extend the duration of the strong poleward and eastward surface flow through the austral winter (August). Maps of MKE and EKE showed that the NWS waters add significant barotropic and baroclinic instability to the equatorward region of the model domain.

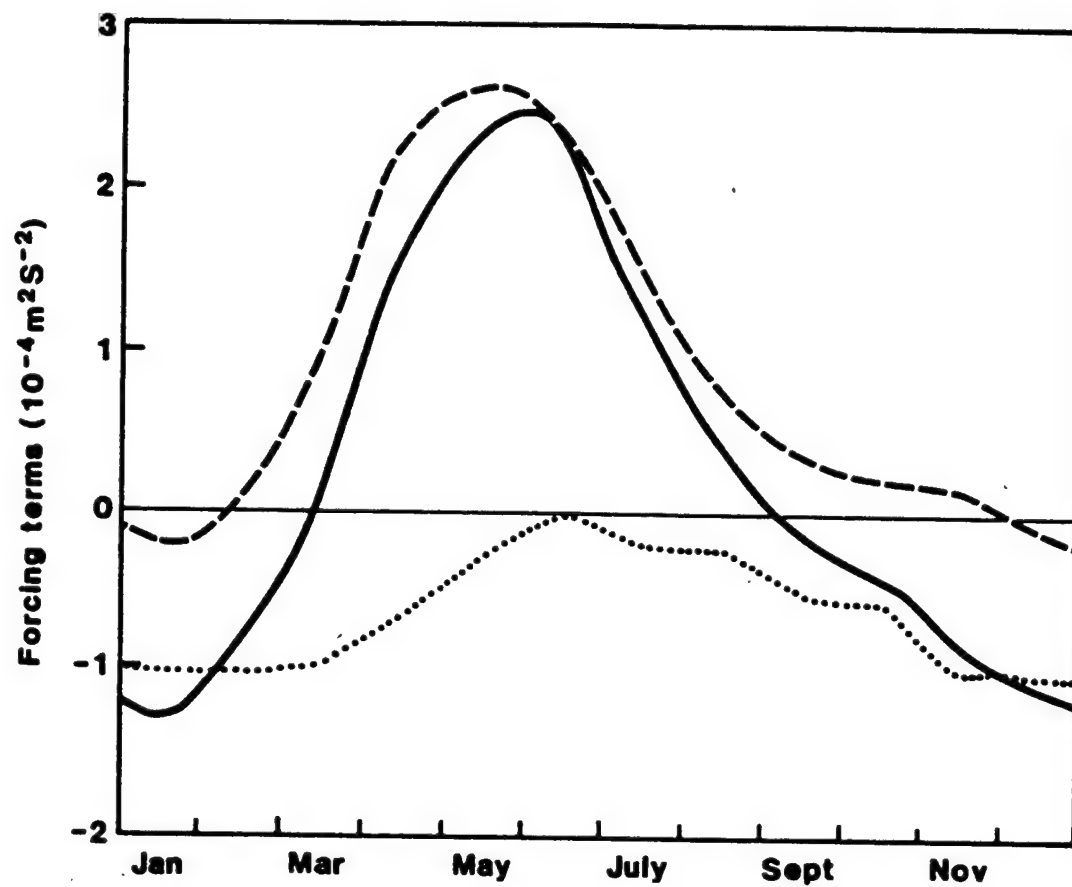
Experiment 6 was designed to investigate the generation mechanism for the undercurrent in the region. A comparison of model results with Experiment 1 showed that along the western coast of Australia the surface flow is sufficient to produce a "headwaters" region near Cape Leeuwin, which drives an equatorward undercurrent. Off the southern coast of Australia, conservation of mass continuity maintains a westward undercurrent in response to an alongshore thermohaline gradient at deeper levels.

Future modeling studies to enhance the simulation and resolution of LCS features should include the addition of bottom topography, increase of horizontal resolution, and expansion of the model domain to include the Great Australian Bight (GAB). Little is known about the interaction of the eastward Leeuwin Current with the circulation within

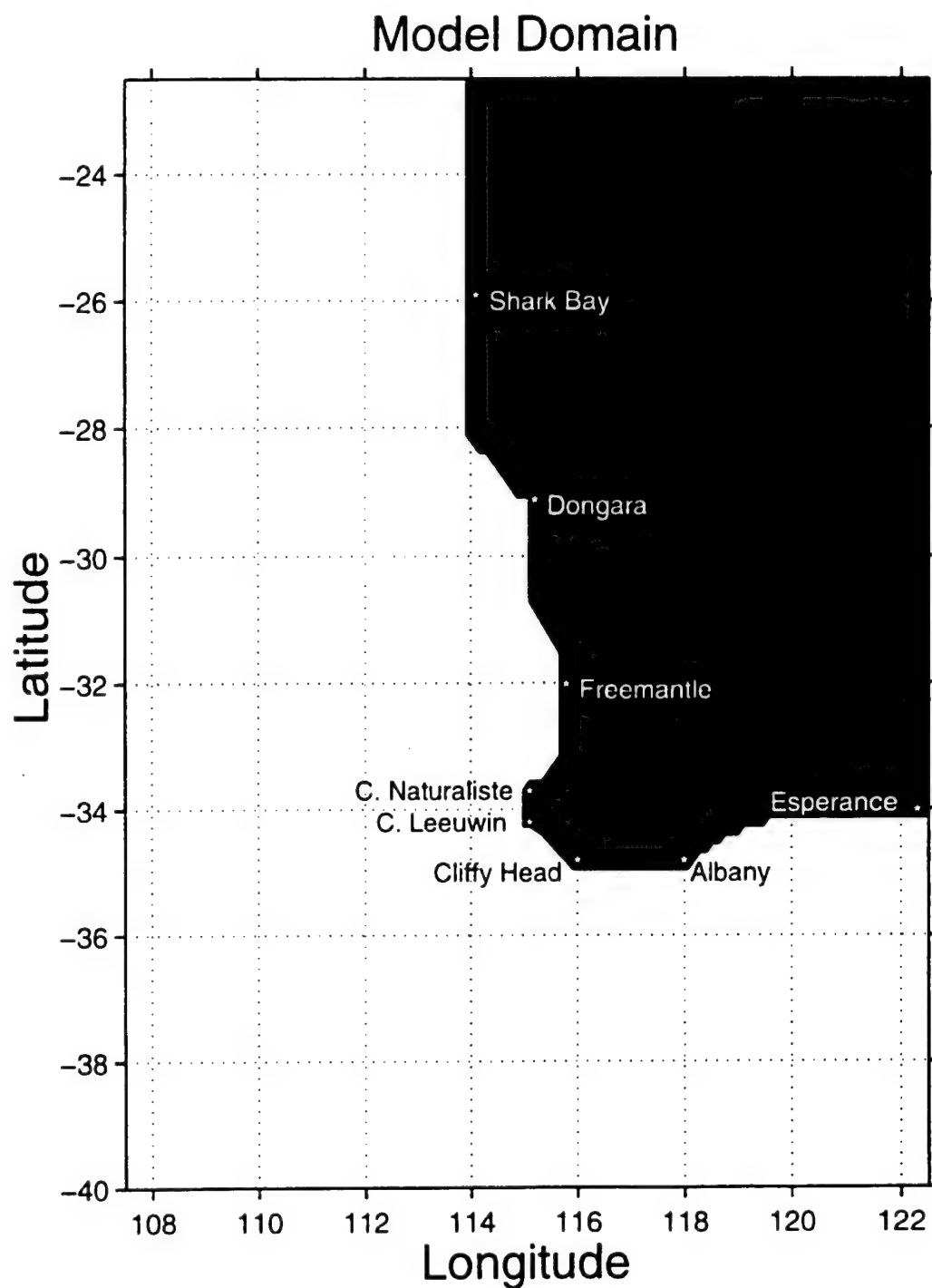
the GAB. Increasing the model domain would allow process oriented studies of the various forcing mechanisms for the GAB and could yield insight into the circulation of this region.

Finally, by using ECMWF winds of relatively coarse spatial resolution, this study focused on the role of seasonal winds in combination with thermohaline gradients in the LCS. It would be of interest to investigate this role using winds of higher spatial and temporal resolution. The use of winds with spatial resolution of  $\sim 1$  km and temporal resolution of  $\sim 1$  day would allow oceanic response to wind events, relaxations, and reversals to be studied. This would be particularly useful off the southwestern coast where the seasonal winds are highly variable over the model year.

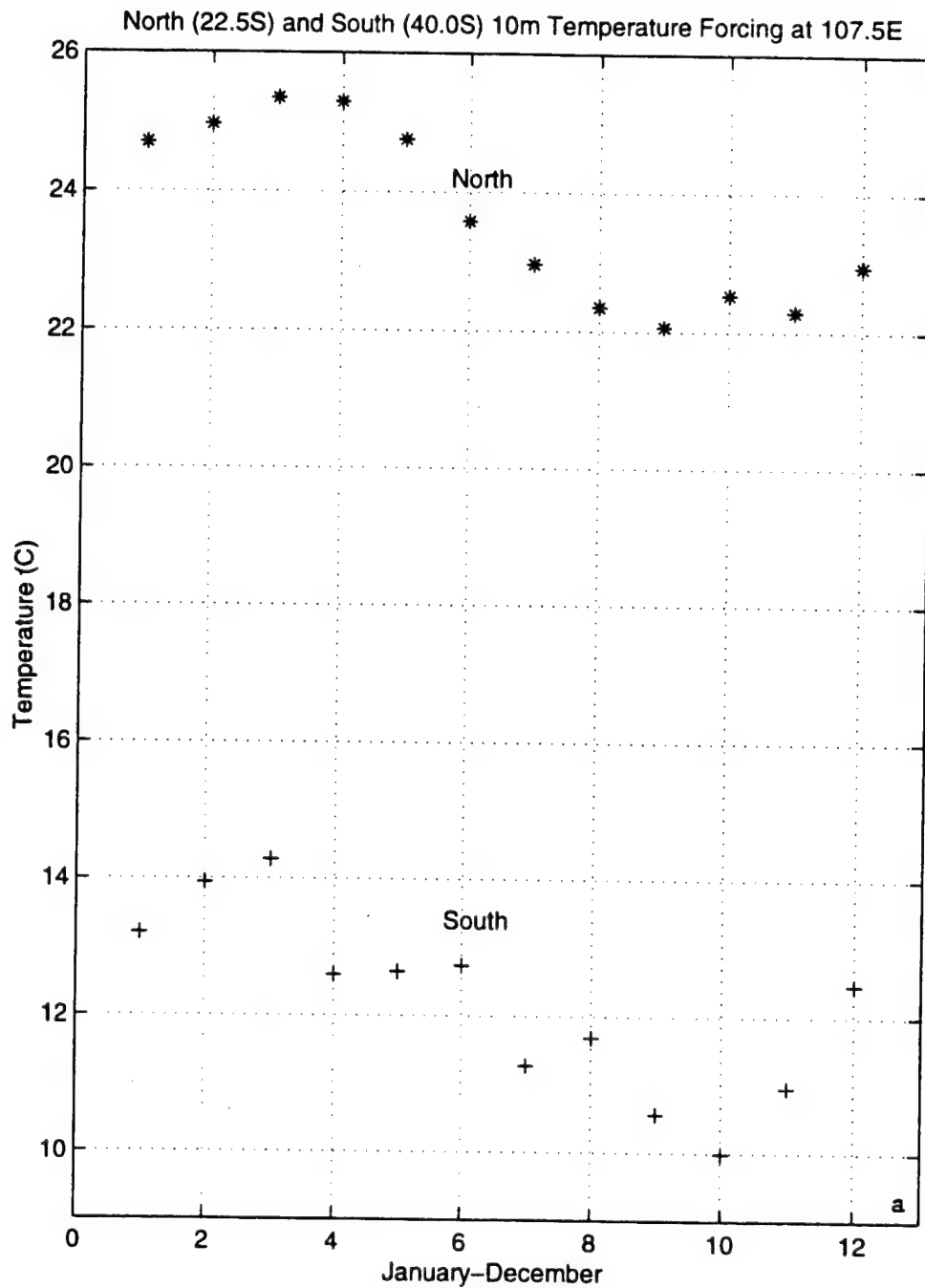
This study provided insight into the interaction of seasonal thermohaline gradients and wind forcing off the western and southwestern coasts of Australia. The model qualitatively reproduced the complex circulation of this region, while yielding insight into the role of each forcing mechanism as well as identifying the important seasonal effects in the LCS.



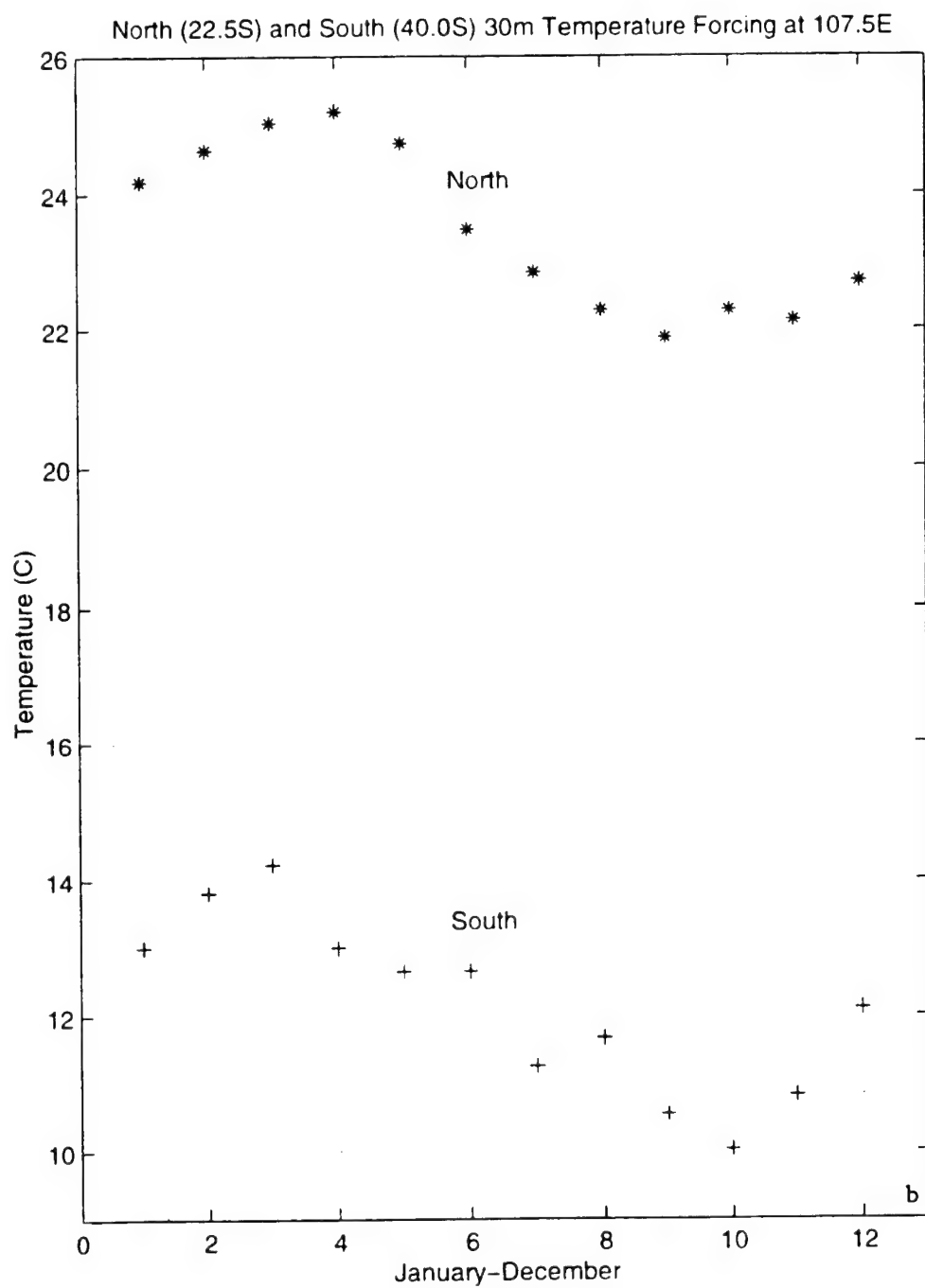
**Figure 1.** Annual cycle of net forcing for the Leeuwin Current between 22°S and 32°: Dashed line is observed pressure gradient forcing; dotted line is observed wind stress; solid line is net forcing. Positive is southward (from Godfrey and Ridgway).

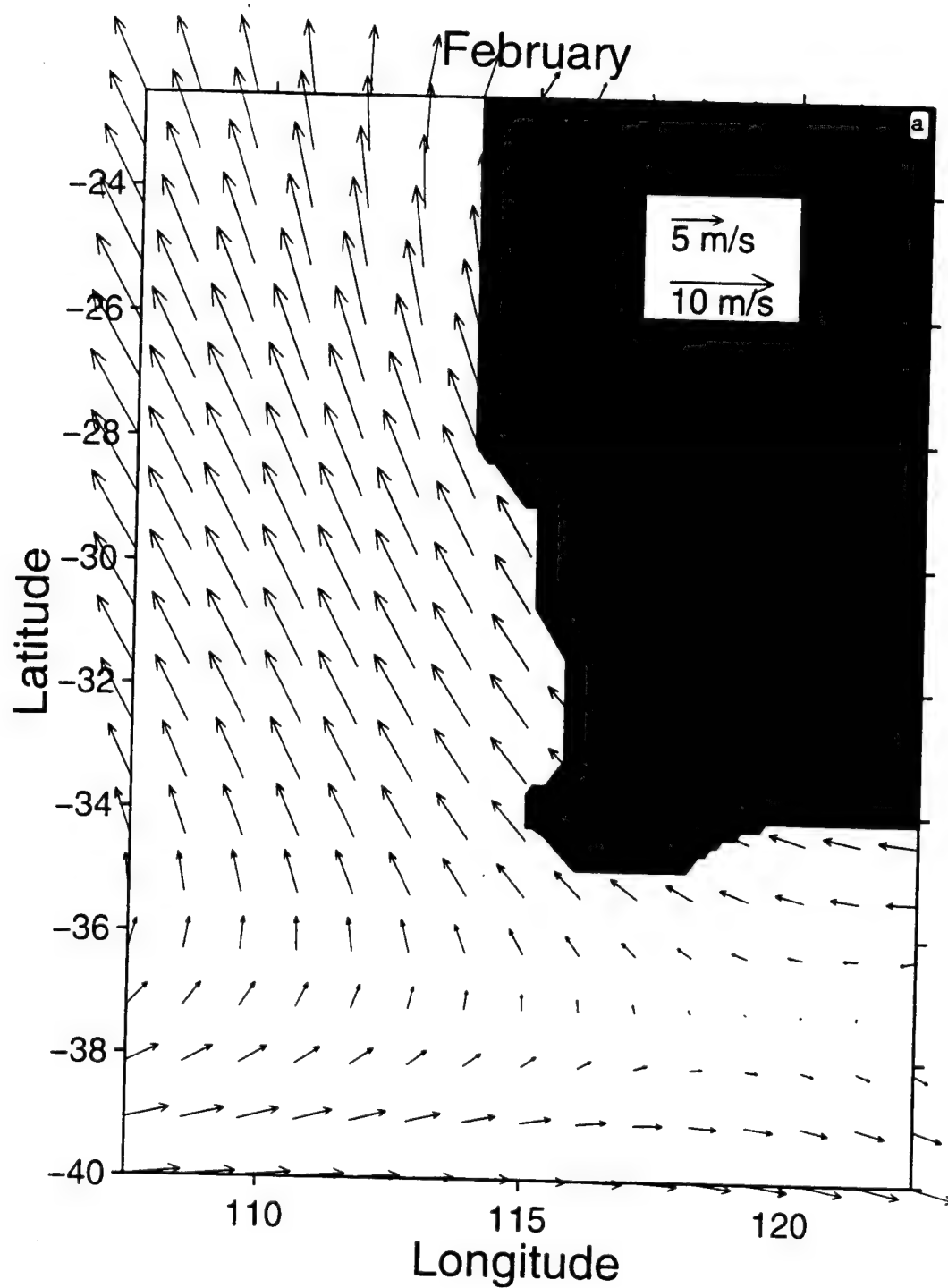


**Figure 2.** Model domain, coastline and geographic locations of the western and southwestern coasts of Australia. The area of study is bounded by 22.5° S to 40° S, 107.5° E to 122.5° E.



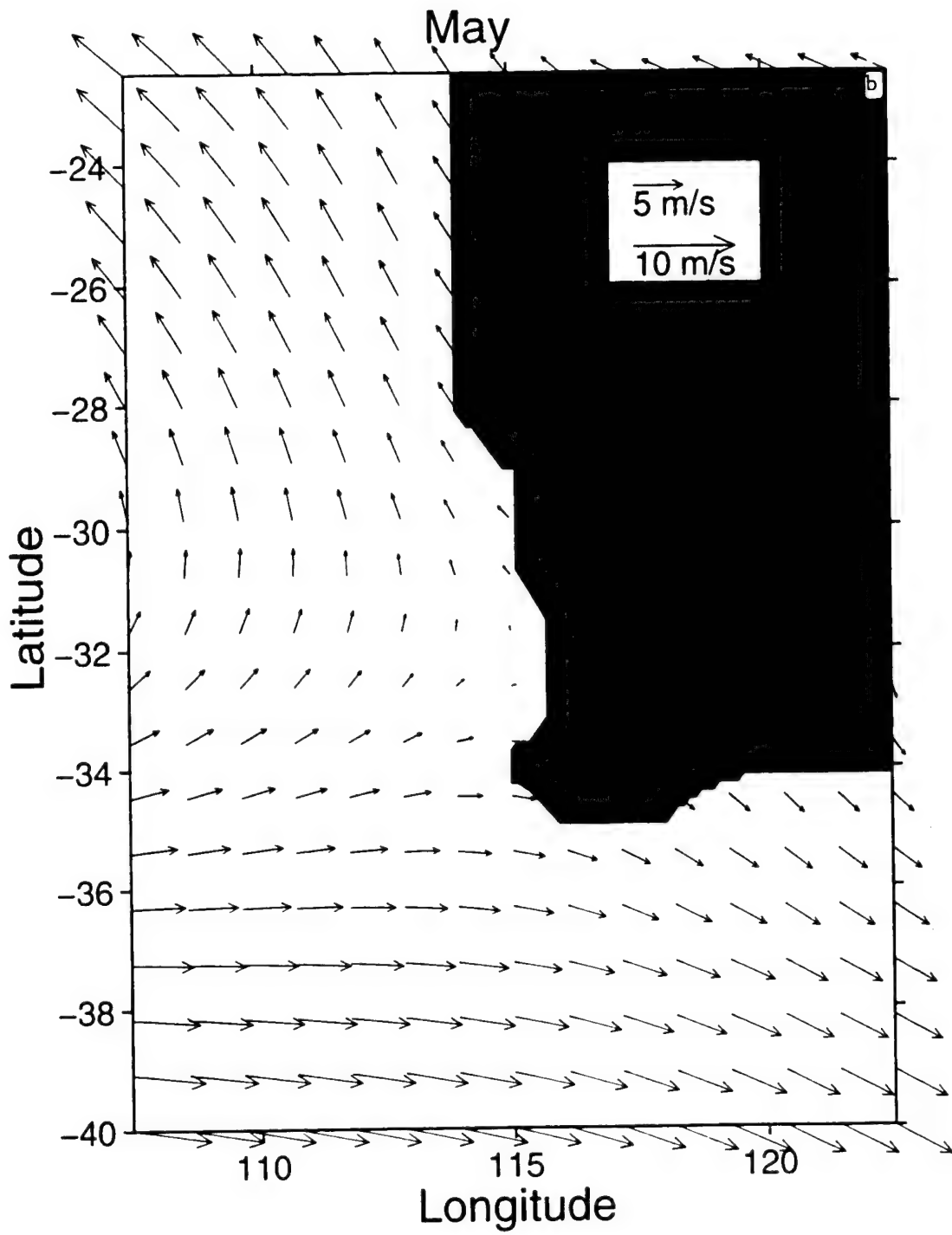
**Figure 3.** Time series plots of monthly temperature fields used as seasonal forcing in the basic simulation. The '\*' symbol represents data at 22.5° S, 107.5° E, while the '+' symbol represents data at 40.5° S, 107.5° E for (a) 10 m and (b) 30 m depth.

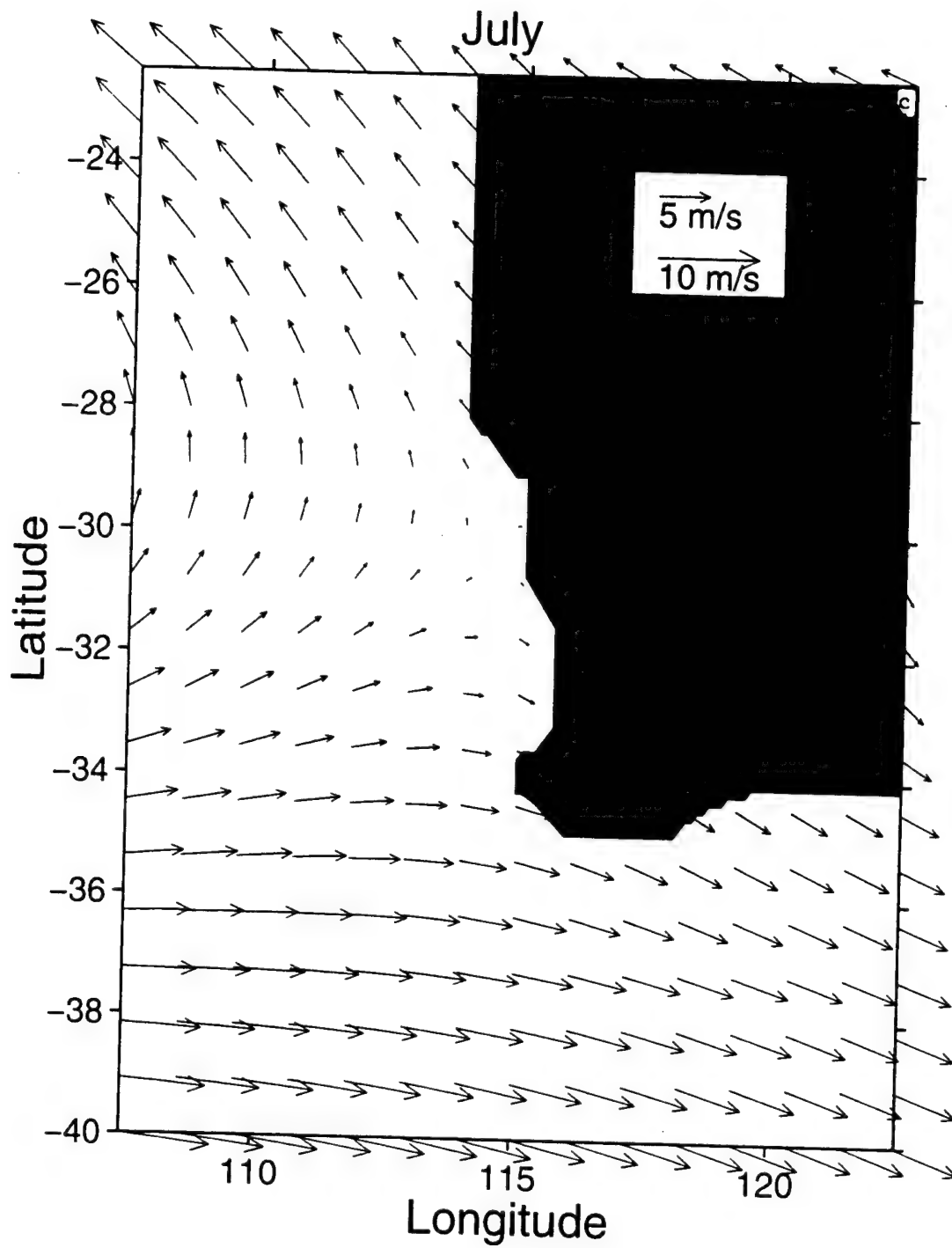


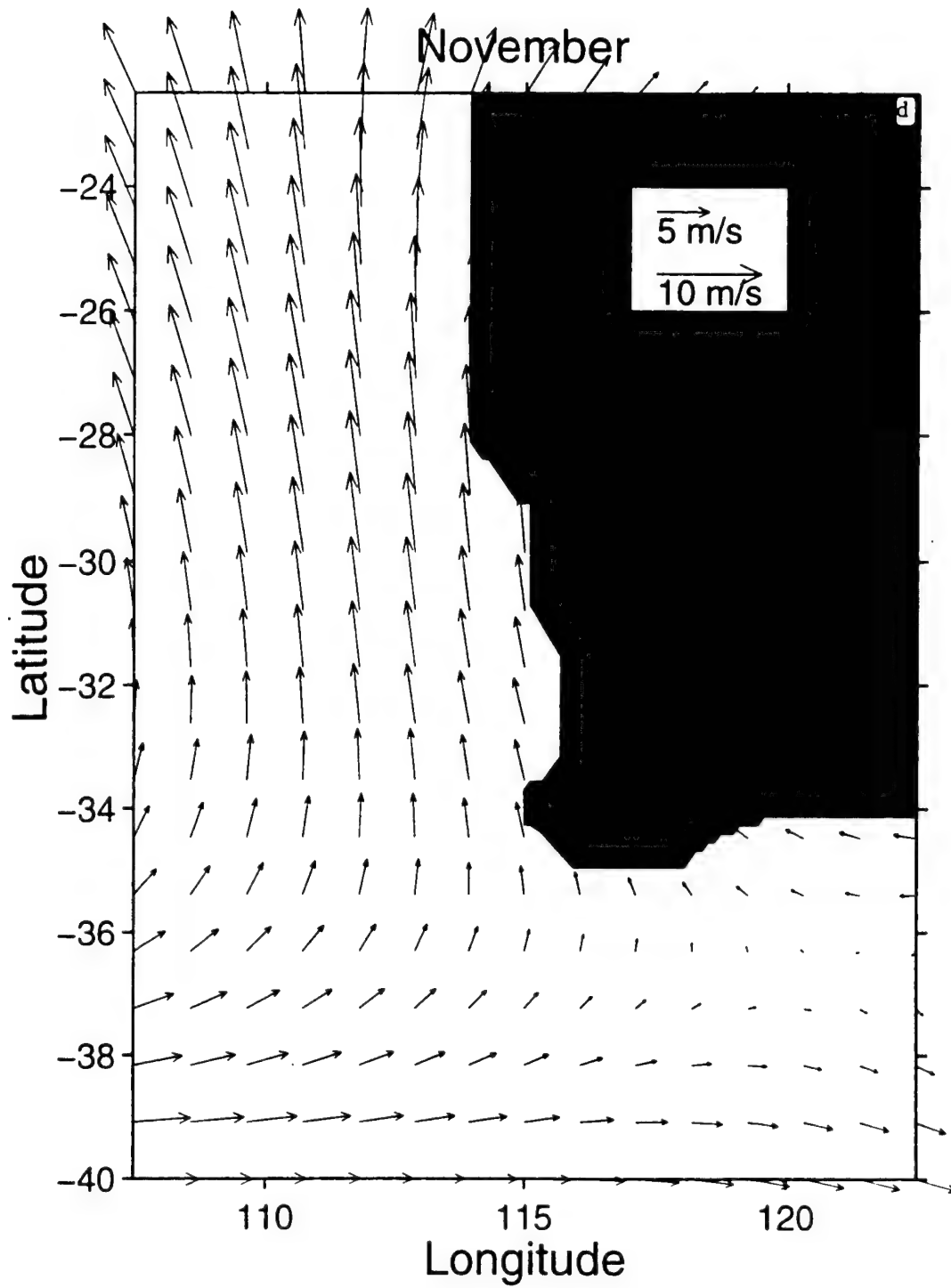


**Figure 4.** Climatological winds over the Leeuwin Current System used to force the model. The climatological (1980-1989) ECMWF winds are shown here for (a) January, (b) April, (c) July, and (d) October









DEPTH : 10m  
T : 3

DATA SET: case1

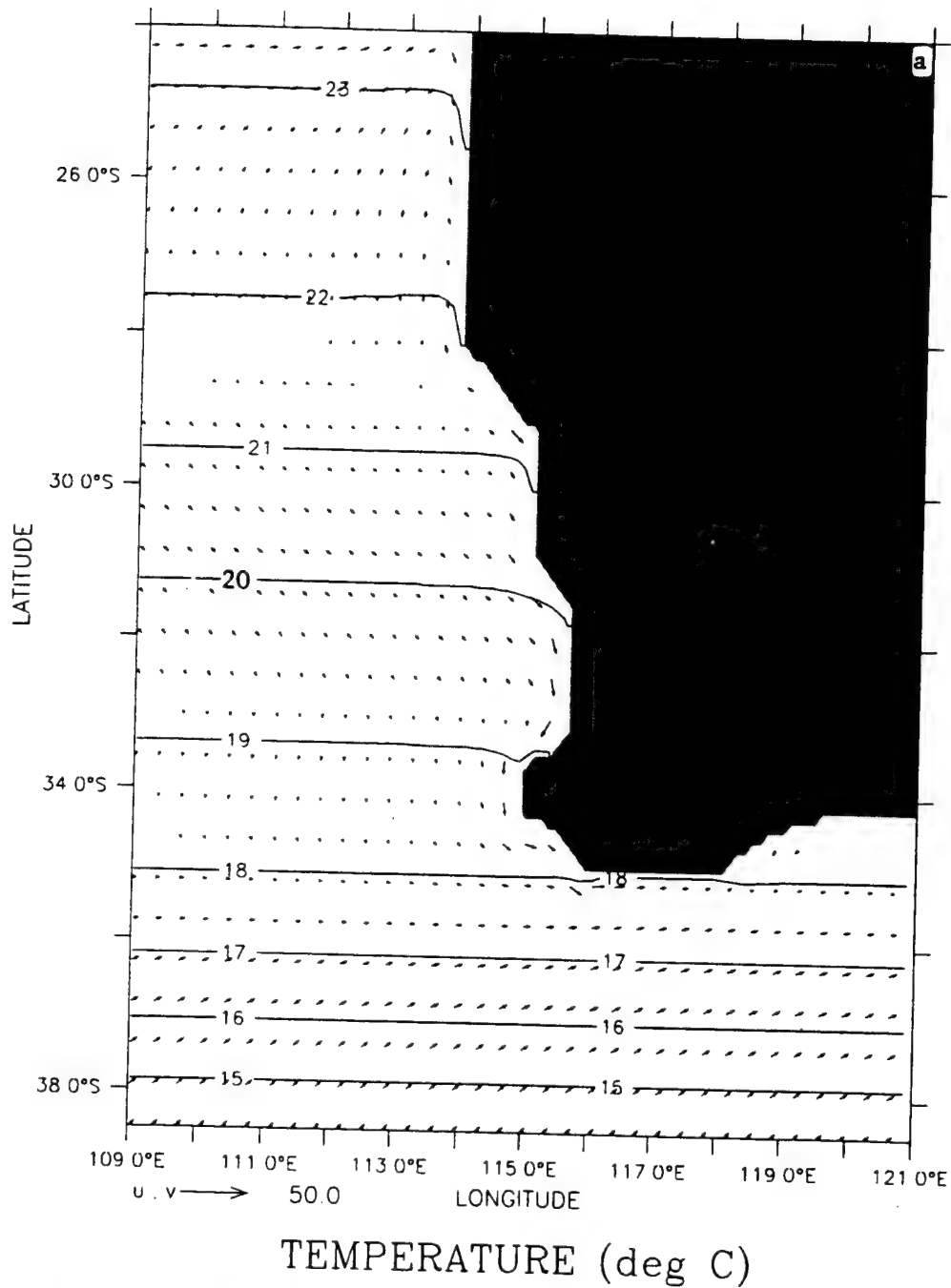
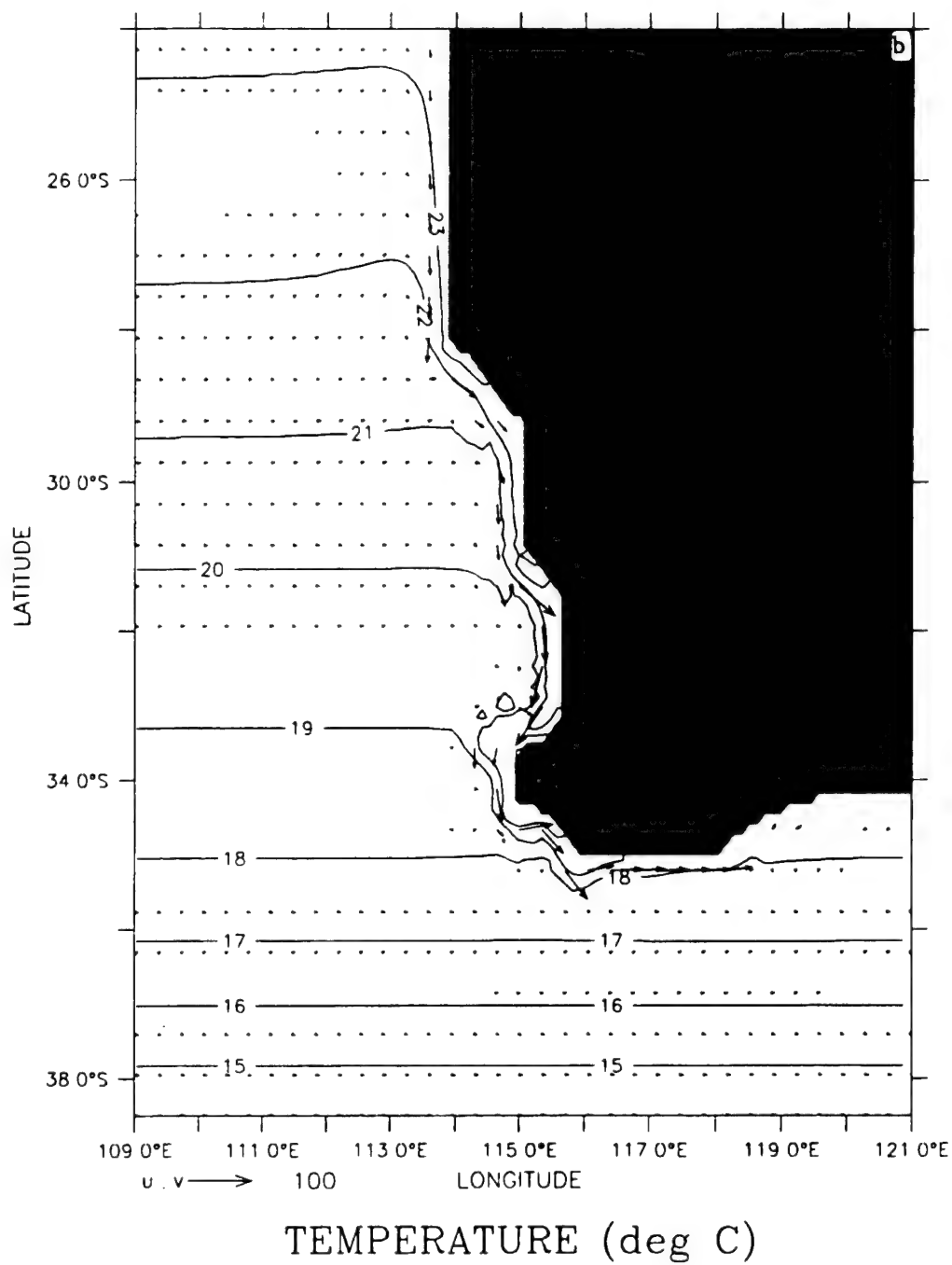


**Figure 5.** Temperature contours and velocity vectors at 10 m depth at days (a) 3, (b) 18, (c) 30, (d) 60, (e) 180, and (f) 360 of Experiment 1. The contour interval is 1°C. To avoid clutter, the velocity vectors are plotted every third grid point in the east-west direction and every fourth grid point in the north-south direction. Maximum velocity is 50 cm/s in (a) and 100 cm/s in (b) - (f).

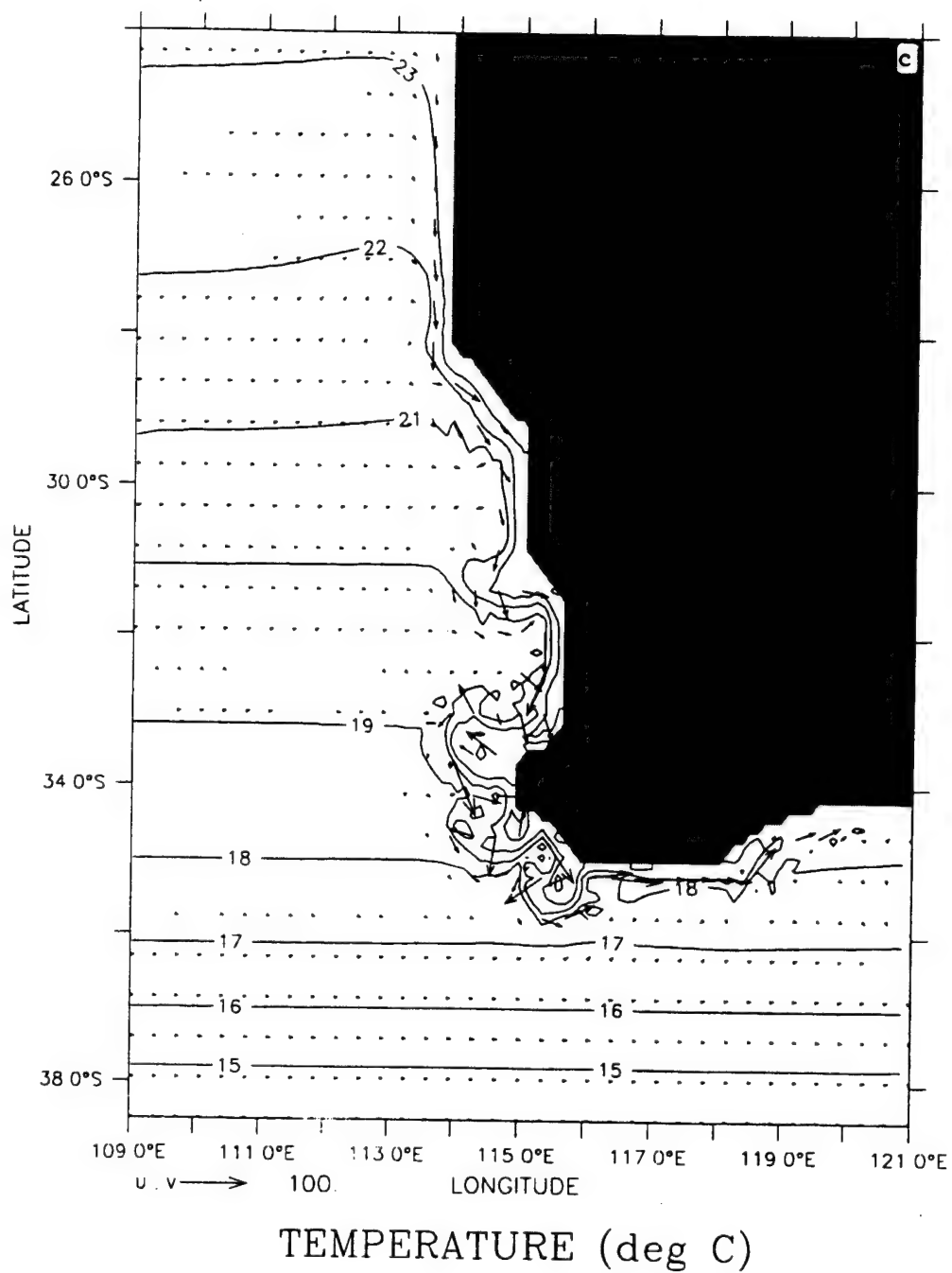
DEPTH 10m  
T 18

DATA SET: case1



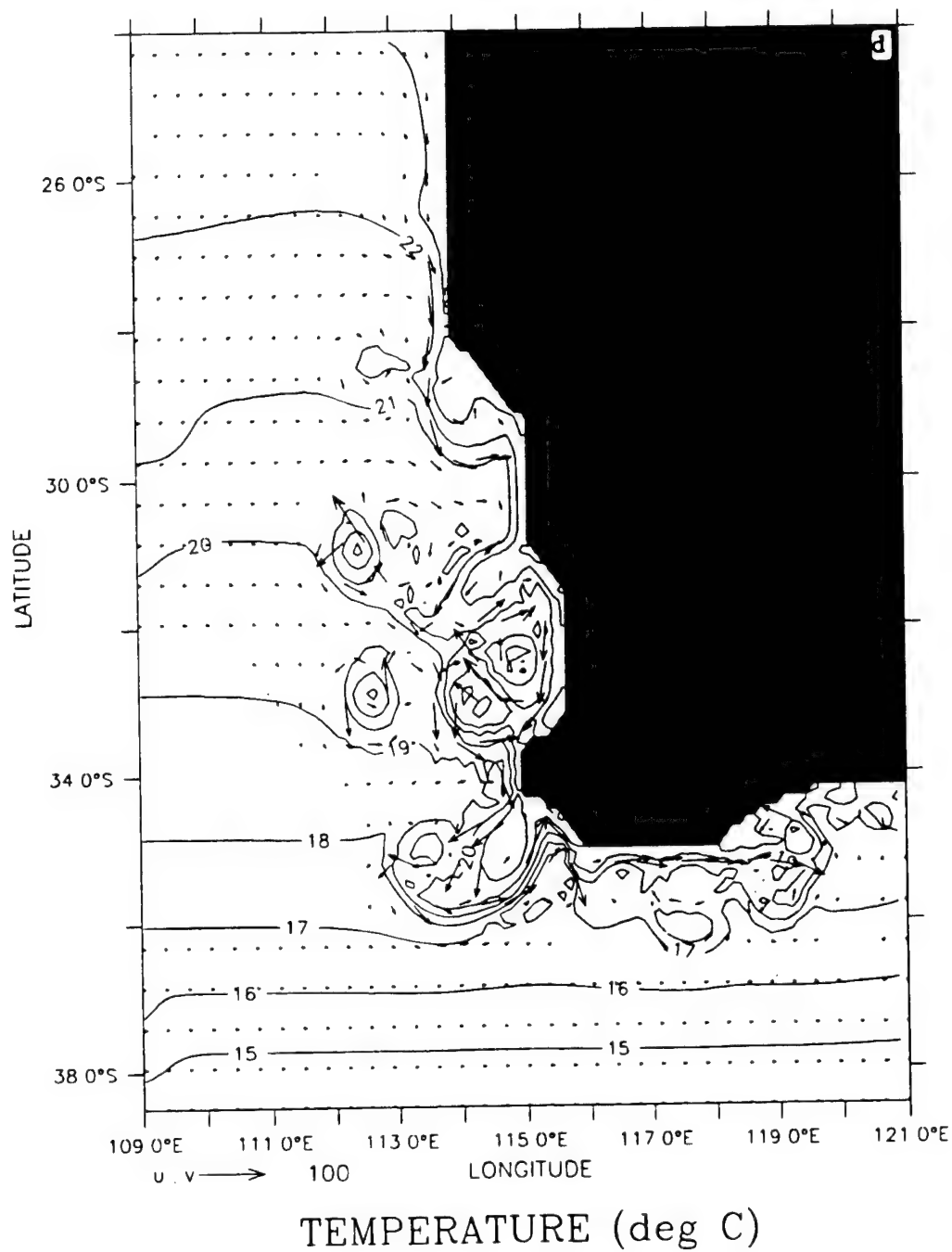
DEPTH : 10m  
T : 30

DATA SET: case1



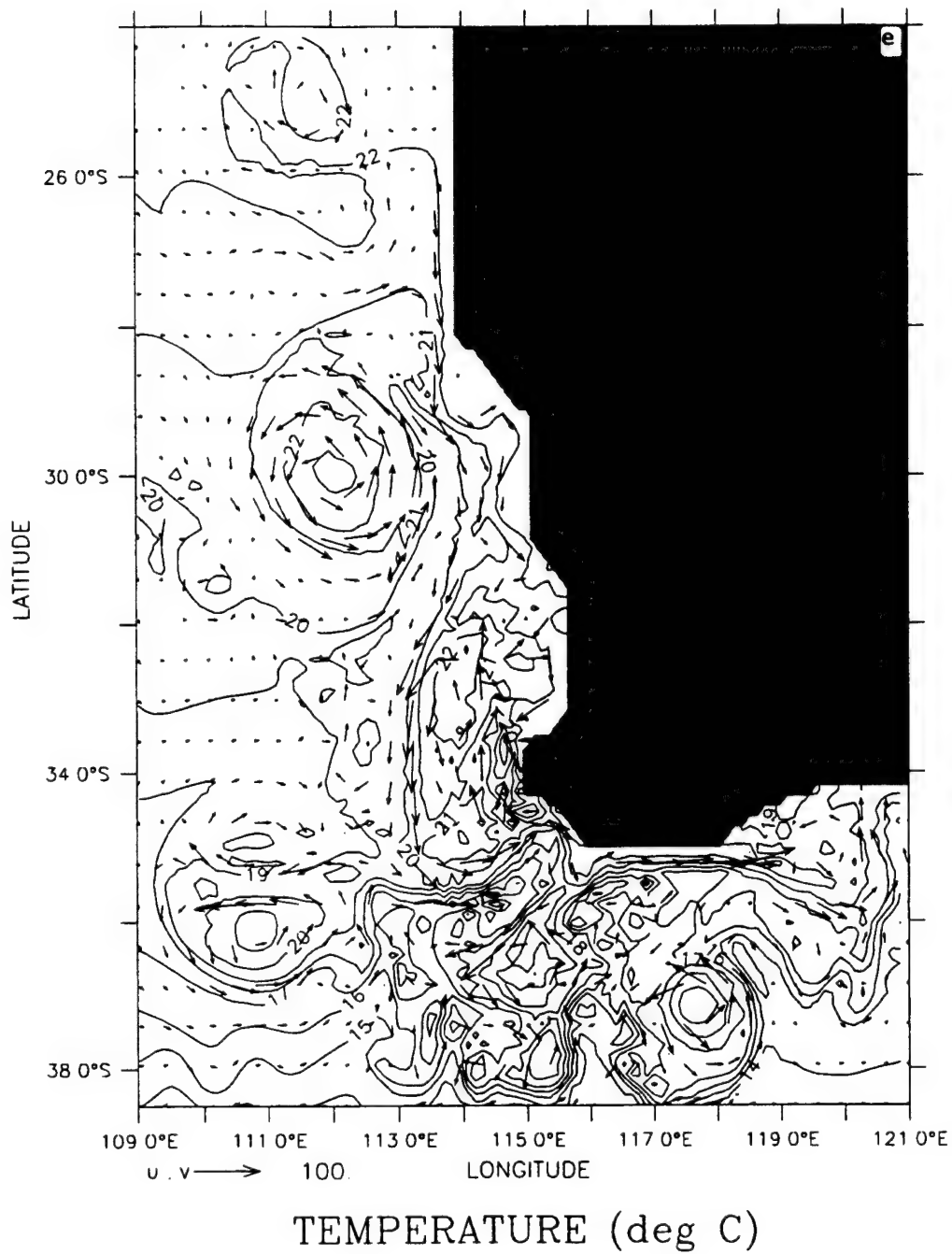
DEPTH : 10m  
T : 60

DATA SET: case1



DEPTH : 10m  
T : 180

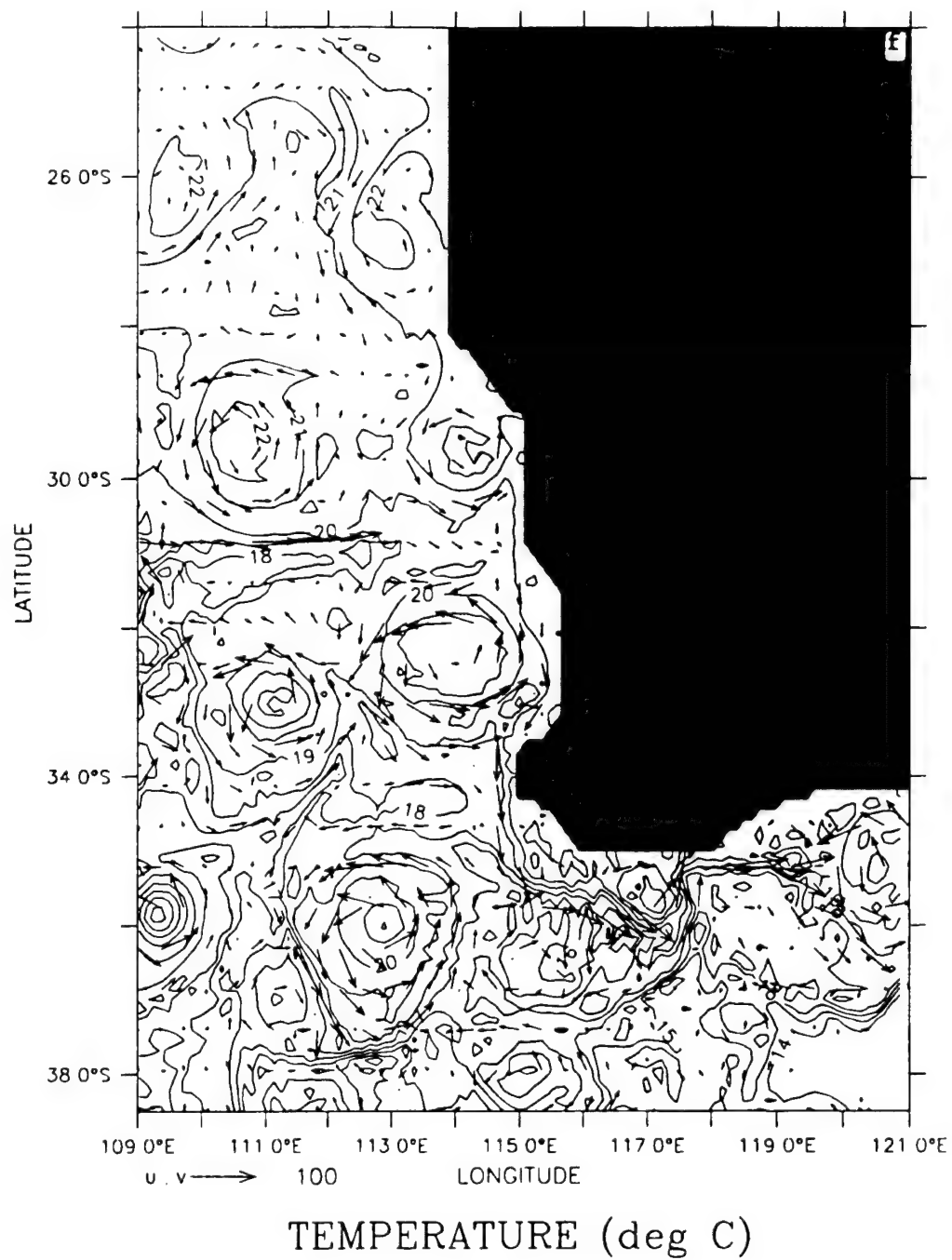
DATA SET: case1



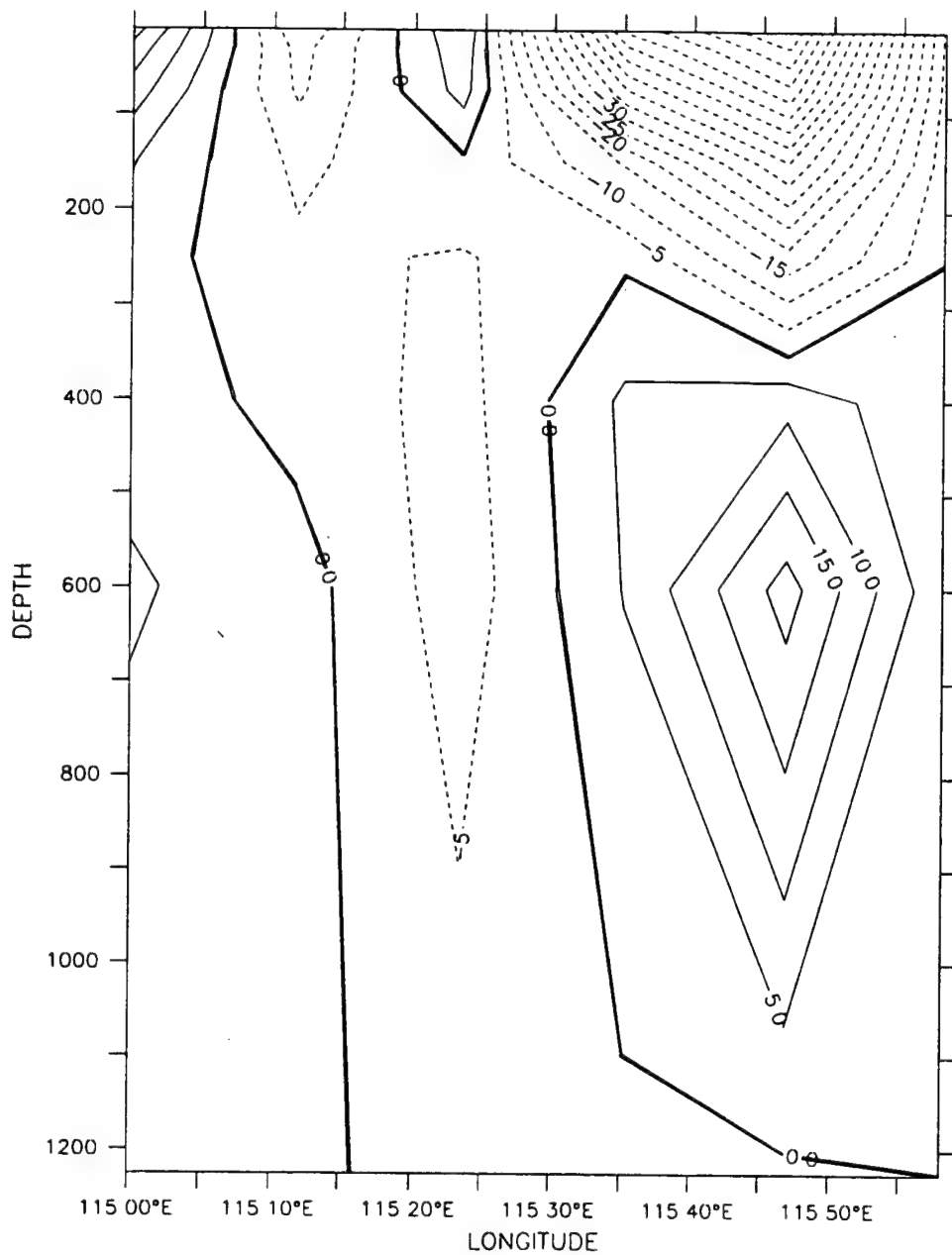


DEPTH 10m  
T 360

DATA SET: case1



LATITUDE : 31.9S  
T : 60



MERID VELOCITY (cm/sec)

**Figure 6.** Cross-shore section of meridional velocity ( $v$ ) at  $\sim 32^\circ$  S (near Freemantle) on day 60 of Experiment 1. The contour interval is 5.0 cm/s. Poleward flow is negative (dashed line) and equatorward flow is positive (solid line).

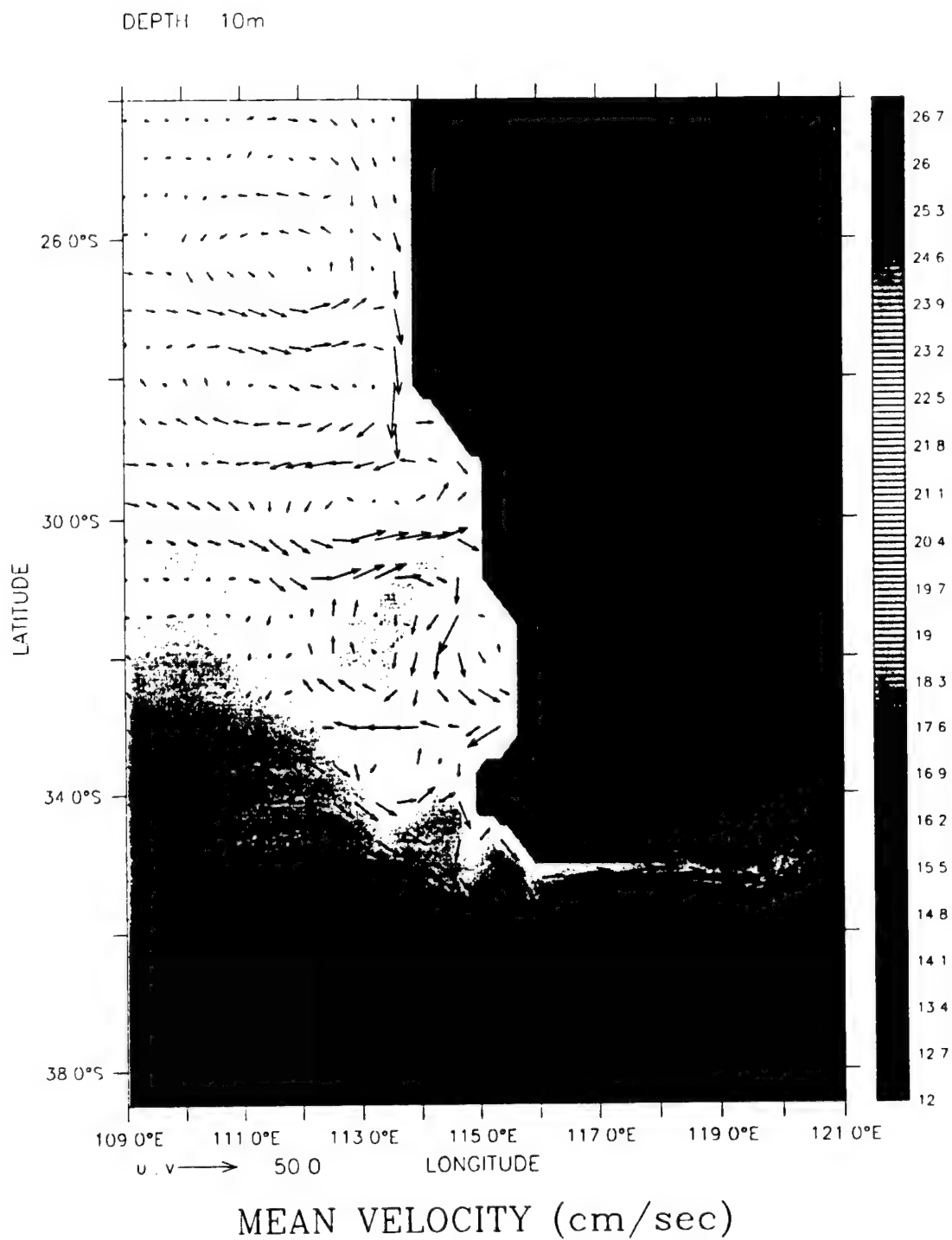


**Figure 7.** Mean temperature and velocity vectors at 10 m depth averaged for days 90 to 270 of Experiment 1. Contour interval is  $0.1^{\circ}\text{C}$  with colder waters in the south end of model domain; maximum velocity vector is 50 cm/s.

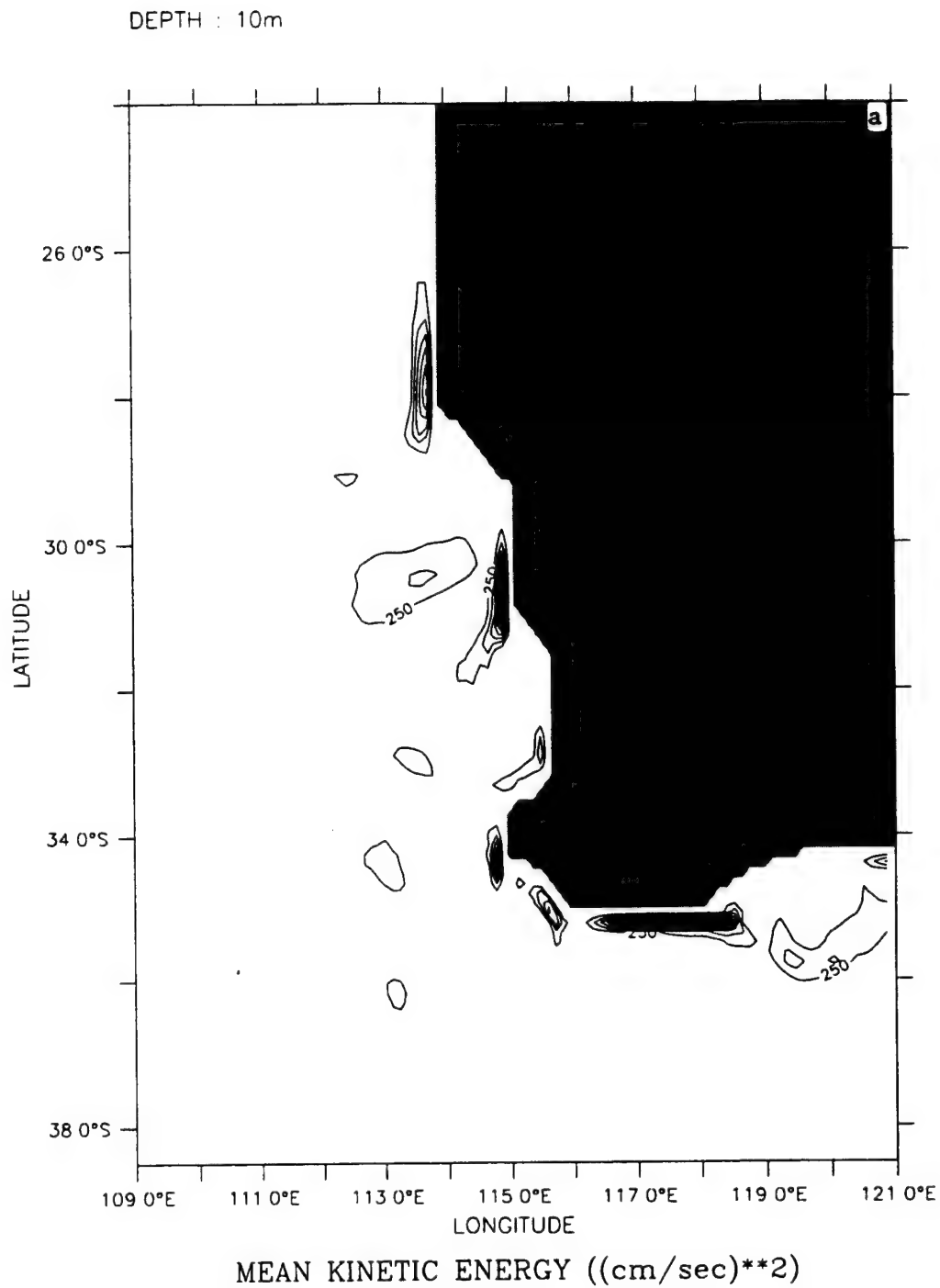
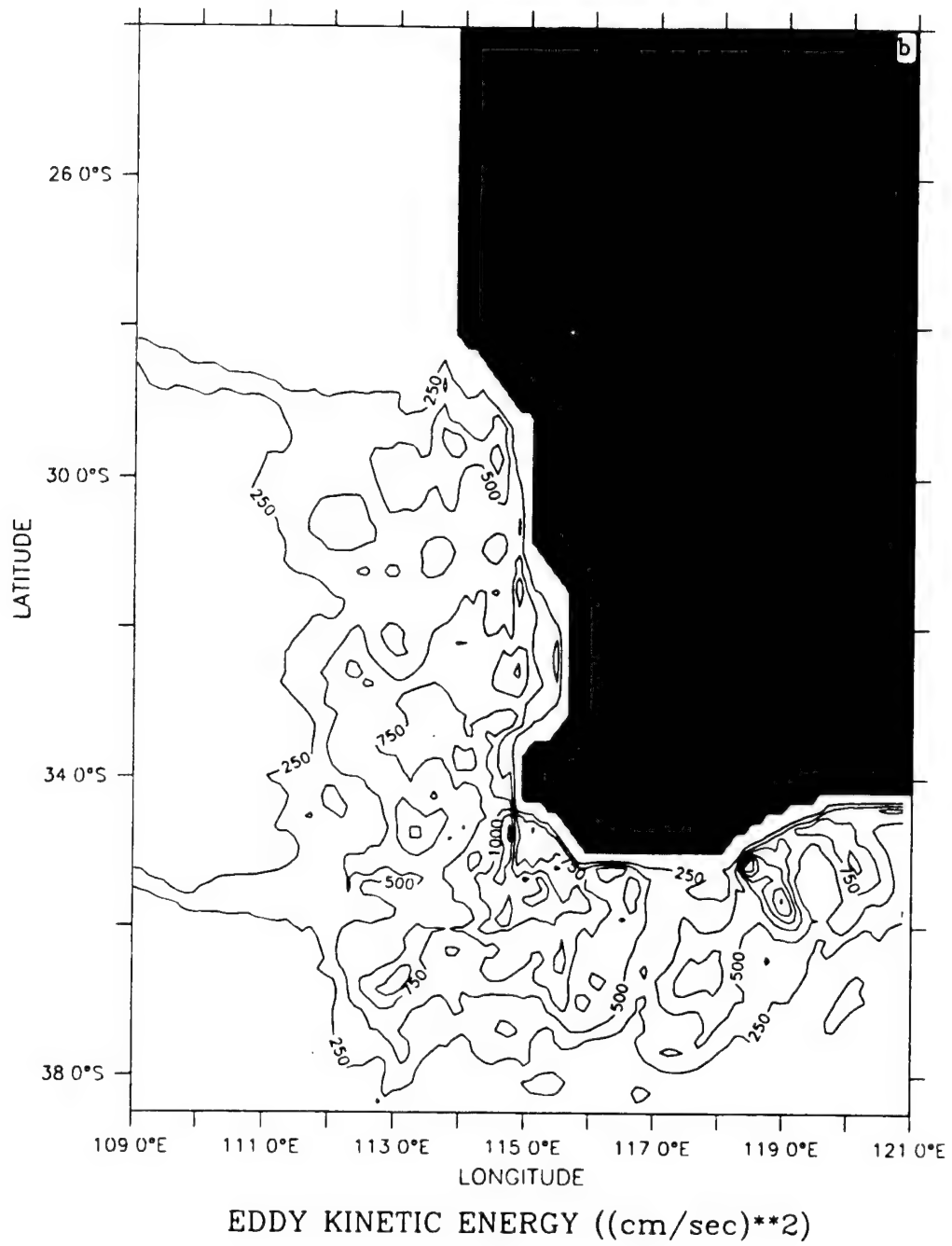


**Figure 8.** Horizontal maps at 10 m depth of (a) mean kinetic energy (MKE) and (b) eddy kinetic energy (EKE) averaged for days 90 to 270 of Experiment 1. Contour interval is 250 cm<sup>2</sup>/s<sup>2</sup>.

DEPTH : 10m



DEPTH : 10m  
T : 90

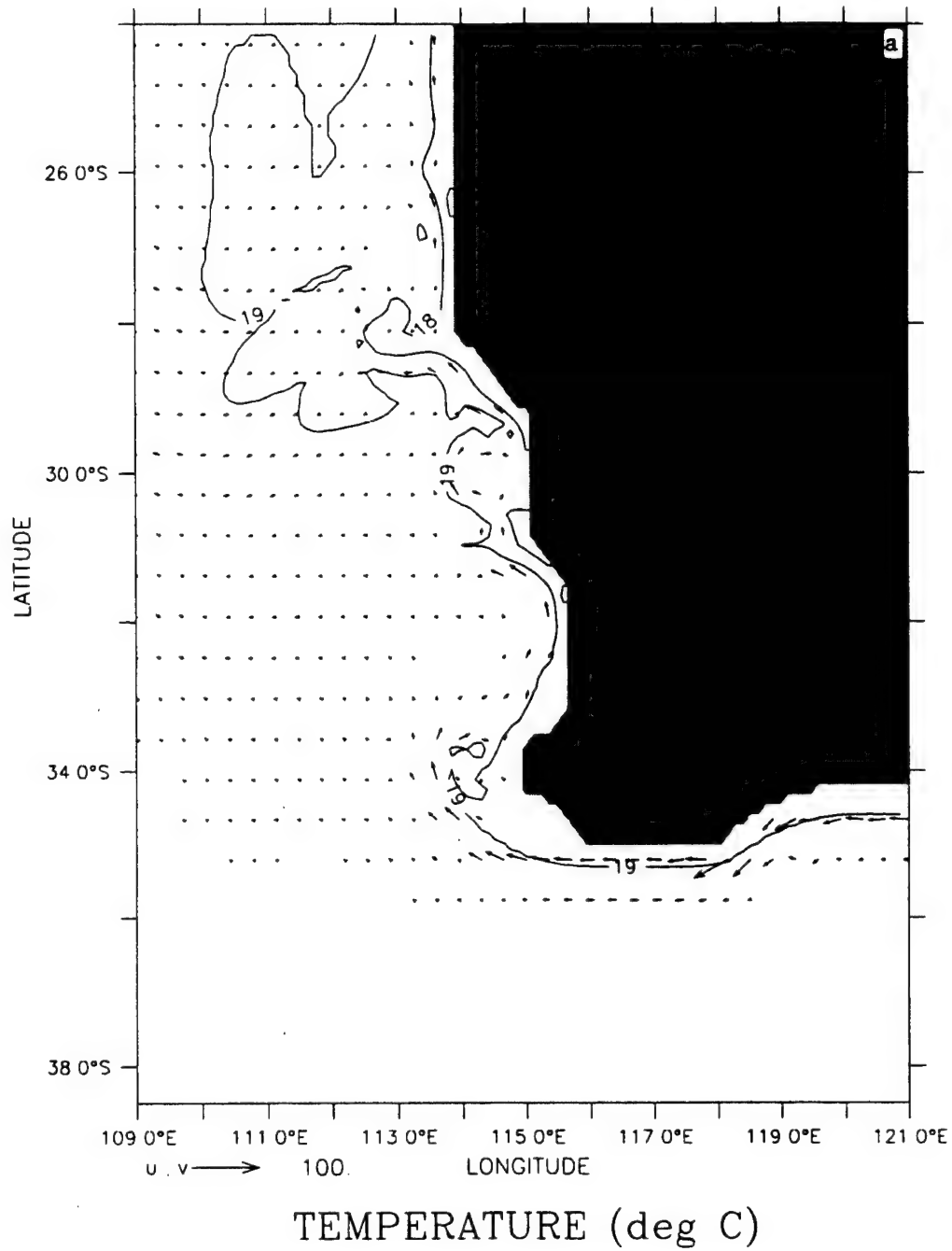
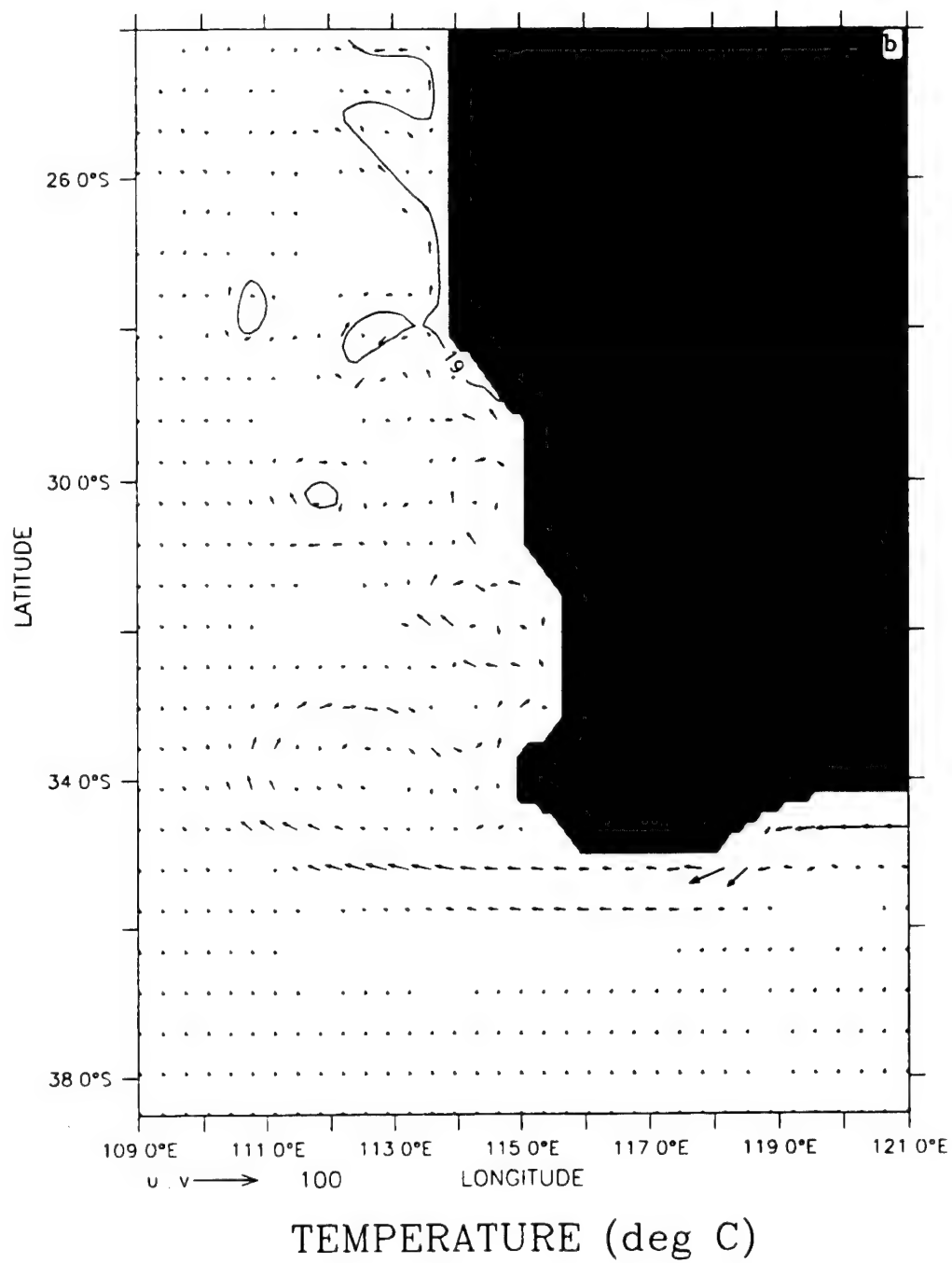
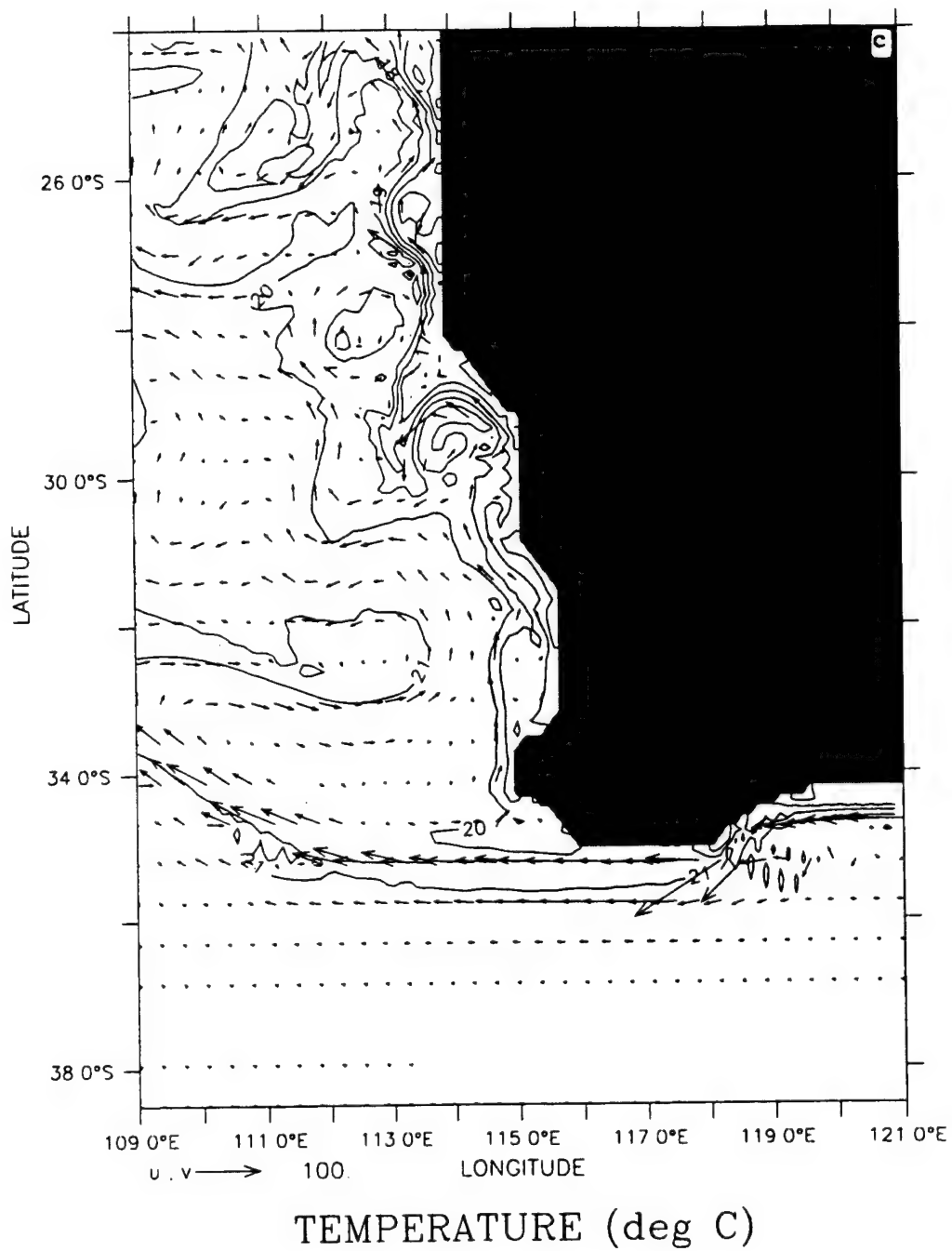


**Figure 9.** Temperature contours and velocity vectors at 10 m depth at days (a) 90, (b) 180, and (c) 360 of Experiment 2. Contour interval is 1°C; maximum velocity vector is 100 cm/s.

DEPTH 10m  
T 180

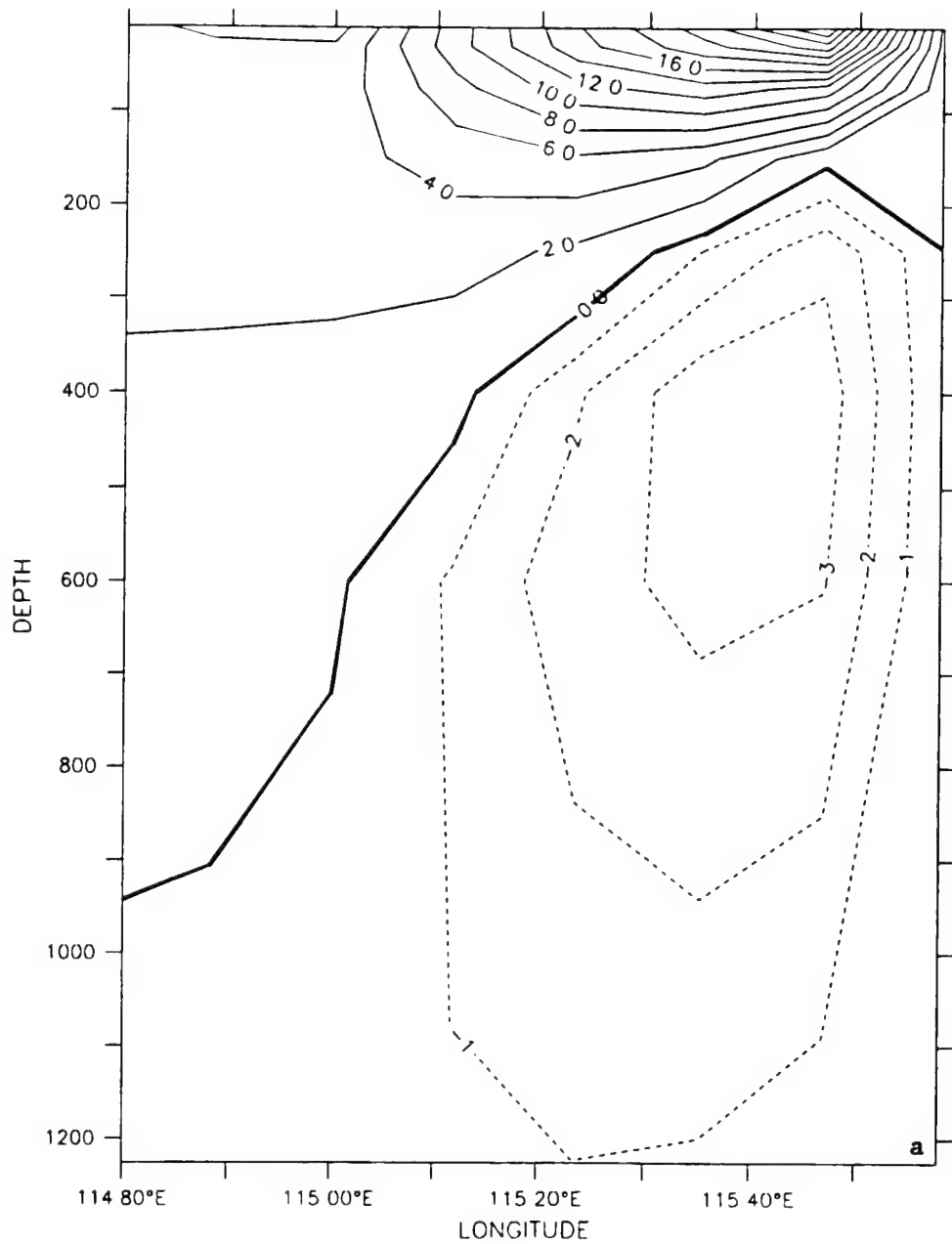


DEPTH : 10m  
T : 360





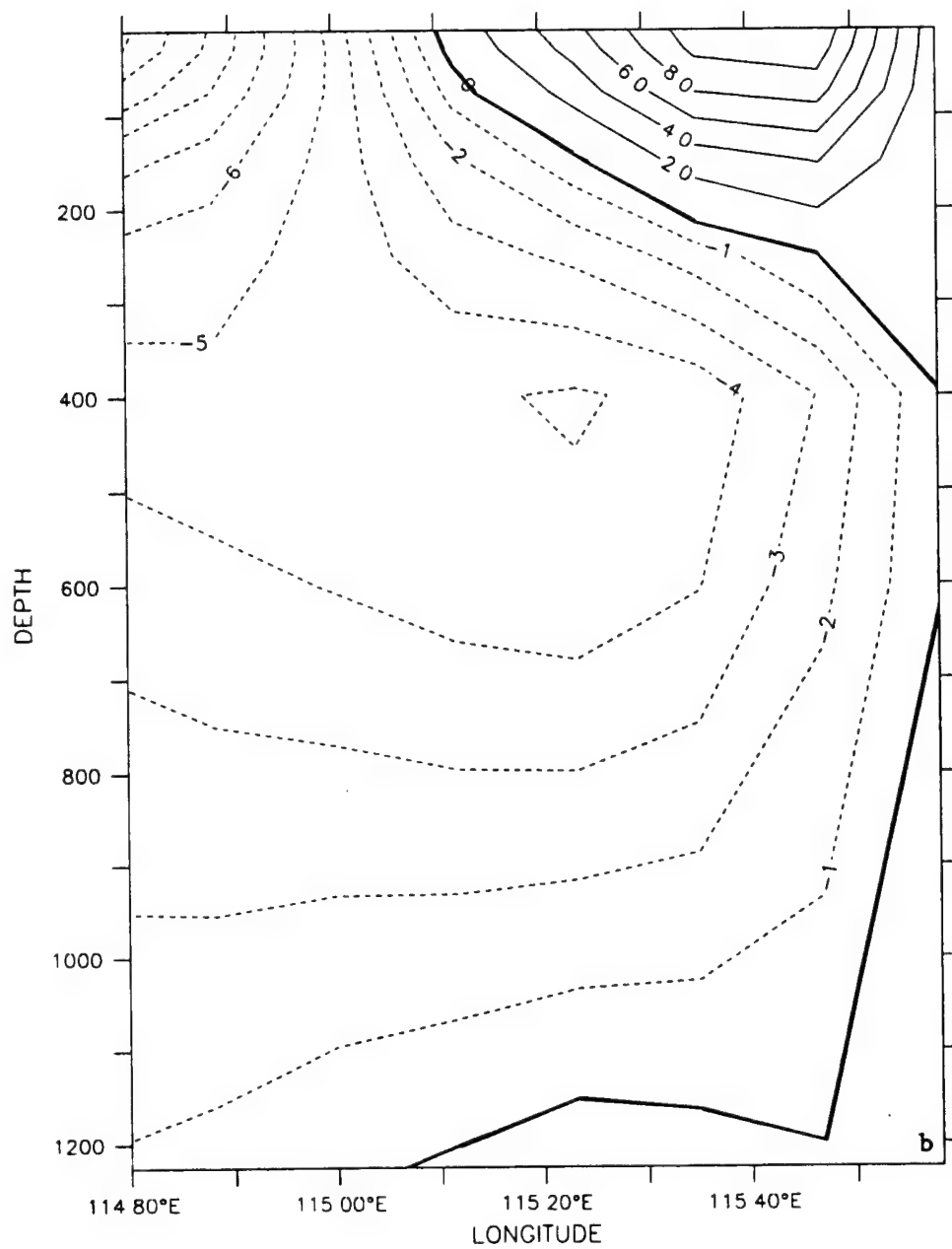
LATITUDE . 31.9S  
T = 90



MERID VELOCITY (cm/sec)

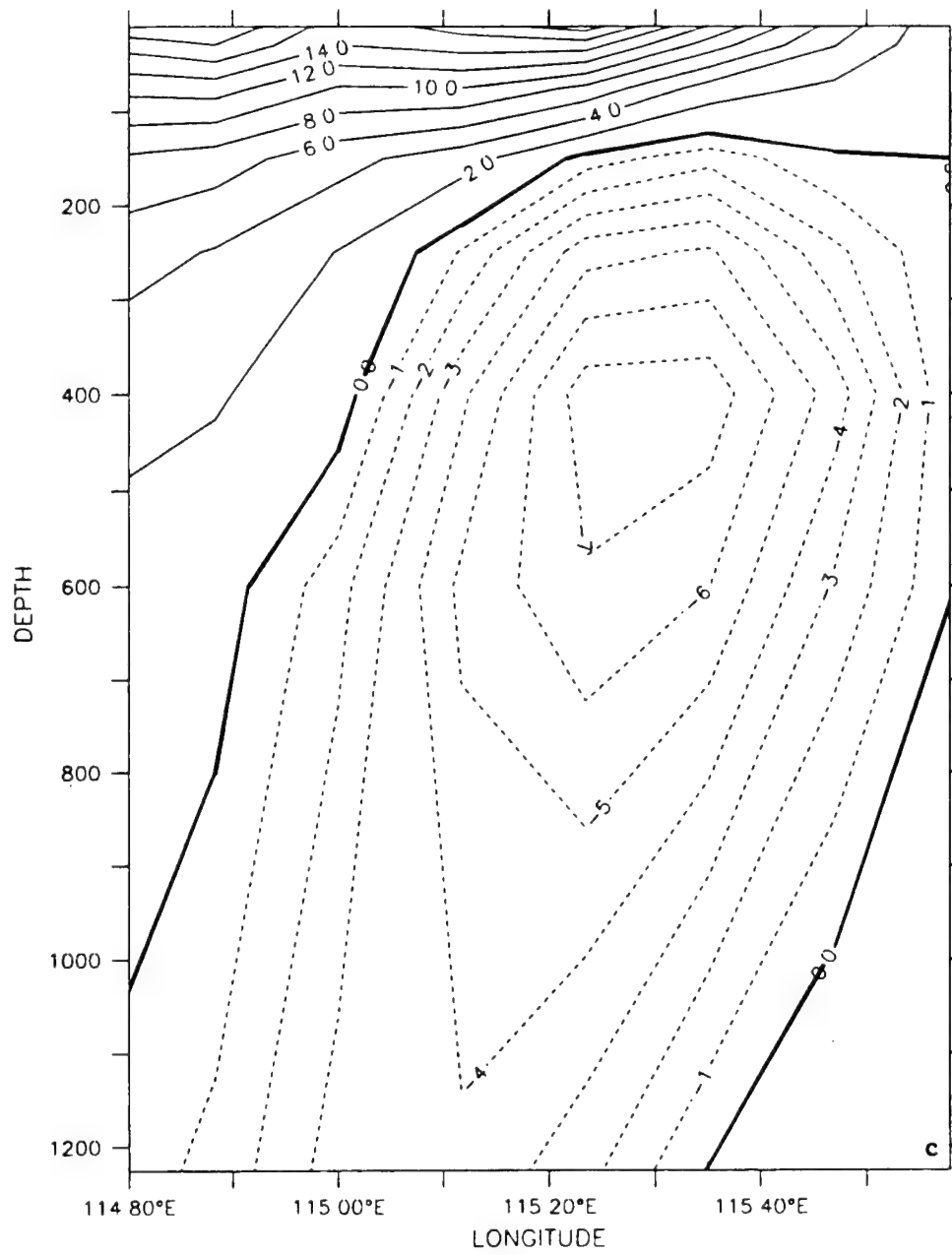
**Figure 10.** Cross-shore section of meridional velocity ( $v$ ) at  $\sim 32^\circ$  S (near Fremantle) on days (a) 90, (b) 180, and (c) 360 of Experiment 2. The contour interval is 1.0 cm/s for poleward (dashed line) flow and 2.0 cm/s for equatorward (solid line) flow.

LATITUDE : 31.9S  
T : 180



MERID VELOCITY (cm/sec)

LATITUDE : 31.9S  
T : 360



MERID VELOCITY (cm/sec)

LATITUDE : 31.9S  
T : 90

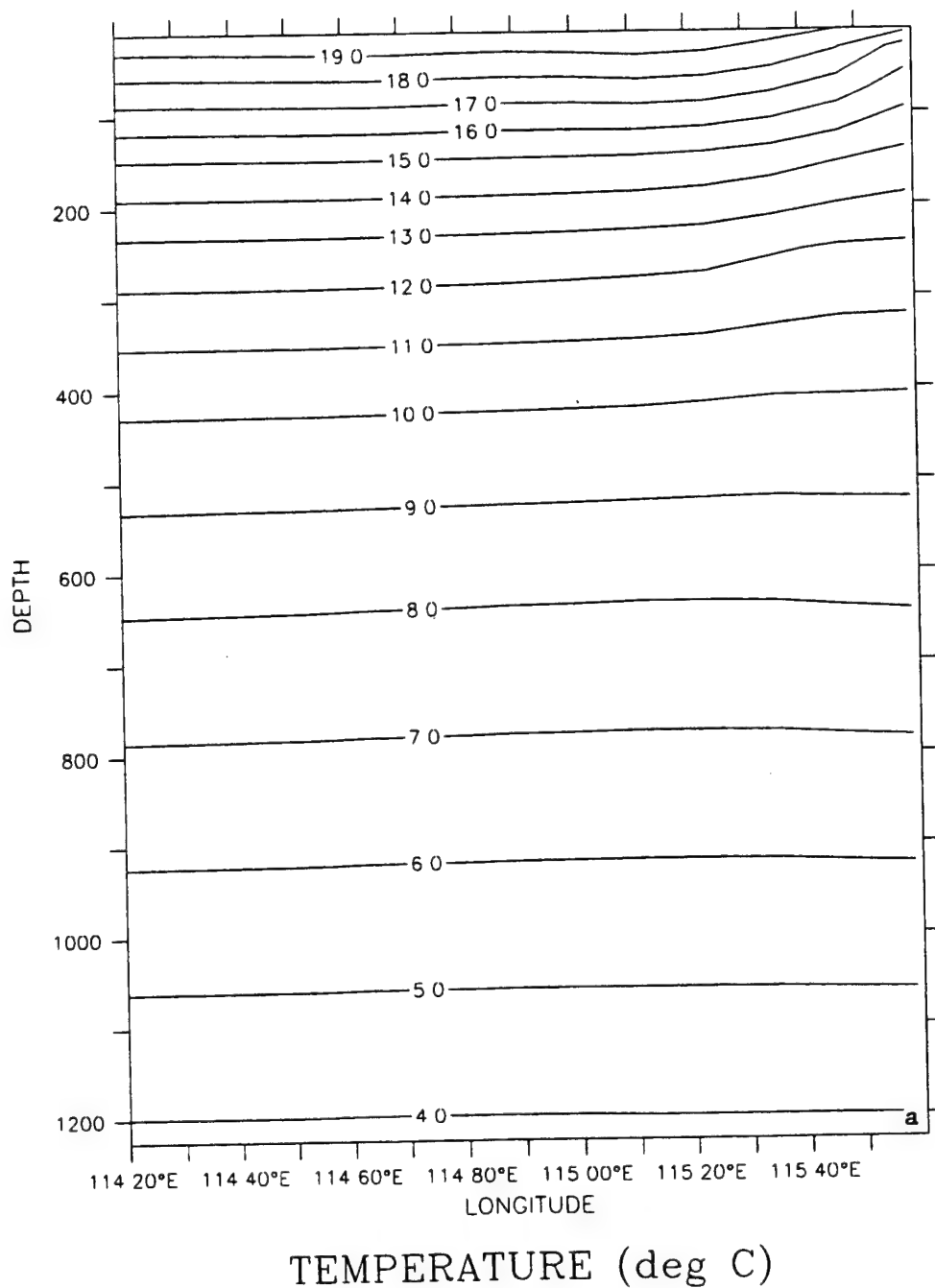
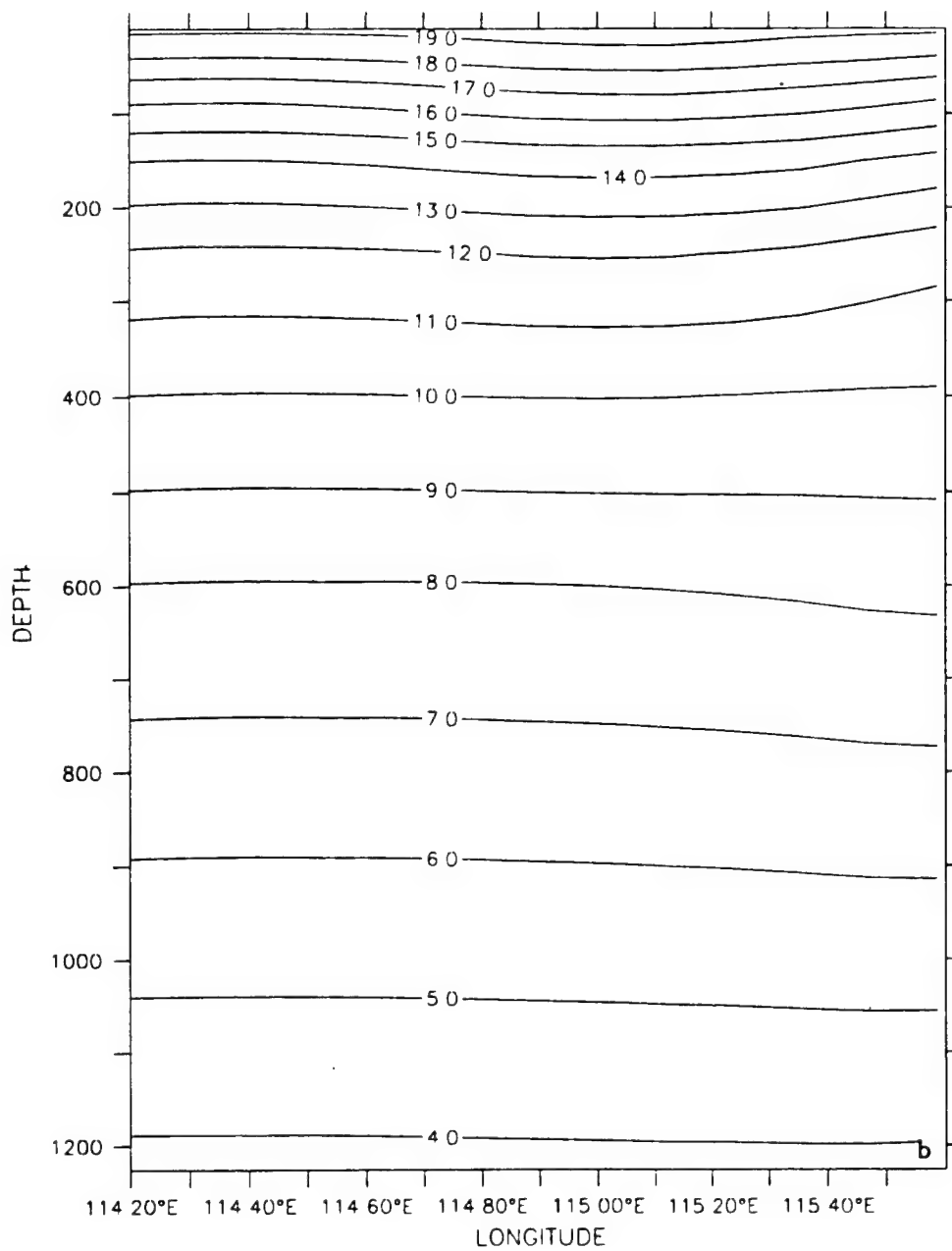


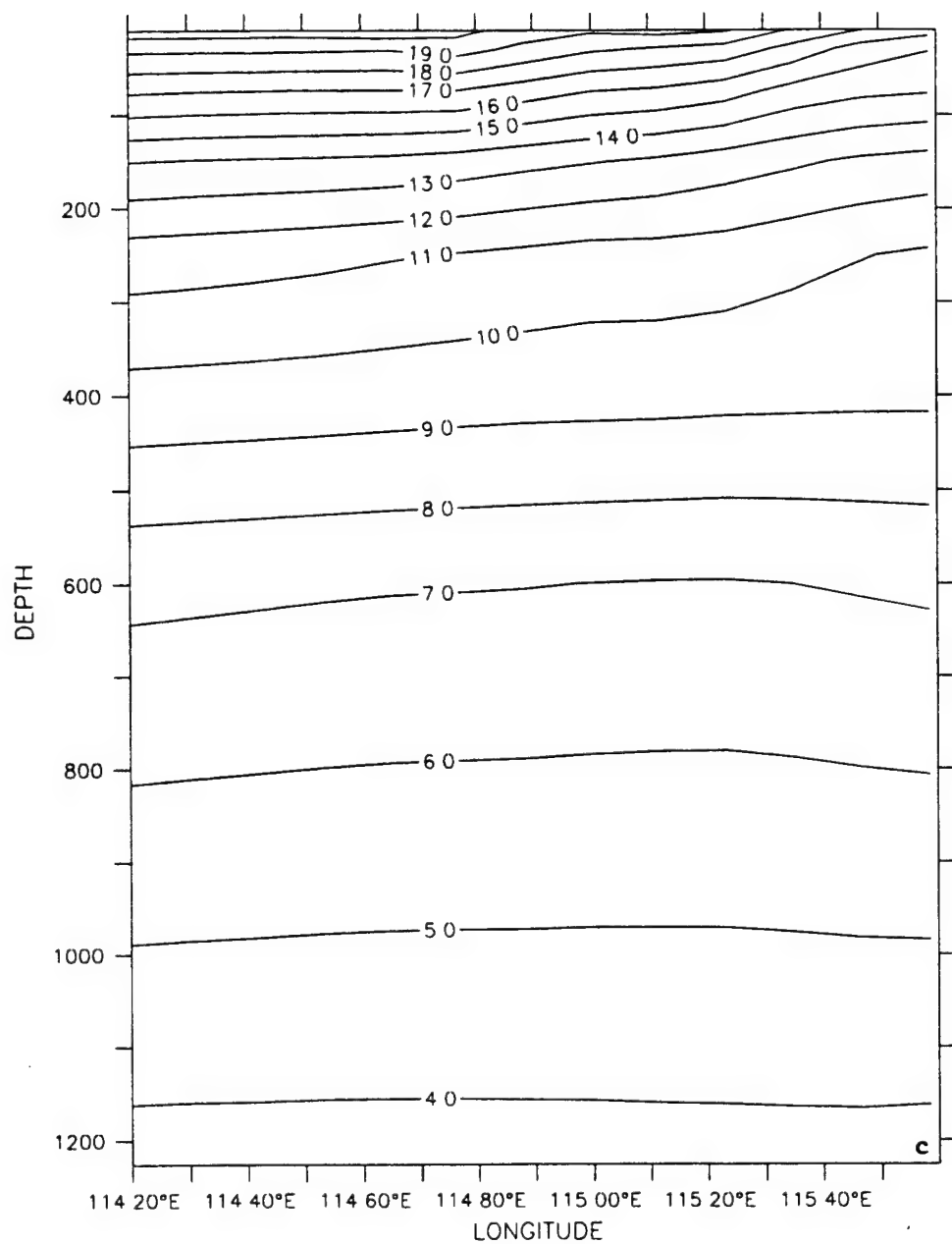
**Figure 11.** Cross-shore sections of temperature at ~ 32°S (near Freemantle) at days (a) 90, (b) 180, (c) 360 of Experiment 2. Contour interval is 1°C.

LATITUDE : 31 9S  
T 180

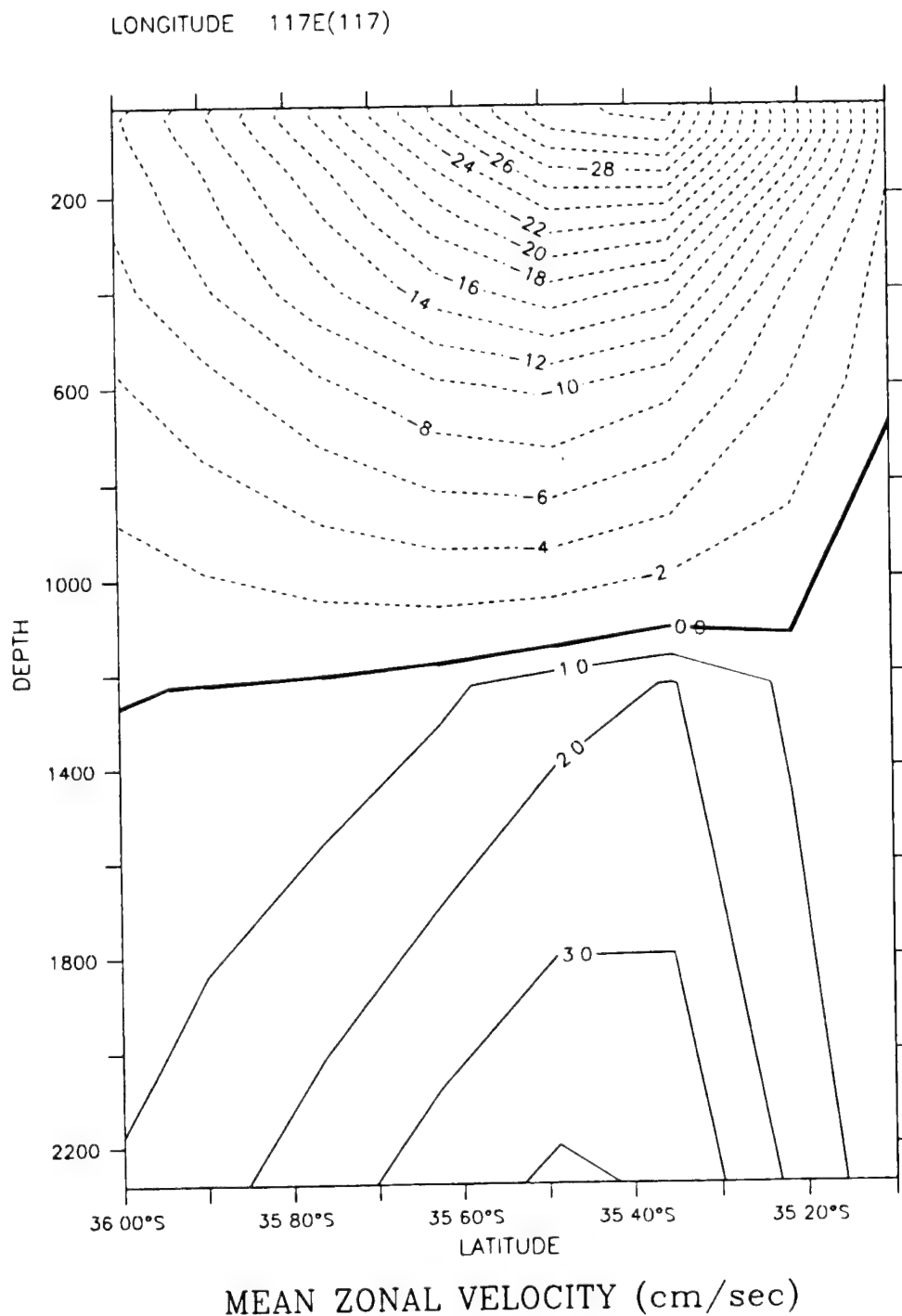


TEMPERATURE (deg C)

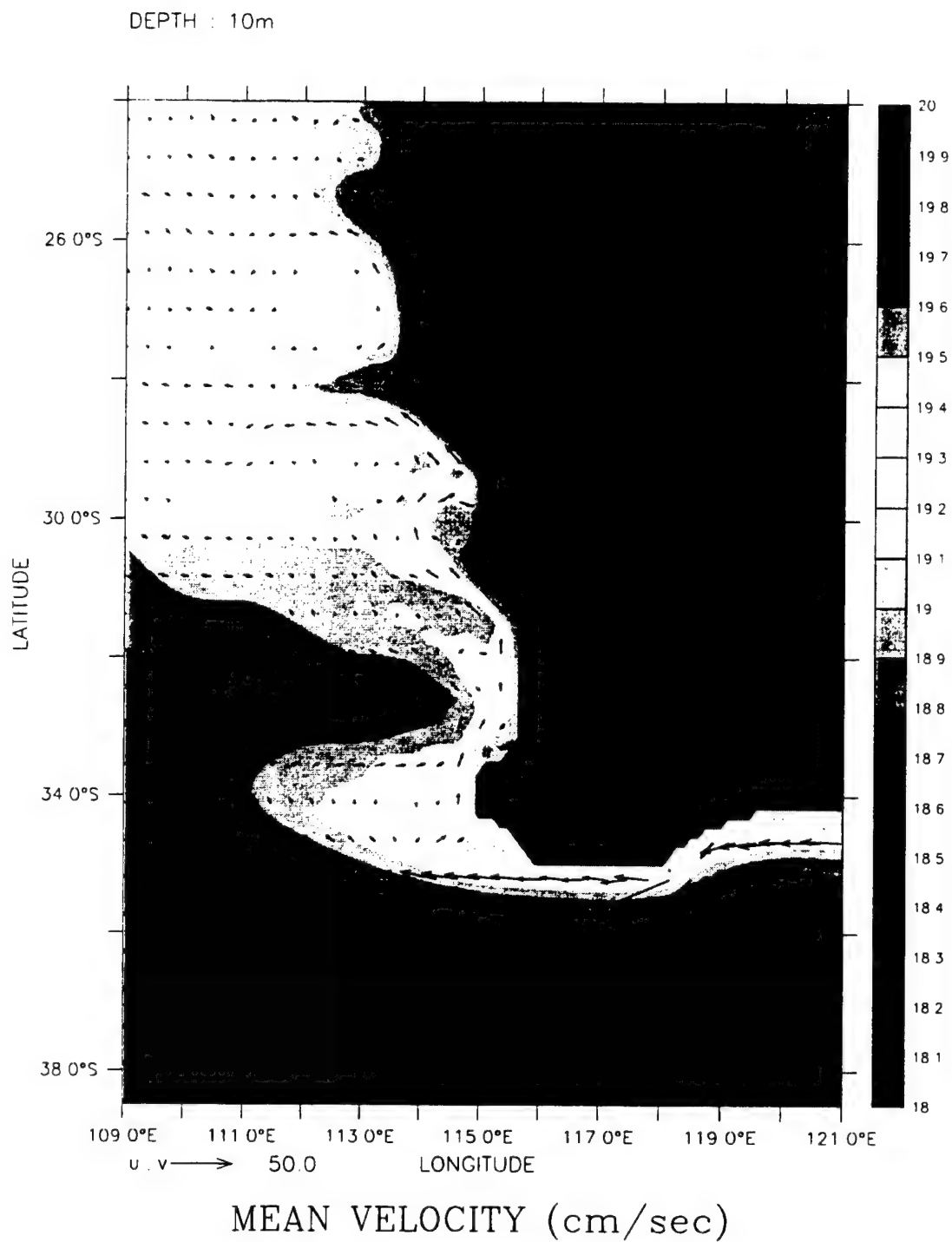
LATITUDE : 31.9S  
T : 360



TEMPERATURE (deg C)

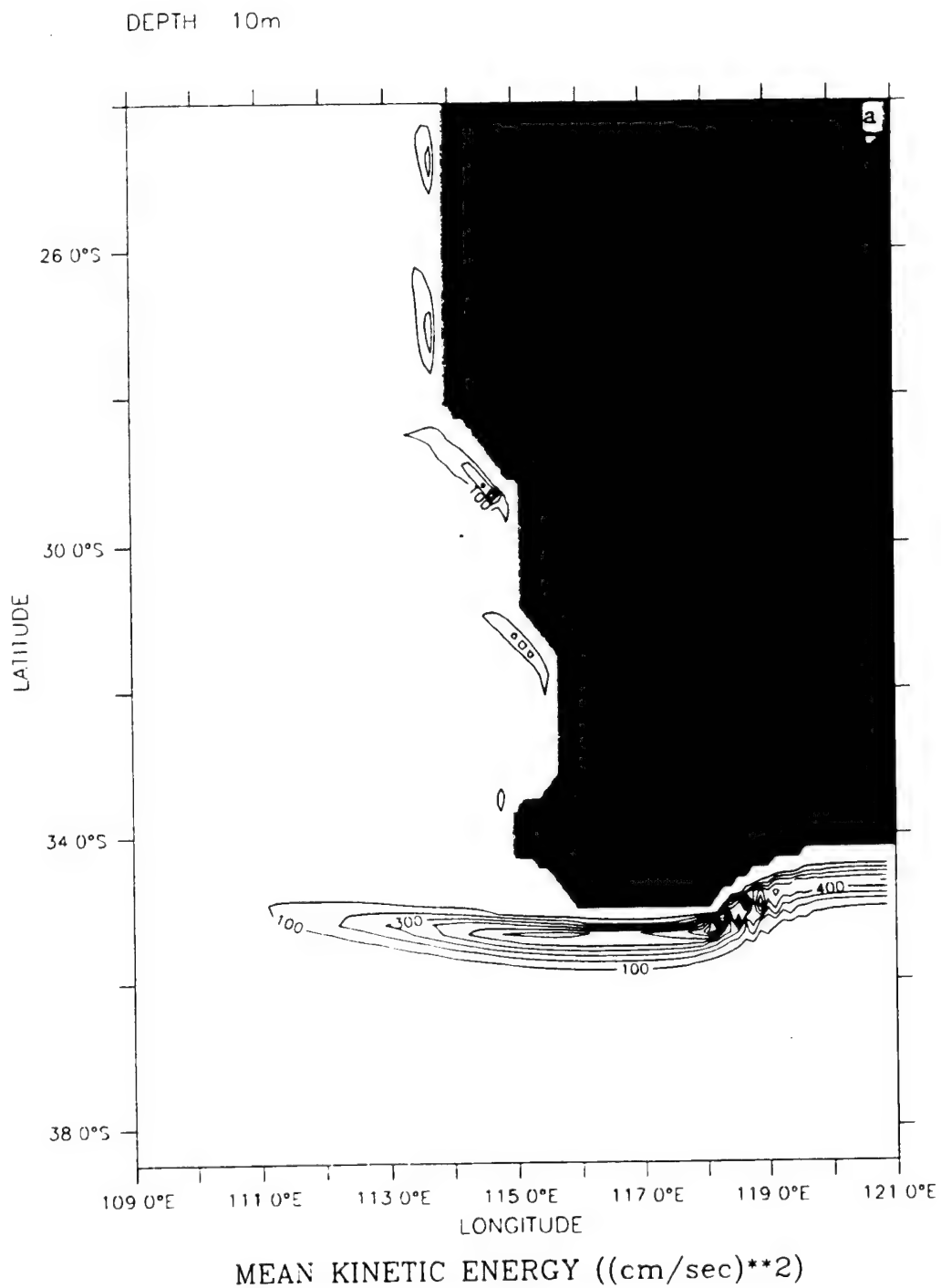


**Figure 12.** Cross-shore section of mean zonal velocity ( $u$ ) at  $\sim 117^\circ$  E averaged for days 90 to 270 of Experiment 2. Contour interval is 1.0 cm/s for eastward (solid line) flow and 2.0 cm/s for westward (dashed line) flow.



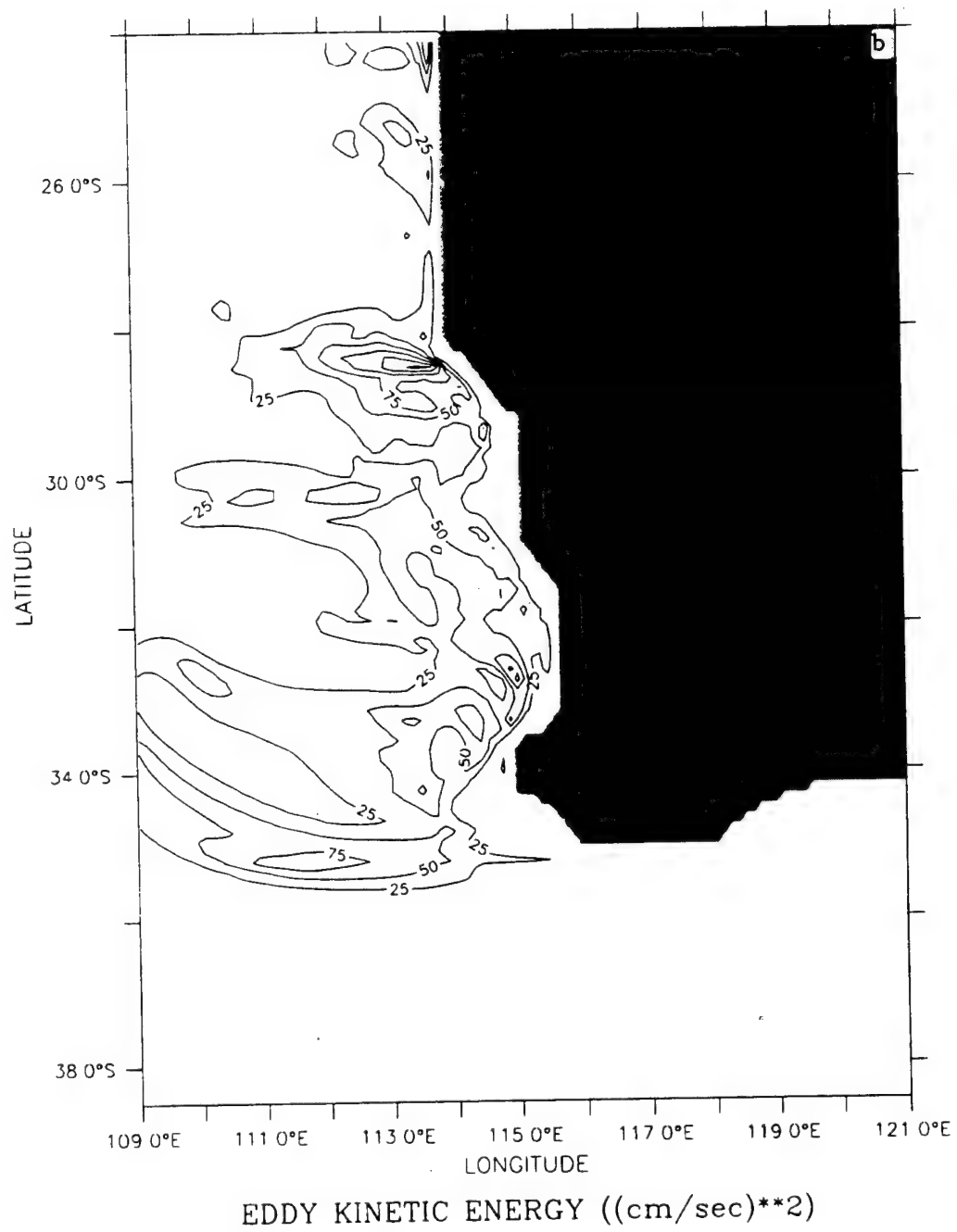
**Figure 13.** Mean temperature and velocity vectors at 10 m depth averaged for days 90 to 270 of Experiment 2. Contour interval is 0.1°C with colder waters in the coastal region of model domain; maximum velocity vector is 50 cm/s





**Figure 14.** Horizontal maps at 10 m depth of (a) mean kinetic energy (MKE) and (b) eddy kinetic energy (EKE) averaged for days 90 to 270 of Experiment 2. Contour interval is  $100 \text{ cm}^2/\text{s}^2$  in (a) and  $25 \text{ cm}^2/\text{s}^2$  in (b).

DEPTH : 10m



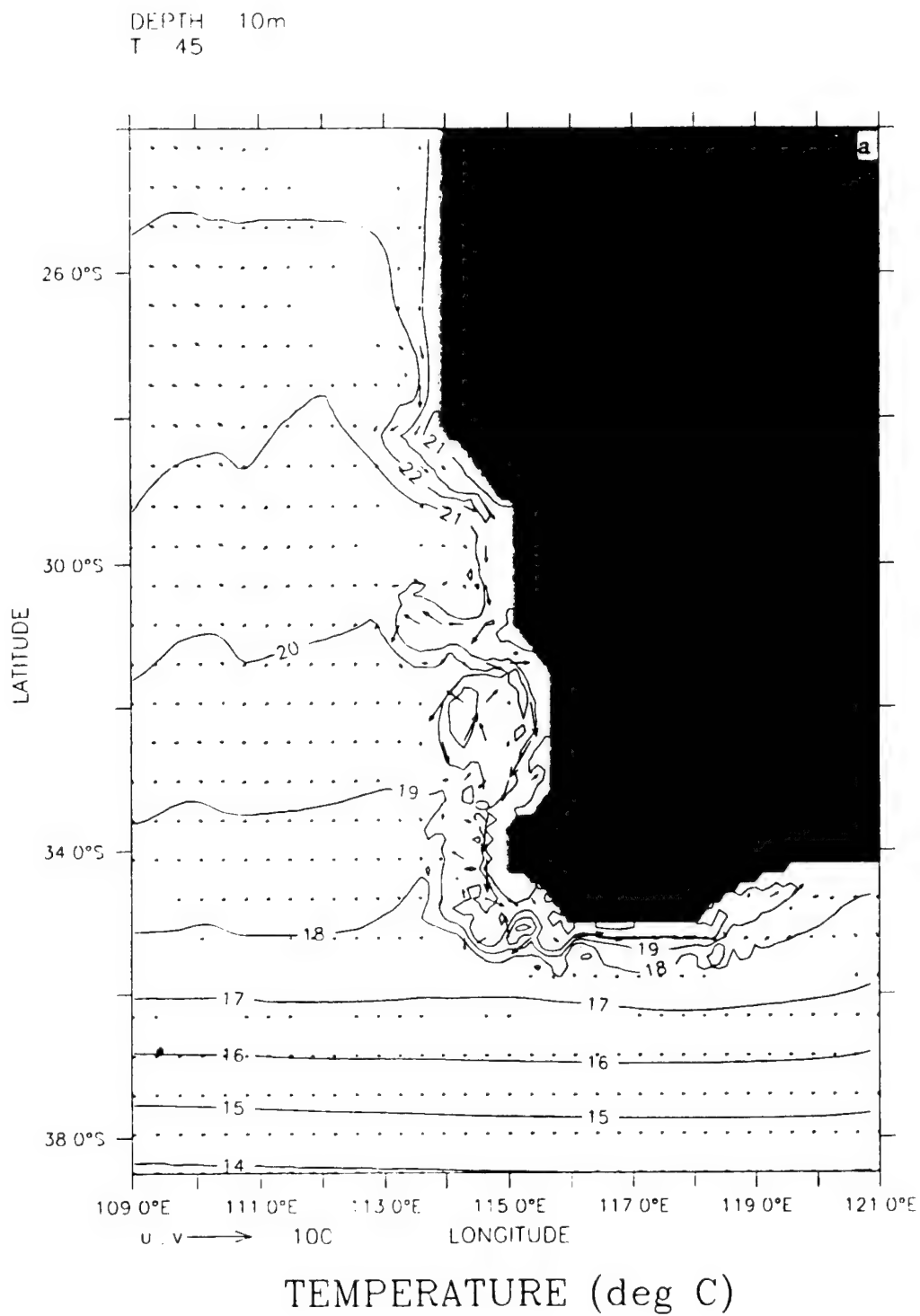
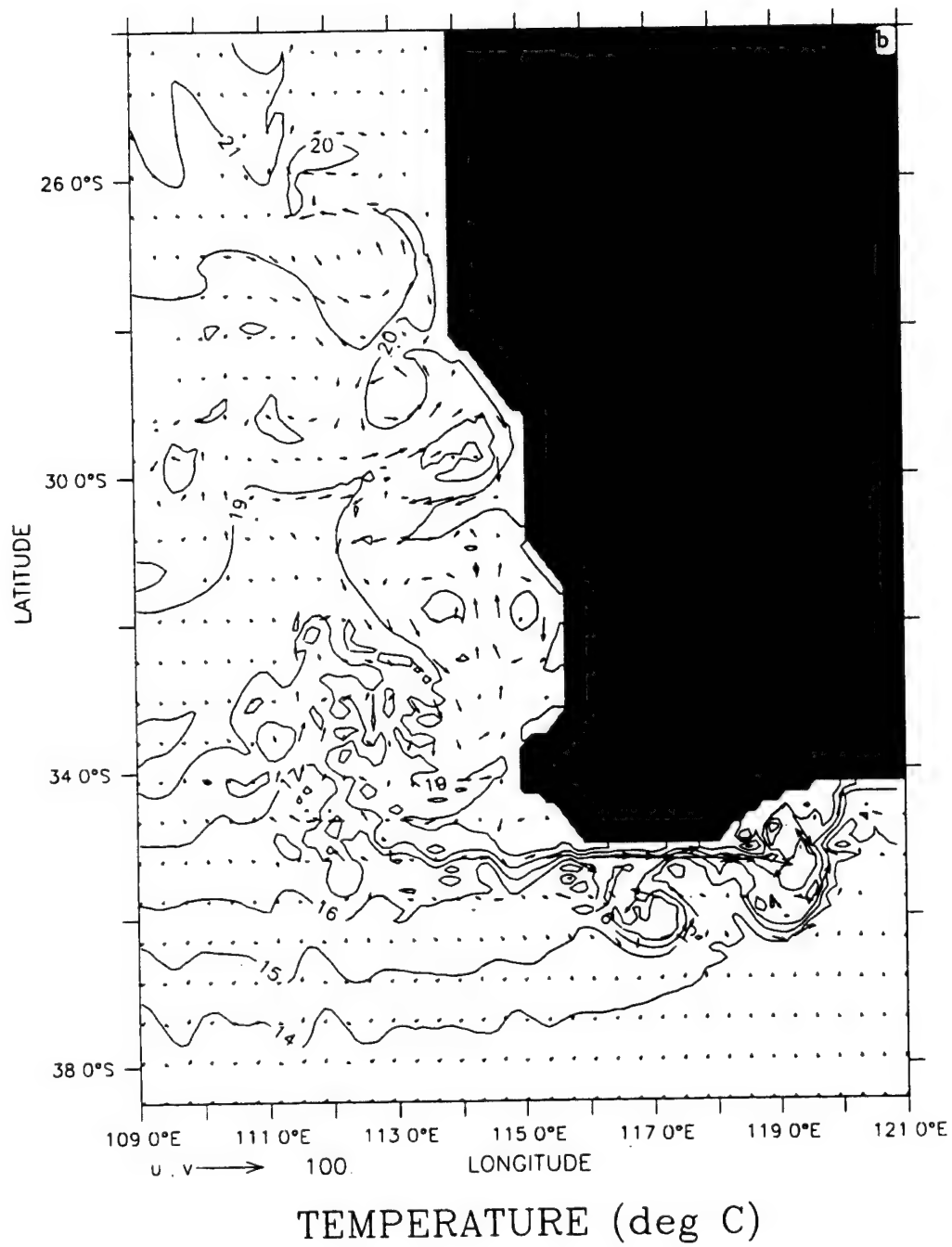
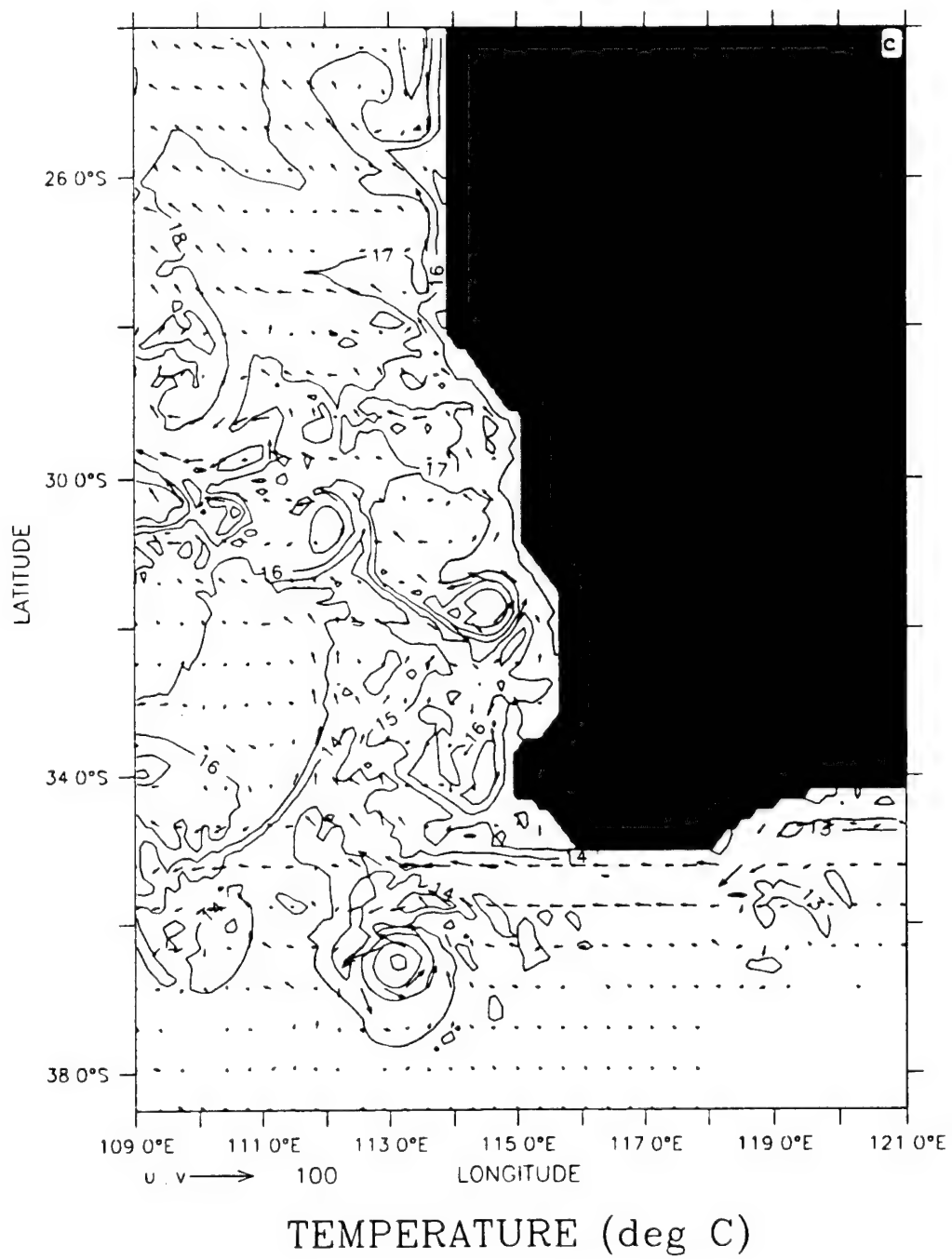


**Figure 15.** Temperature contours and velocity vectors at 10 m depth at days (a) 45, (b) 180, and (c) 360 of Experiment 3. Contour interval is 1°C; maximum velocity vector is 100 cm/s.

DEPTH : 10m  
T : 180



DEPTH 10m  
T 360



LATITUDE : 34S  
T : 180

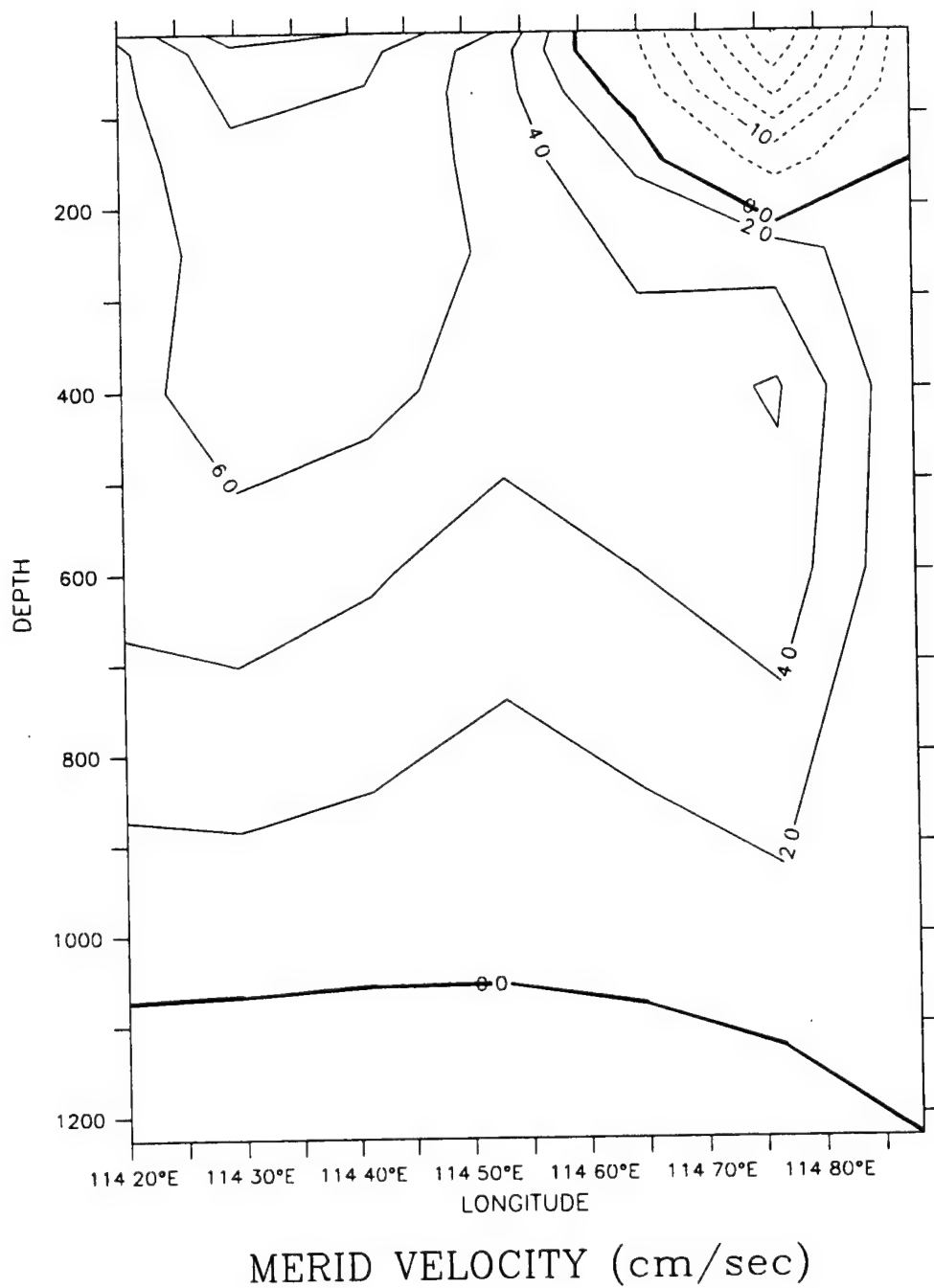


**Figure 16.** Cross-shore section of meridional velocity ( $v$ ) at 34° S (off Cape Leeuwin), for day 180 of Experiment 3. The contour interval is 5.0 cm/s for poleward (dashed line) flow and 2.0 cm/s for equatorward (solid line) flow.

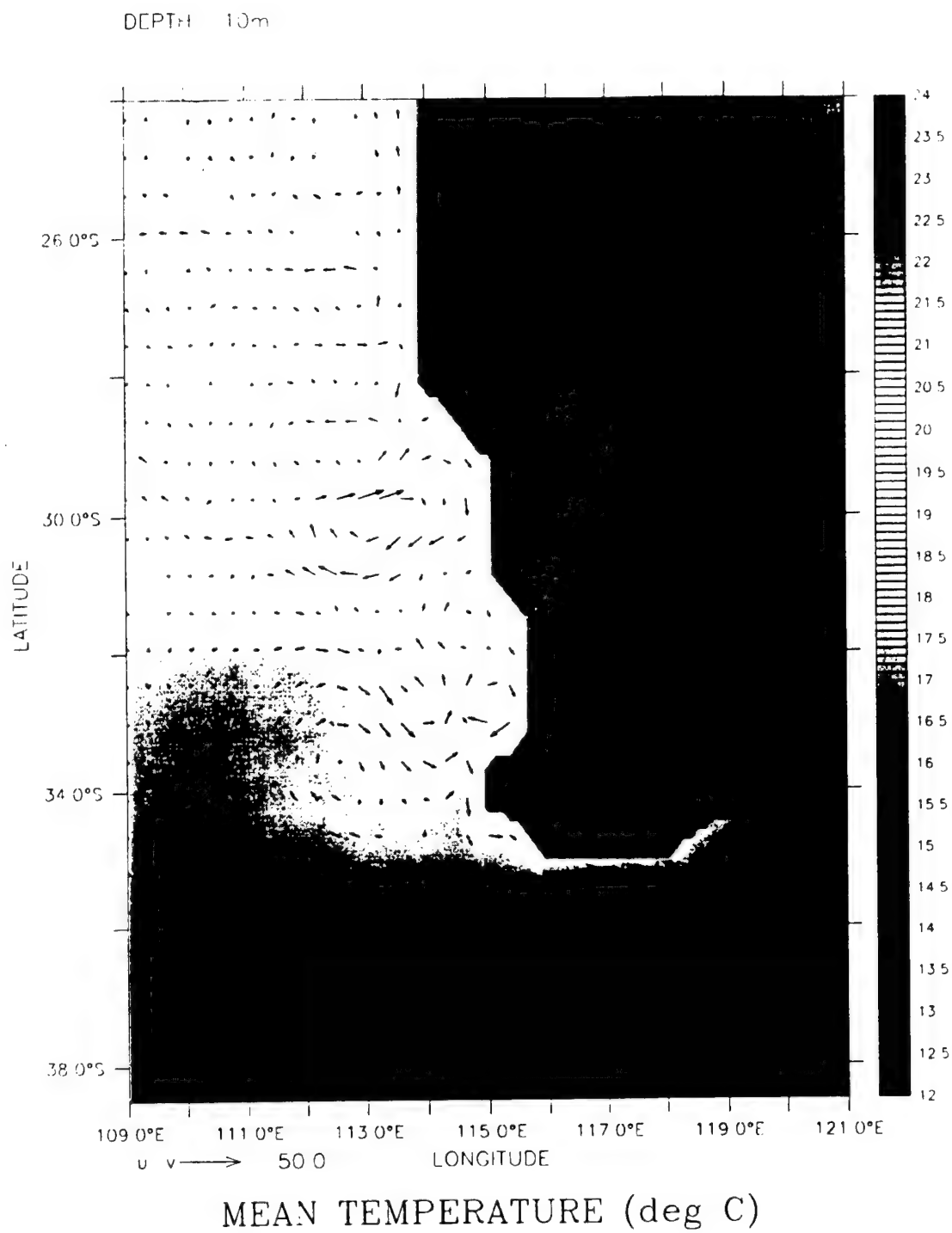


**Figure 17.** Mean temperature and velocity vectors at 10 m depth averaged for days 90 to 270 of Experiment 3. Contour interval is 1°C; maximum velocity vector is 50 cm/s.

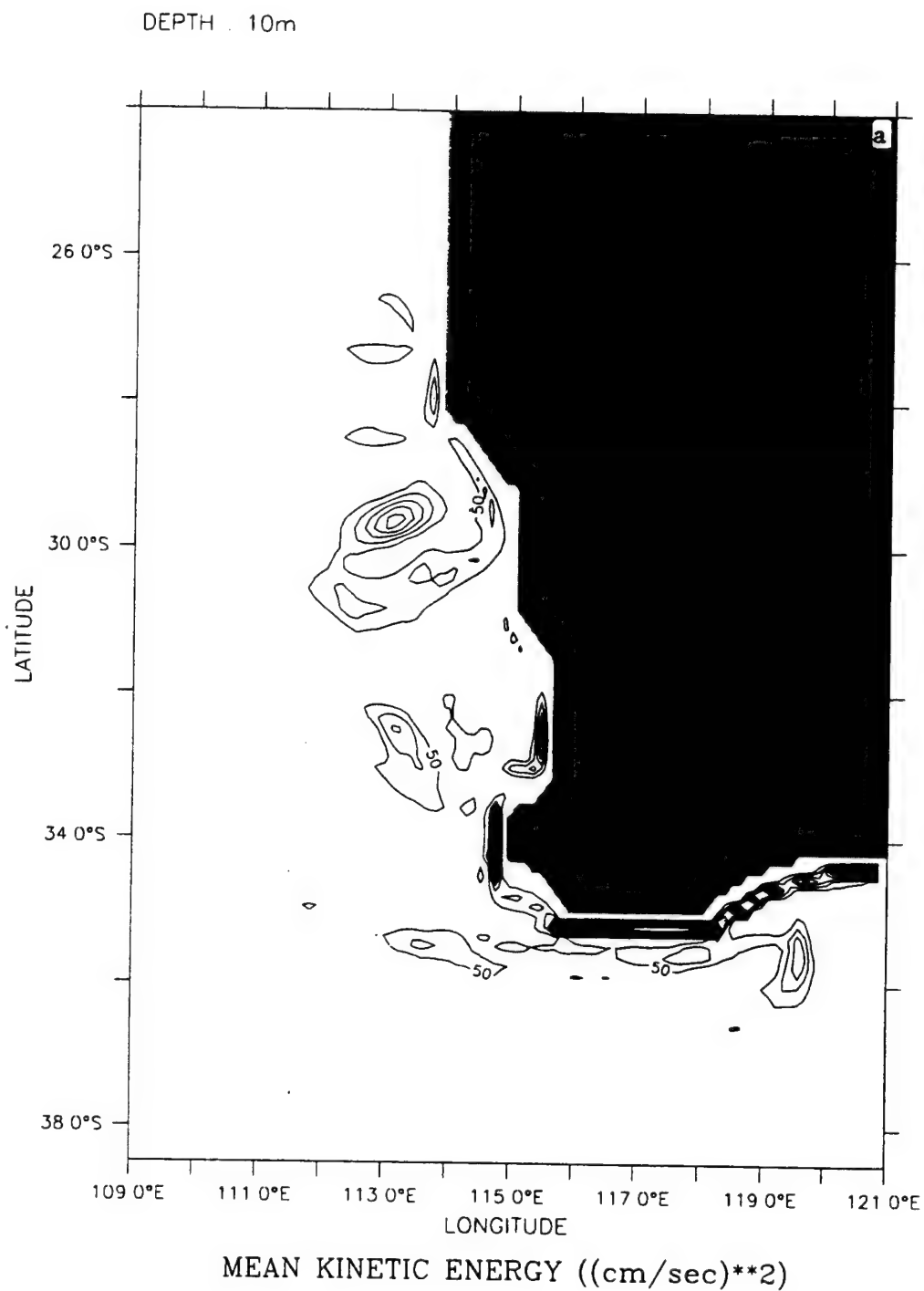
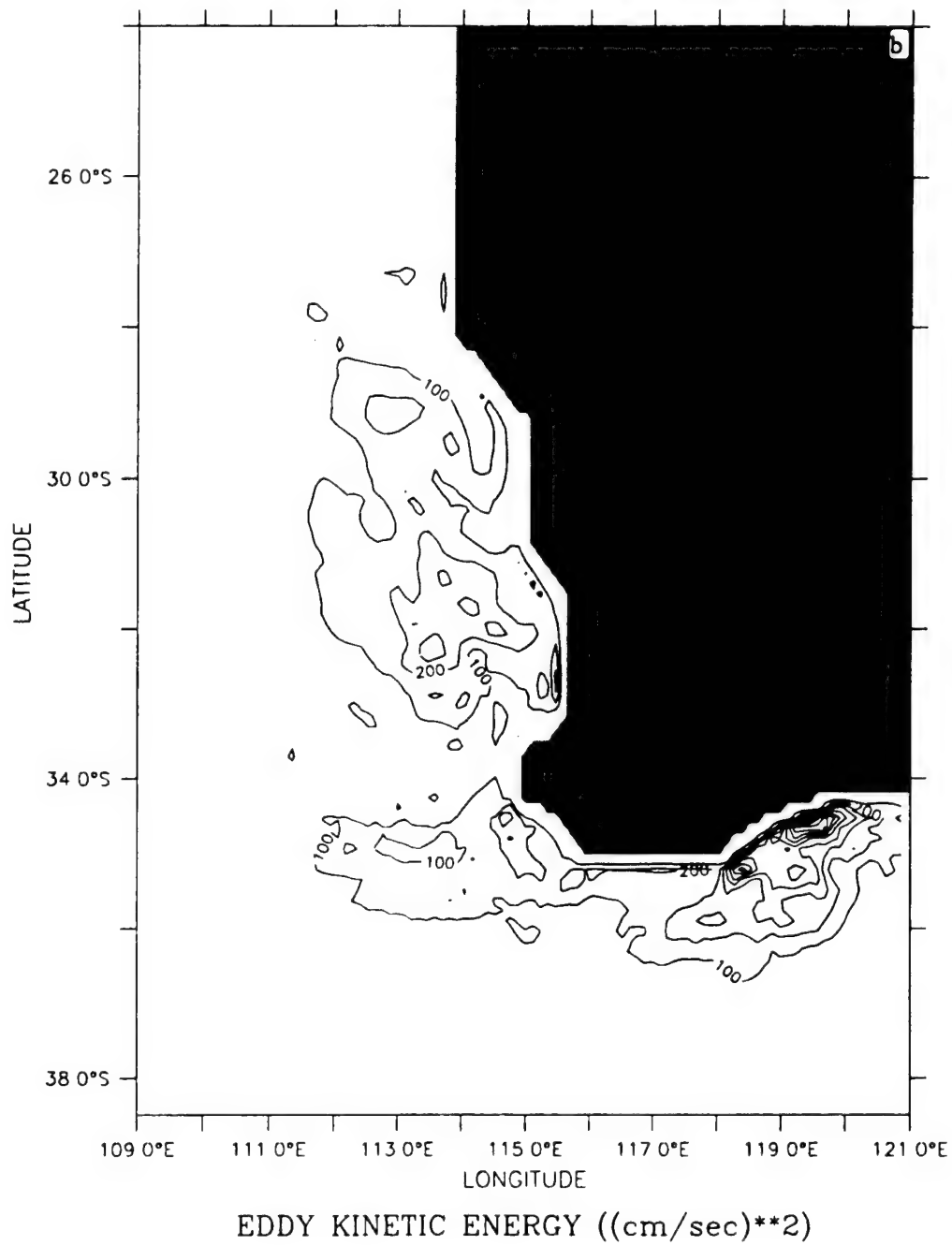


**Figure 18.** Horizontal maps at 10 m depth of (a) mean kinetic energy (MKE) and (b) eddy kinetic energy (EKE) averaged for days 90 to 270 of Experiment 3. Contour interval is  $50 \text{ cm}^2/\text{s}^2$  in (a) and  $100 \text{ cm}^2/\text{s}^2$  in (b).



DEPTH 10m



DEPTH : 10m  
T : 15

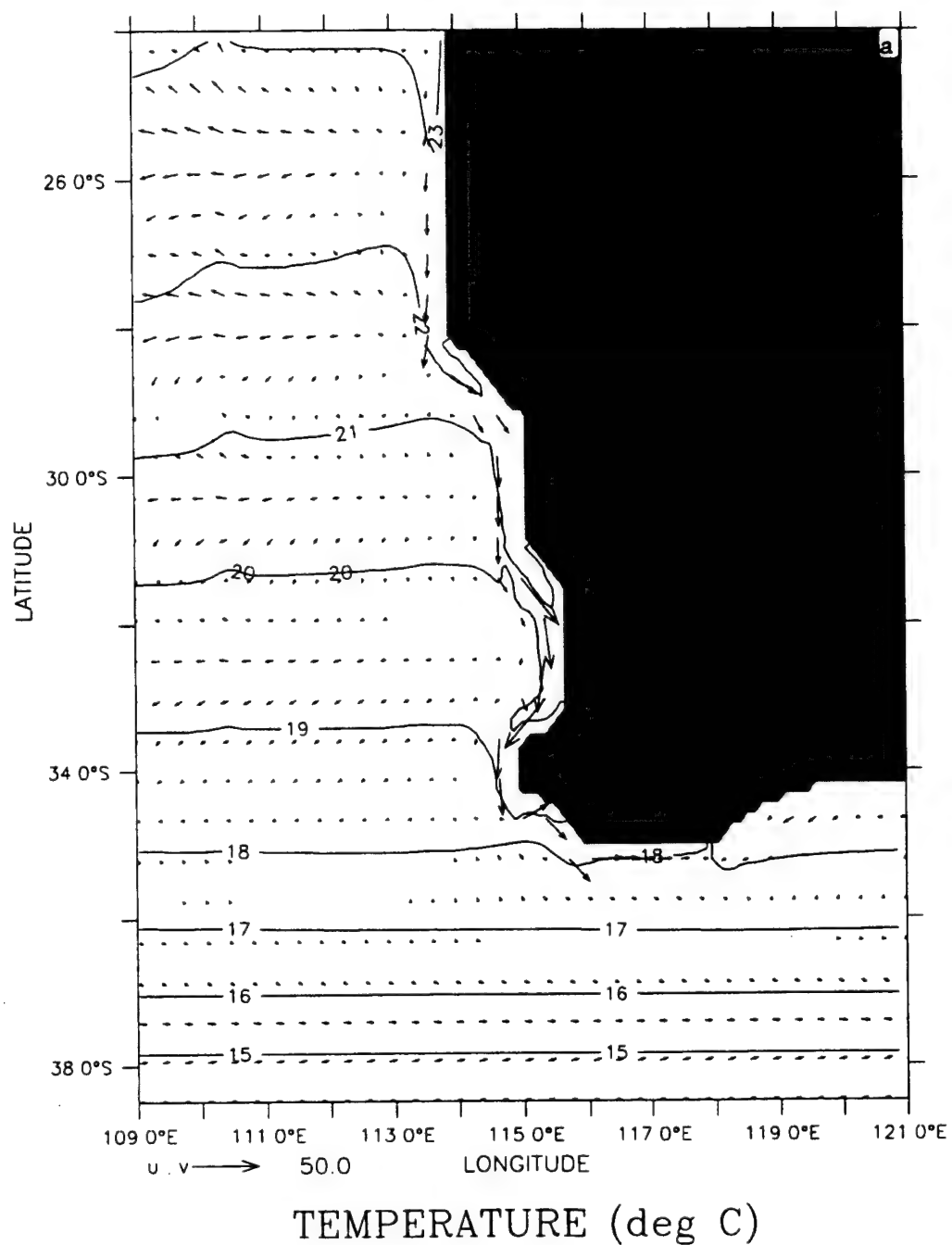
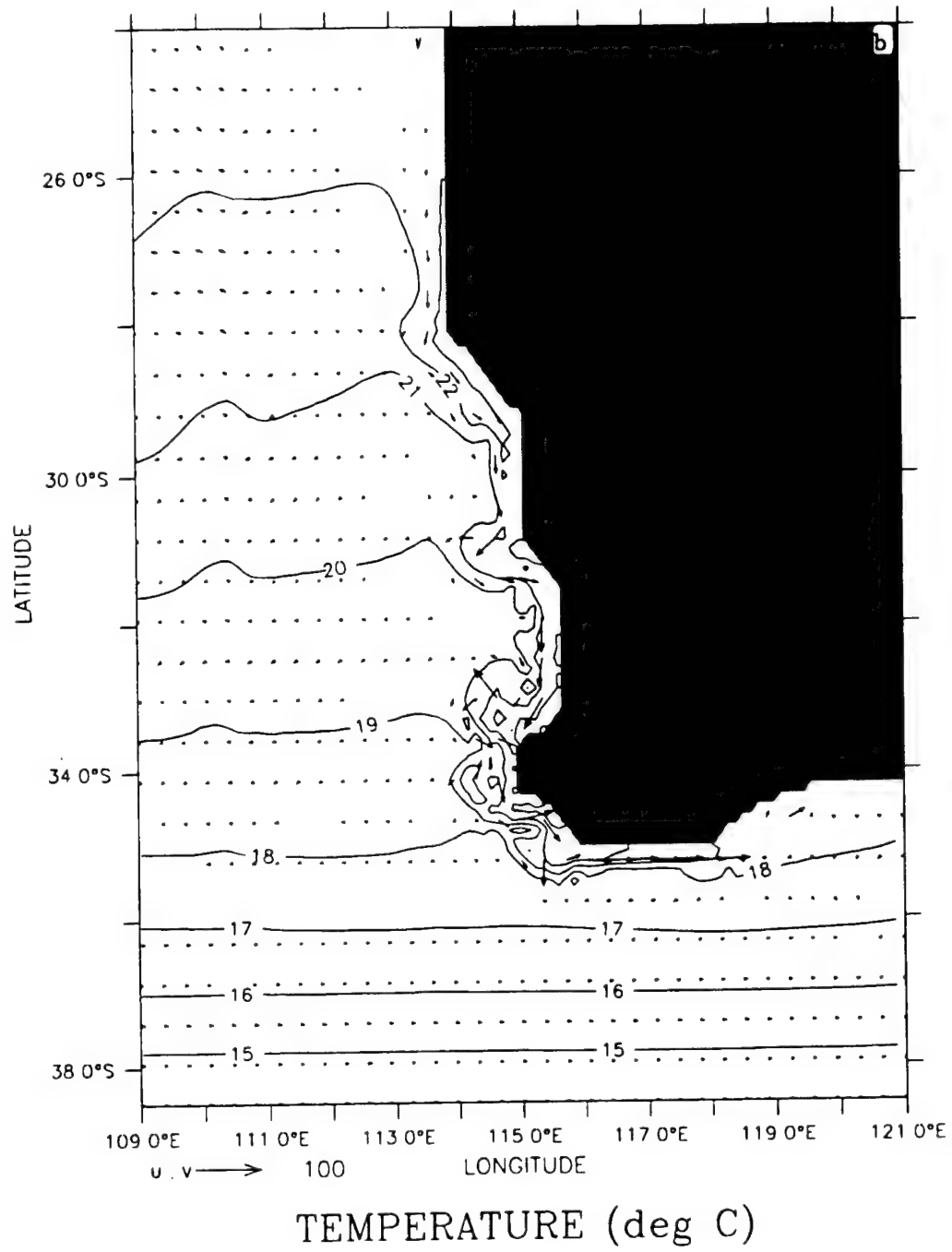
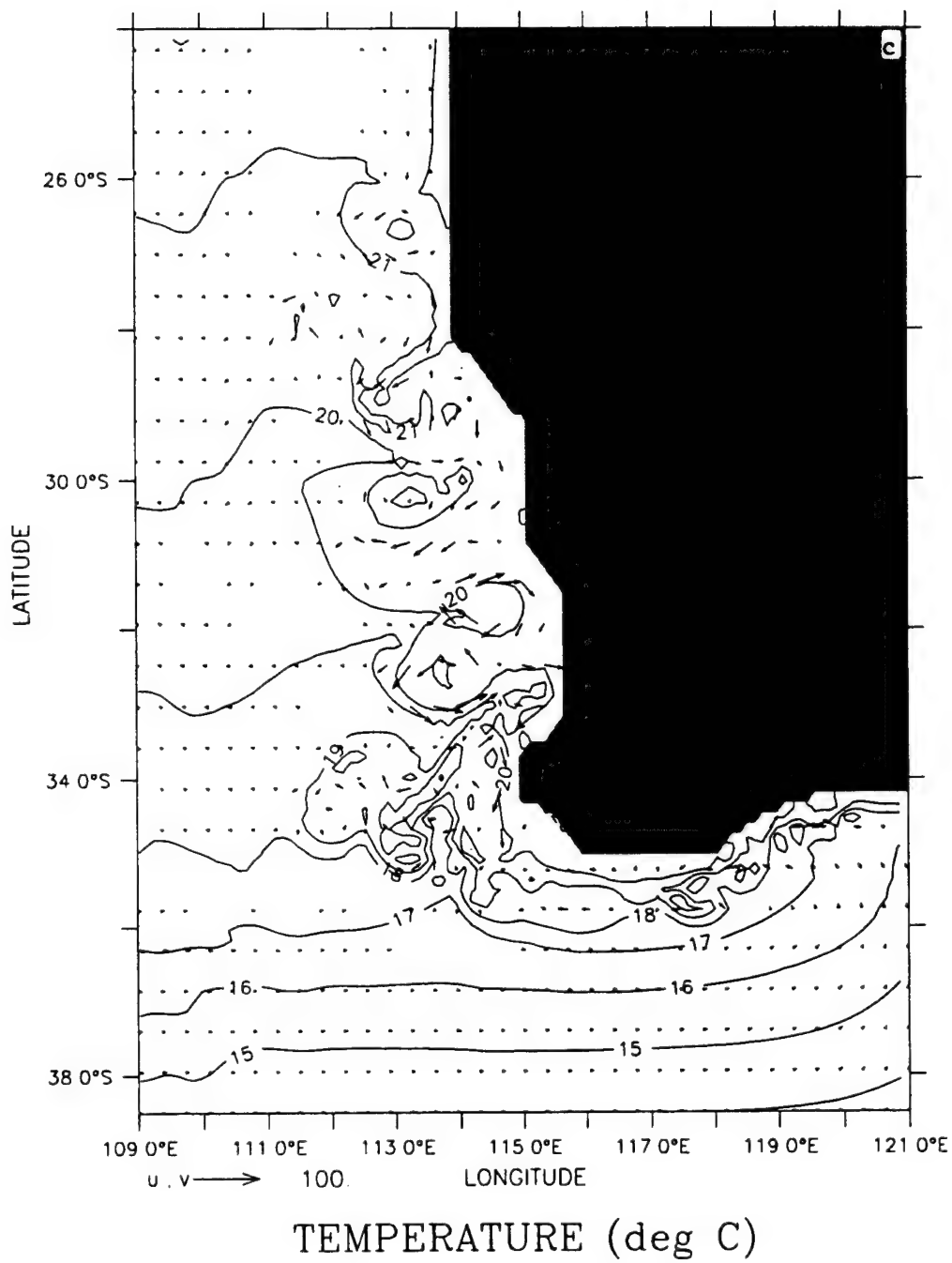


**Figure 19.** Temperature contours and velocity vectors at 10 m depth at days (a) 15, (b) 30, (c) 90, (d) 180, and (e) 345 of Experiment 4. The contour interval is 1°C; maximum velocity vector is 50 cm/s in (a) and 100 cm/c in (b) – (e).

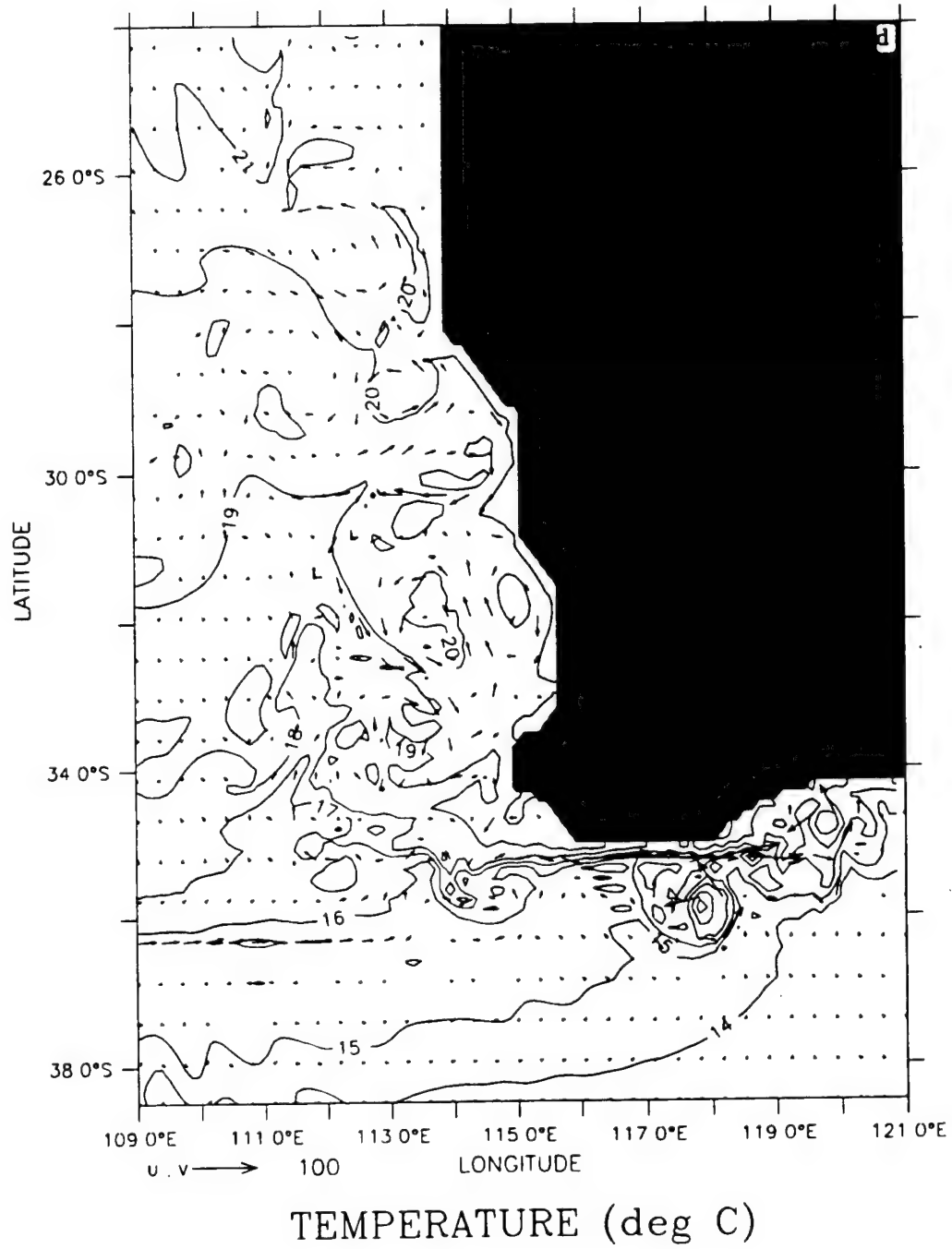
DEPTH : 10m  
T : 30



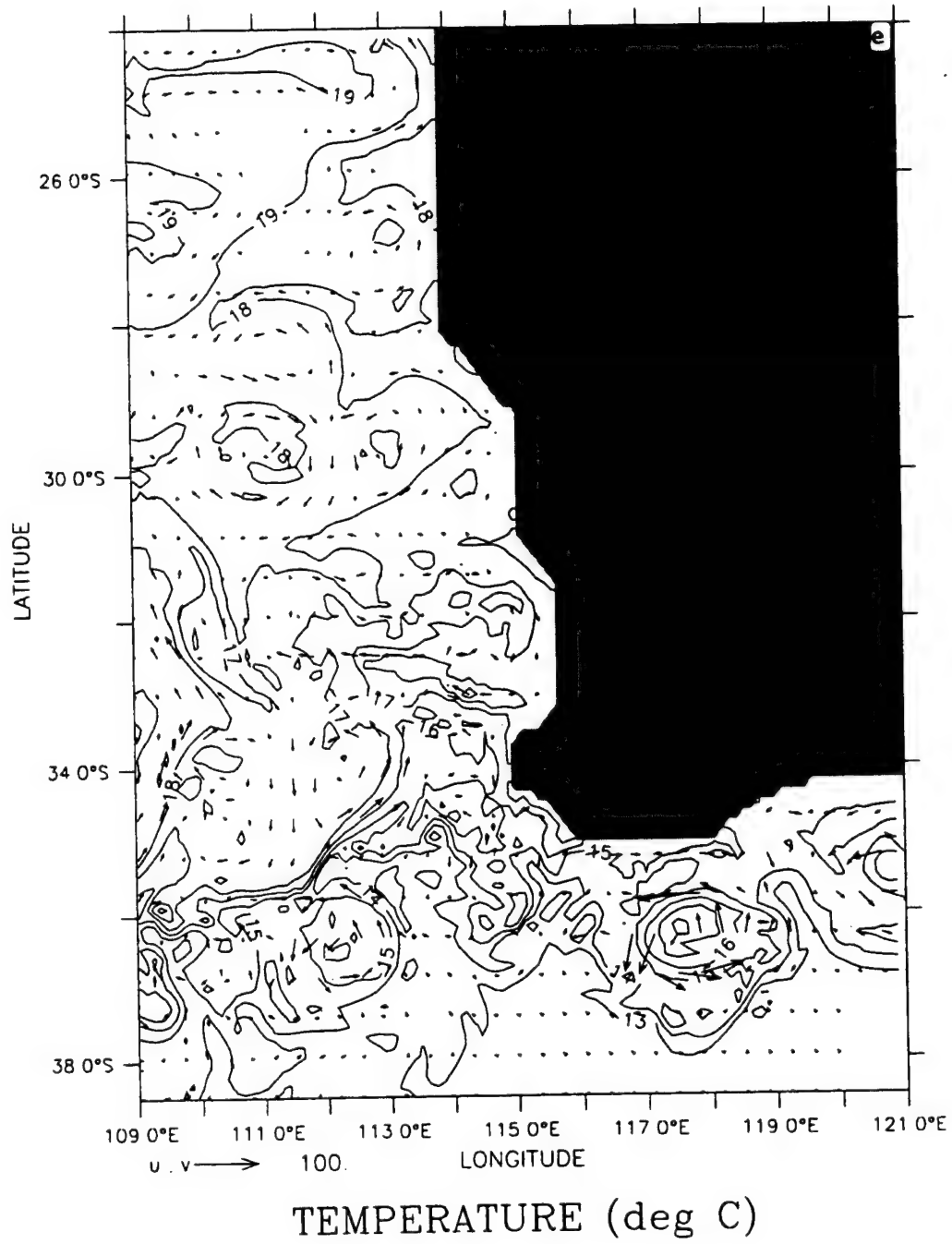
DEPTH : 10m  
T : 90



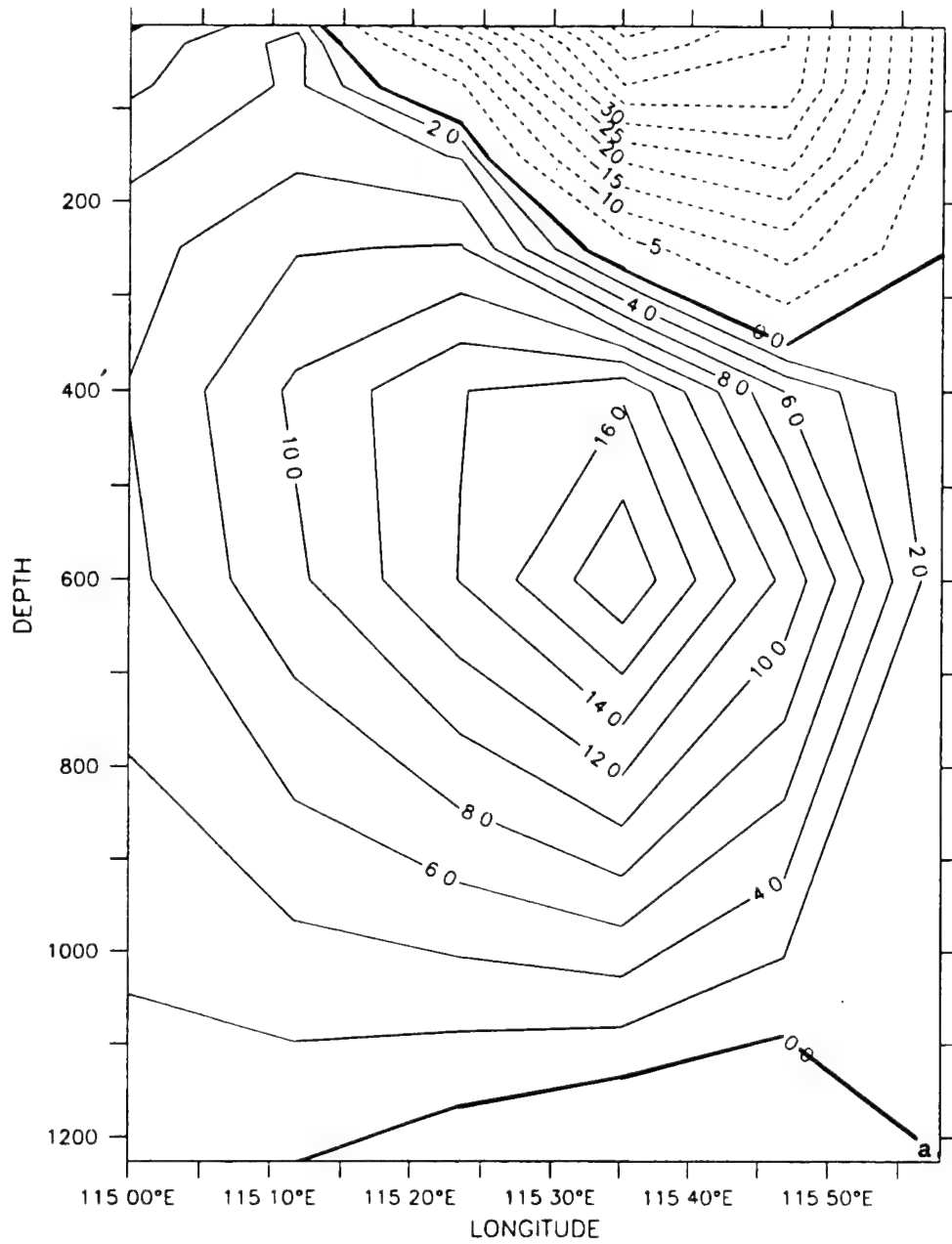
DEPTH : 10m  
T : 180



DEPTH : 10m  
T : 345



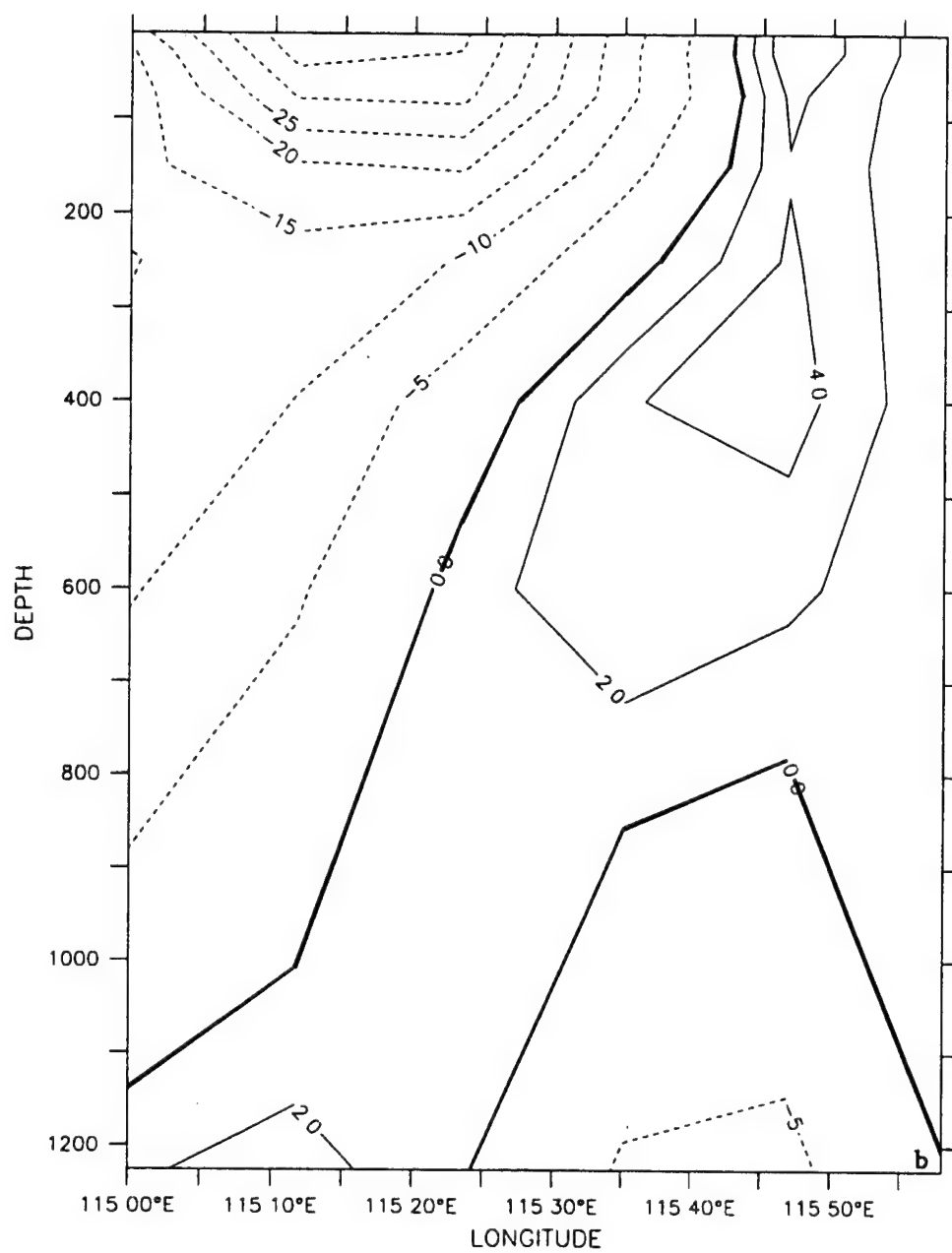
LATITUDE : 31.9S  
T : 30



MERID VELOCITY (cm/sec)

**Figure 20.** Cross-shore section of meridional velocity ( $v$ ) at  $\sim 32^\circ$  S (near Fremantle) for days (a) 30 and (b) 90, and at  $34^\circ$  S (off Cape Leeuwin) for days (c) 180 and (d) 345 of Experiment 3. The contour interval is 5.0 cm/s for poleward (dashed line) flow and 2.0 cm/s in (a), (b) and 1.0 cm/s in (c), (d) for equatorward (solid line) flow.

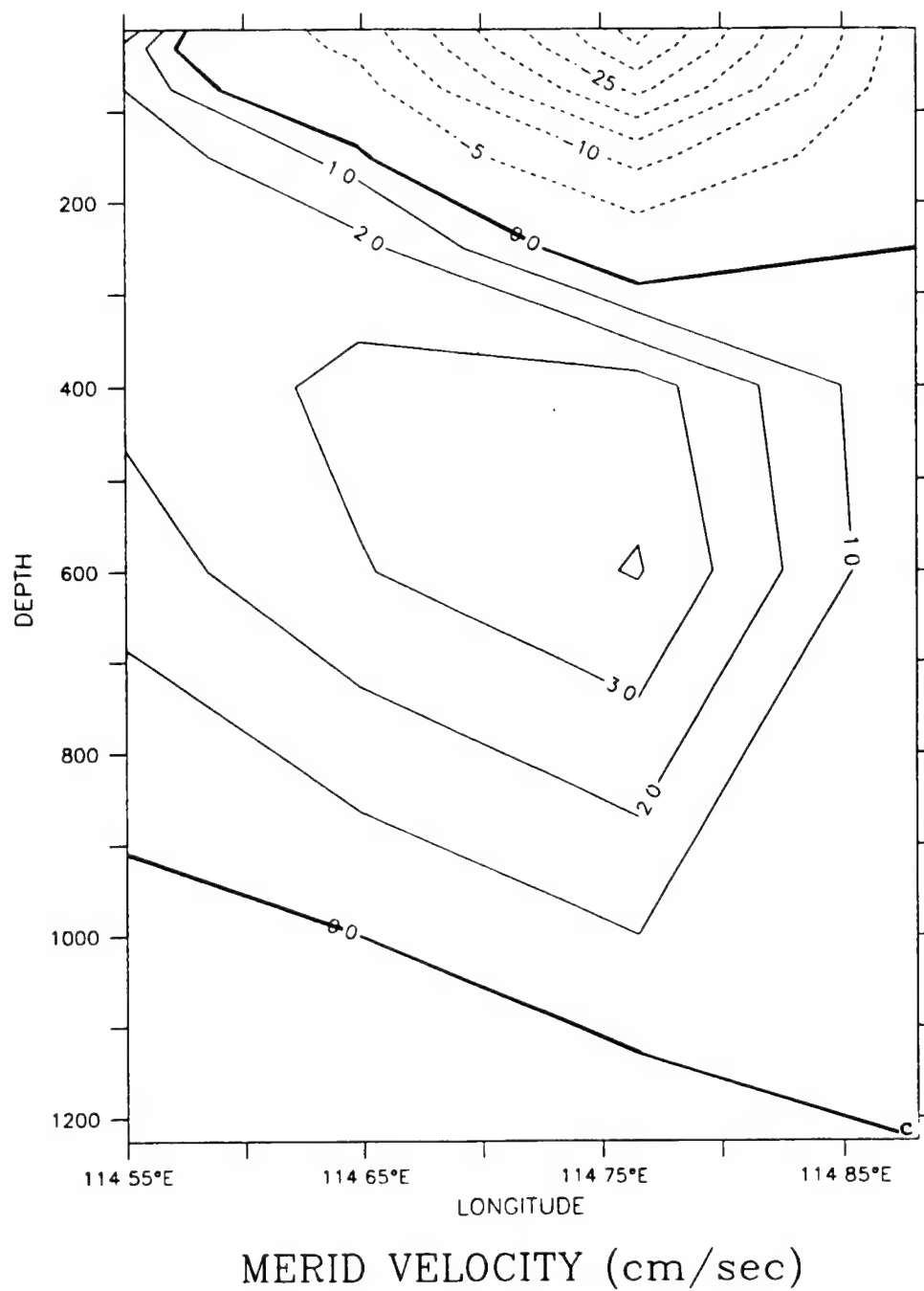
LATITUDE : 31.9S  
T : 90



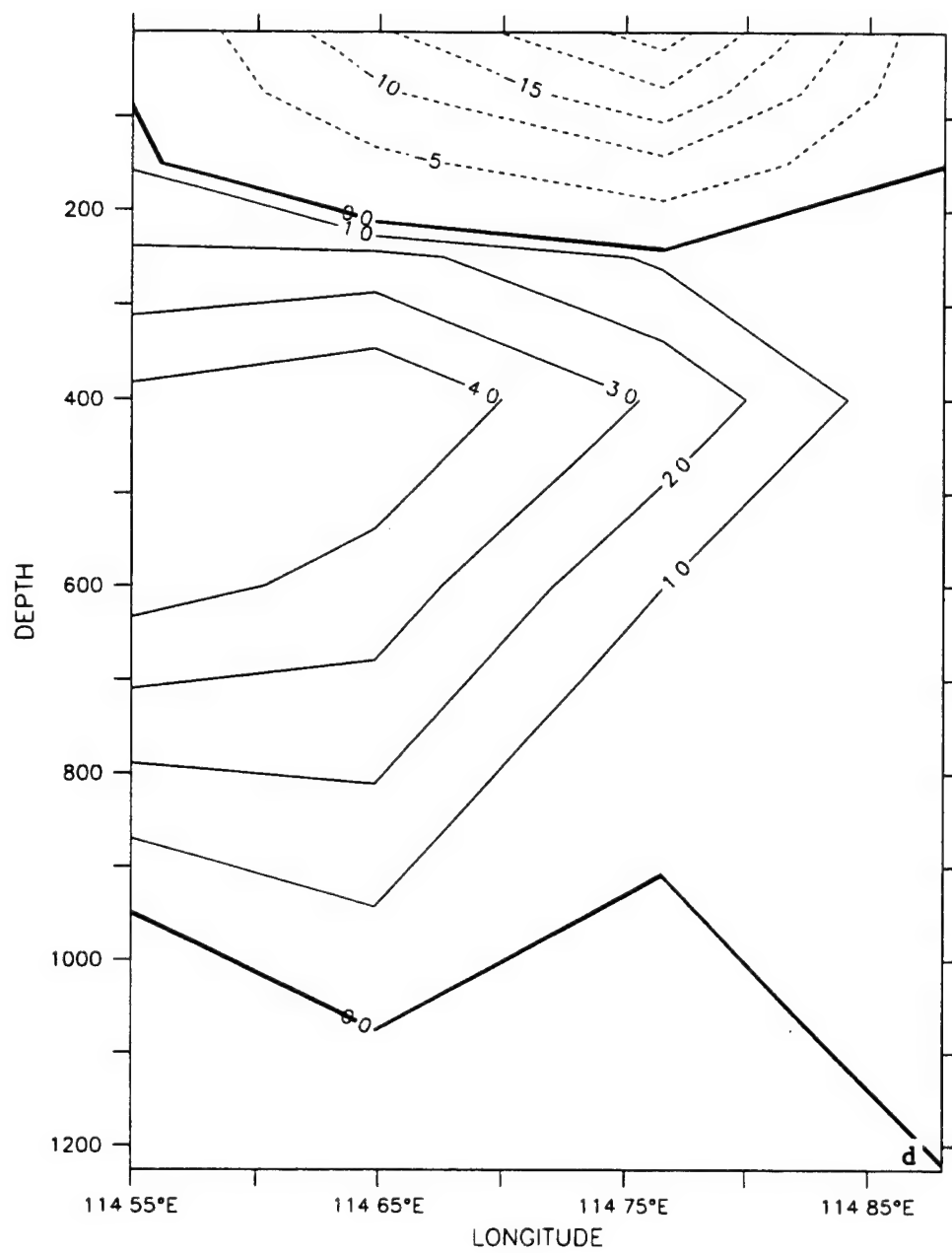
MERID VELOCITY (cm/sec)



LATITUDE : 34S  
T : 180



LATITUDE : 34S  
T : 345



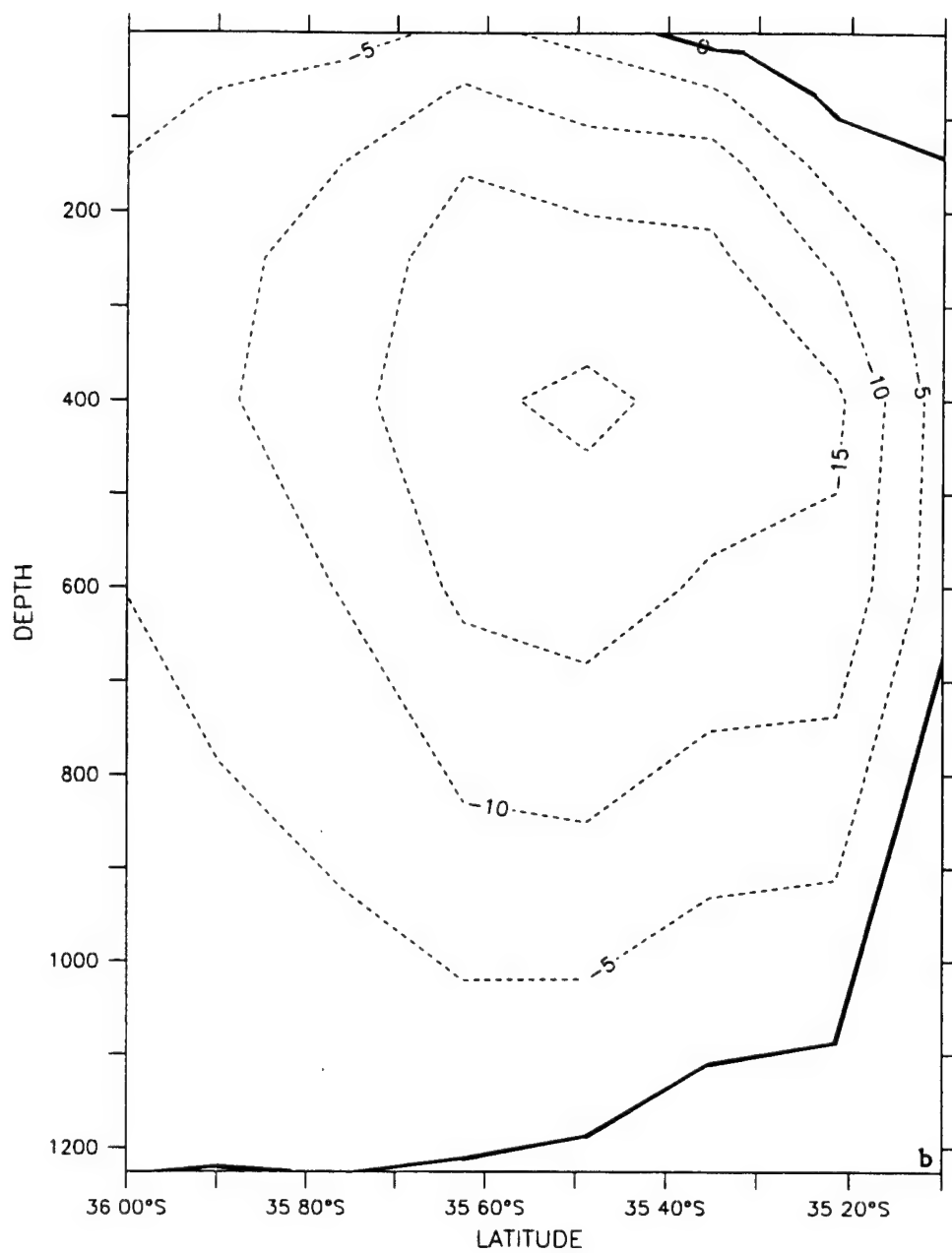
MERID VELOCITY (cm/sec)

LONGITUDE 117E(117)  
T : 30



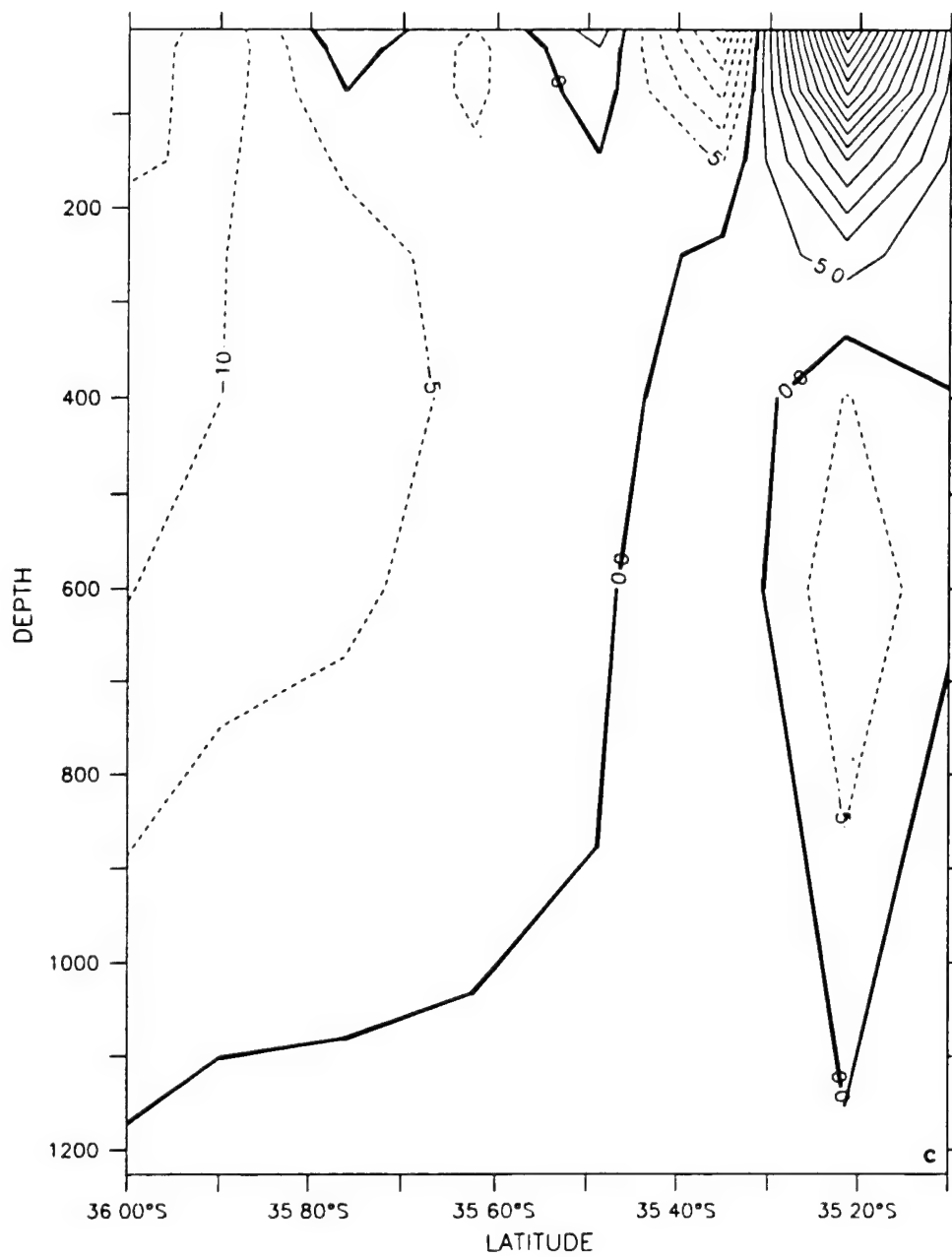
**Figure 21.** Cross-shore section of zonal velocity ( $u$ ) at  $\sim 117^\circ$  E for days (a) 30, (b) 90, (c) 180, and (d) 345 of Experiment 4. Contour interval is 5.0 cm/s in (a) – (c) and 2.0 cm/s for eastward (solid line) flow and 5.0 cm/s for westward (dashed line) flow in (d).

LONGITUDE : 117E(117)  
T : 90



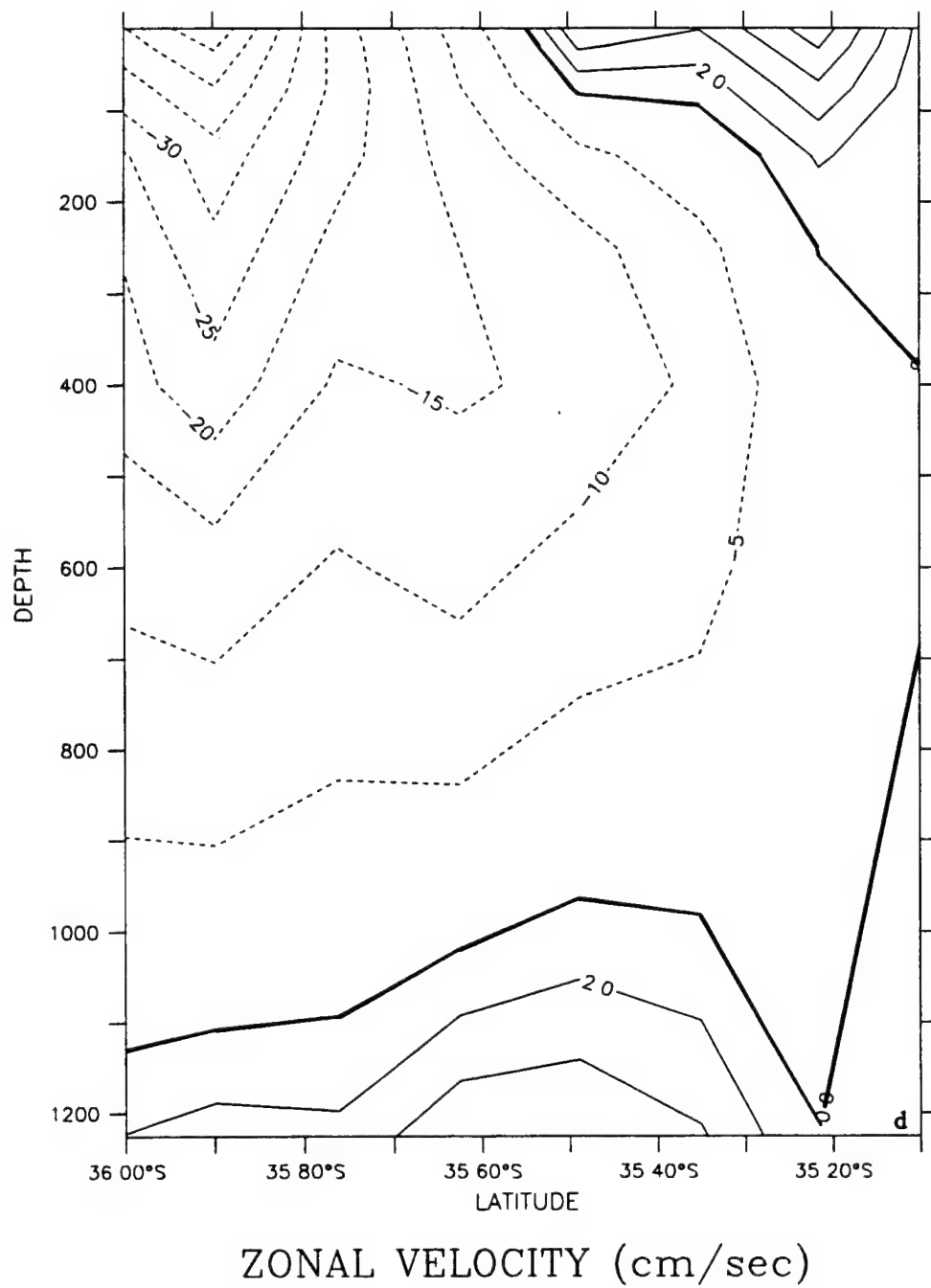
ZONAL VELOCITY (cm/sec)

LONGITUDE 117E(117)  
T : 180



ZONAL VELOCITY (cm/sec)

LONGITUDE : 117E(117)  
T : 345



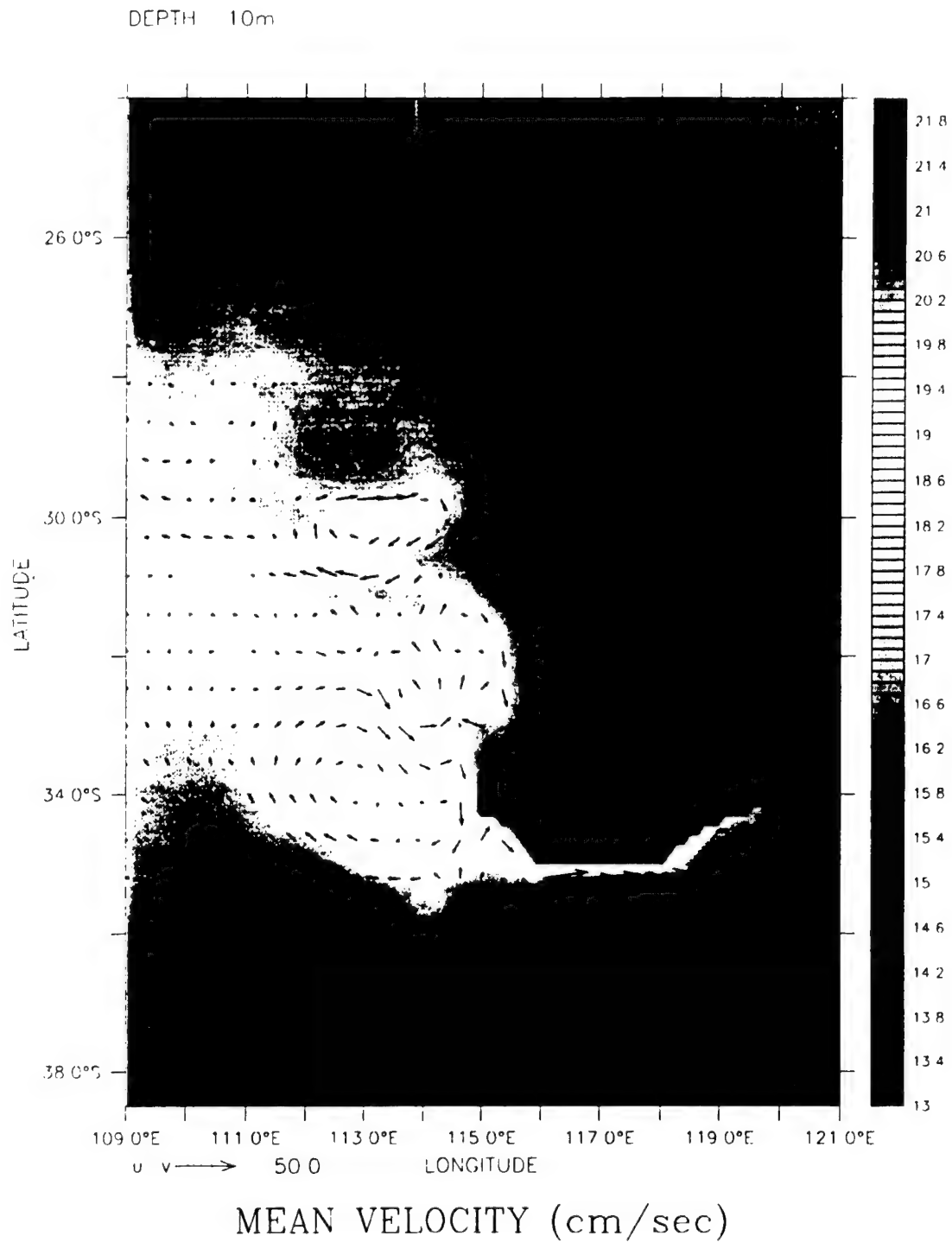


**Figure 22.** Mean temperature and velocity vectors at 10 m depth averaged for days 90 to 270 of Experiment 4. Contour interval is 0.1°C with colder waters in the south end of the model domain; maximum velocity vector is 50 cm/s.

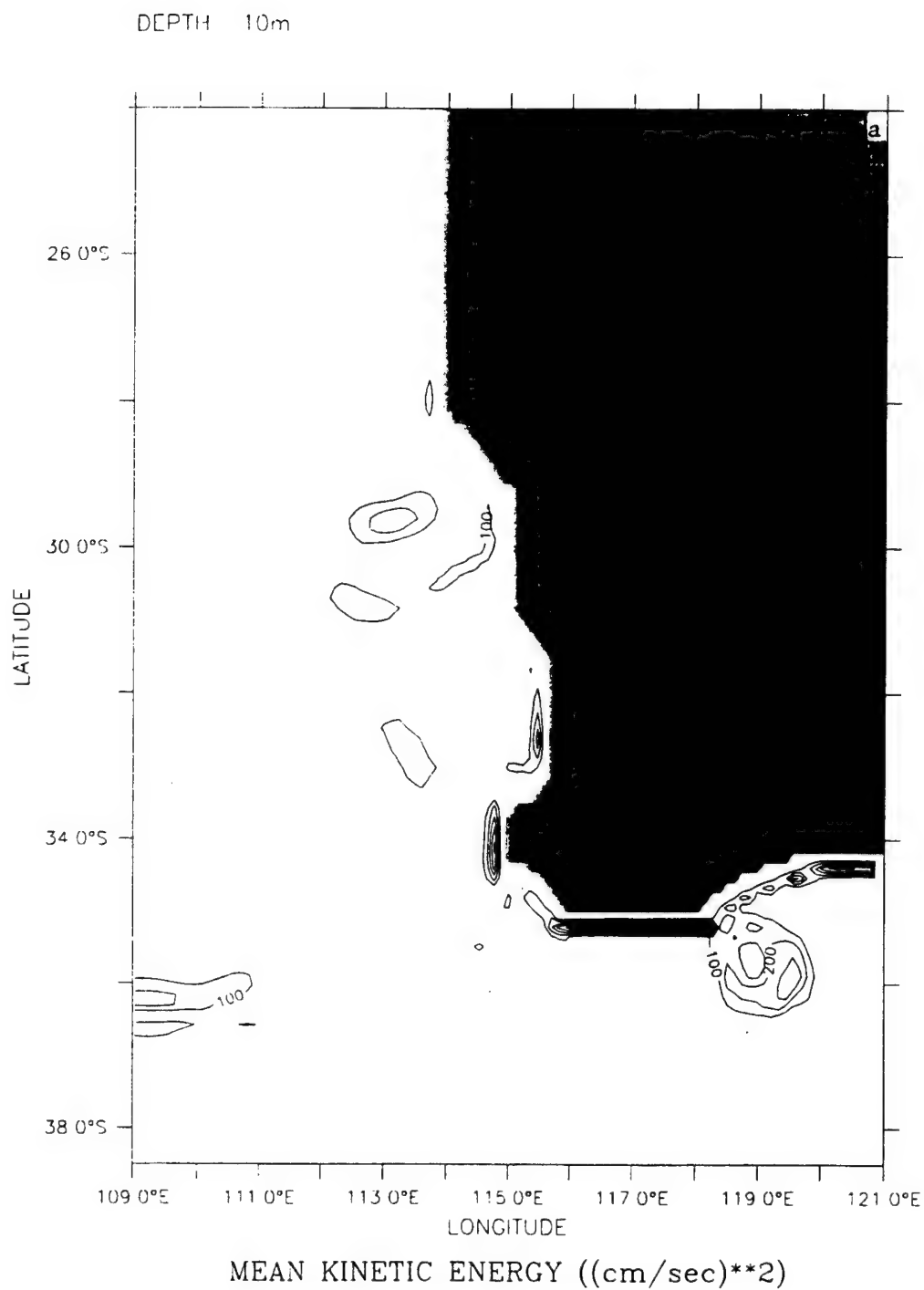
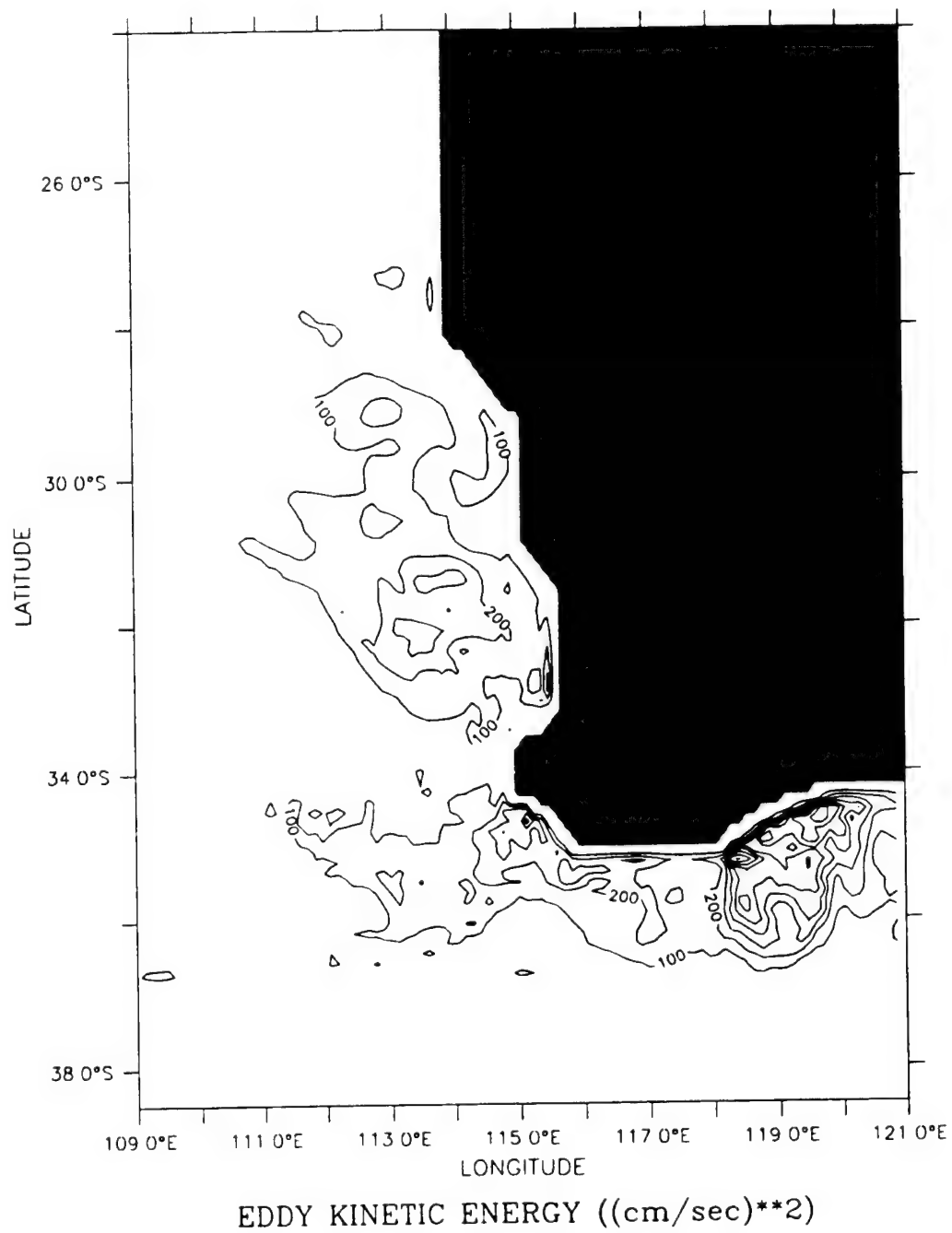


**Figure 23.** Horizontal maps at 10 m depth of (a) mean kinetic energy (MKE) and (b) eddy kinetic energy (EKE) averaged for days 90 to 270 of Experiment 4. Contour interval is  $100 \text{ cm}^2/\text{s}^2$ .



DEPTH : 10m



DEPTH : 10m  
T : 78

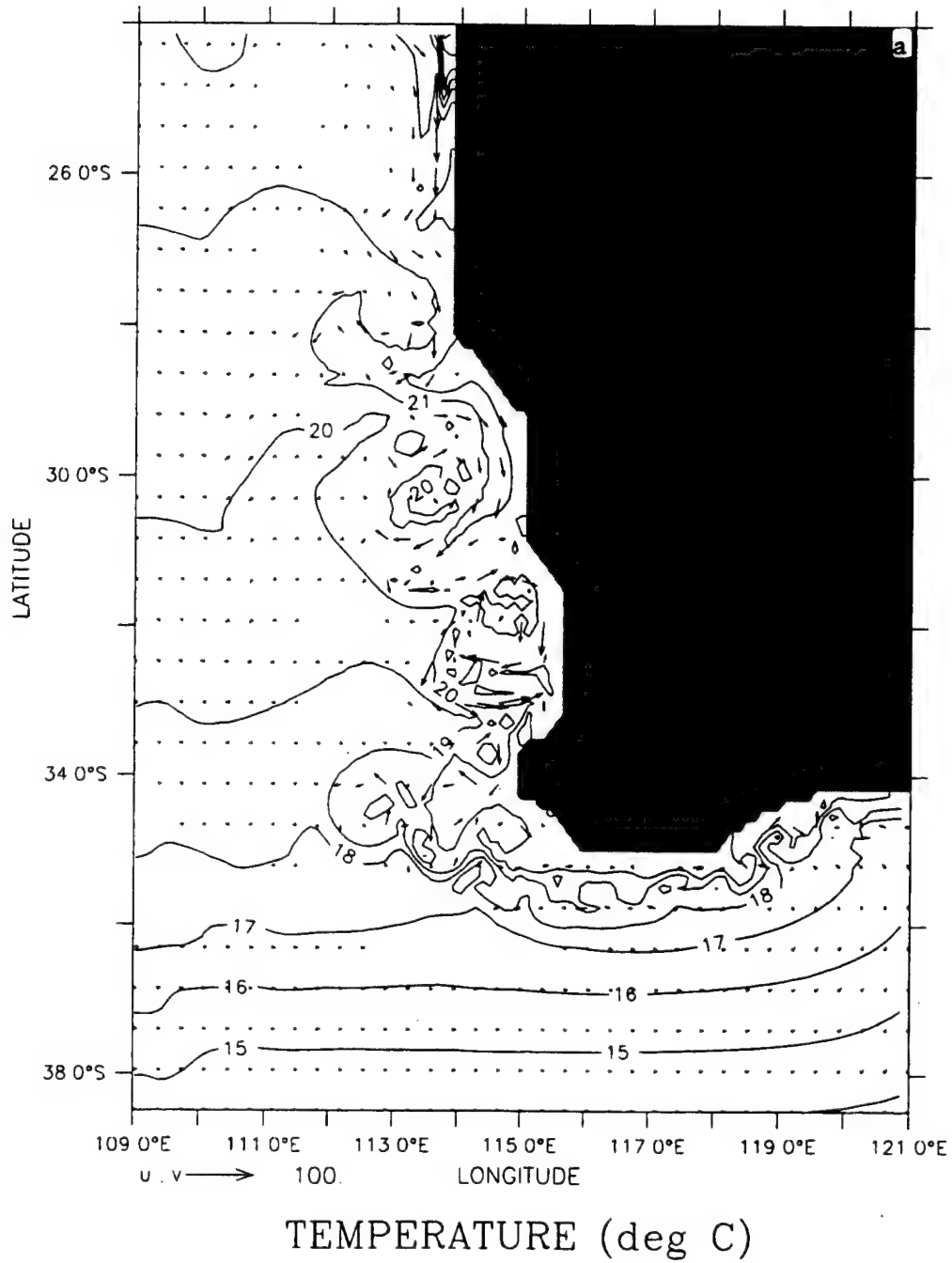
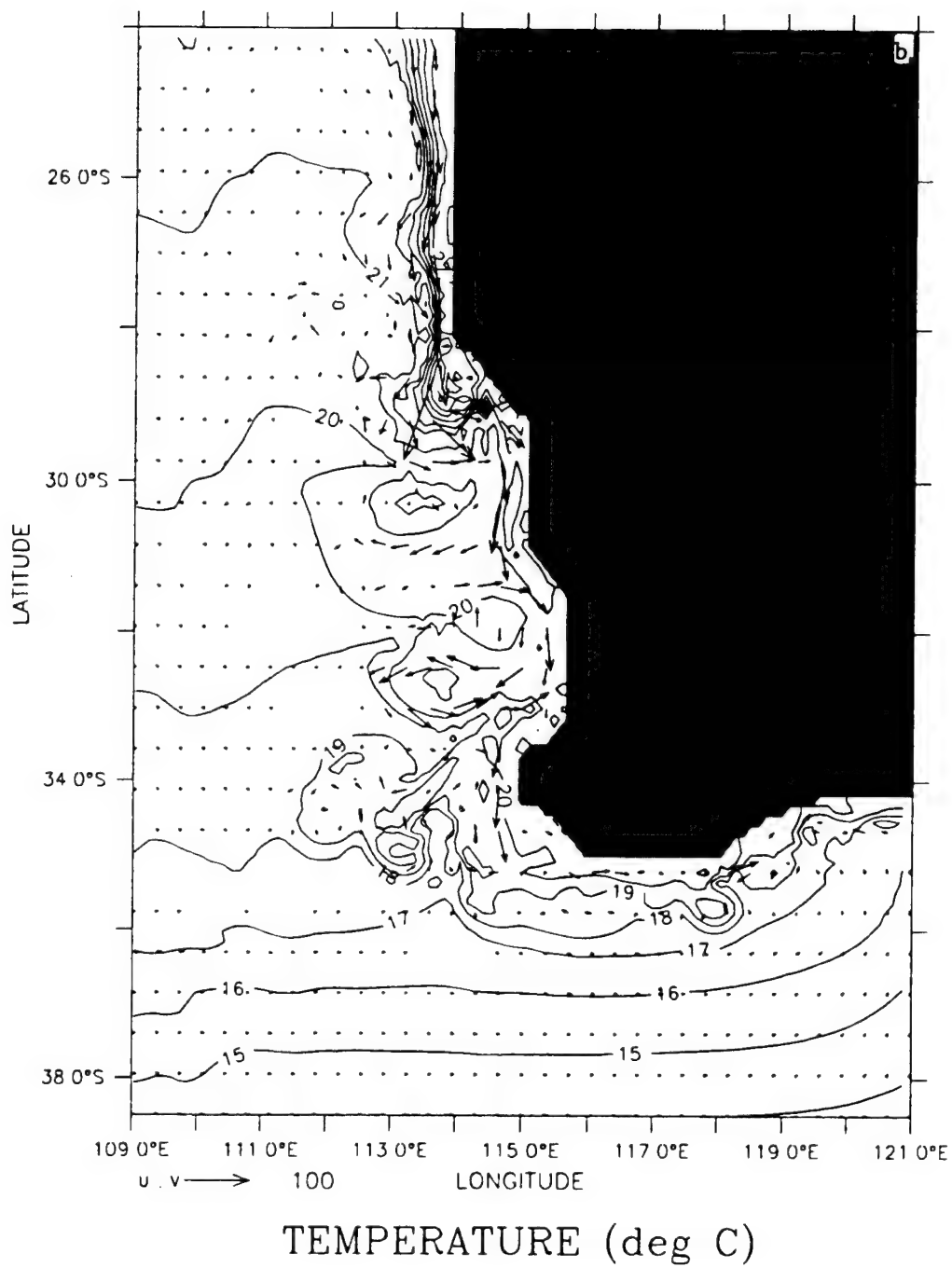


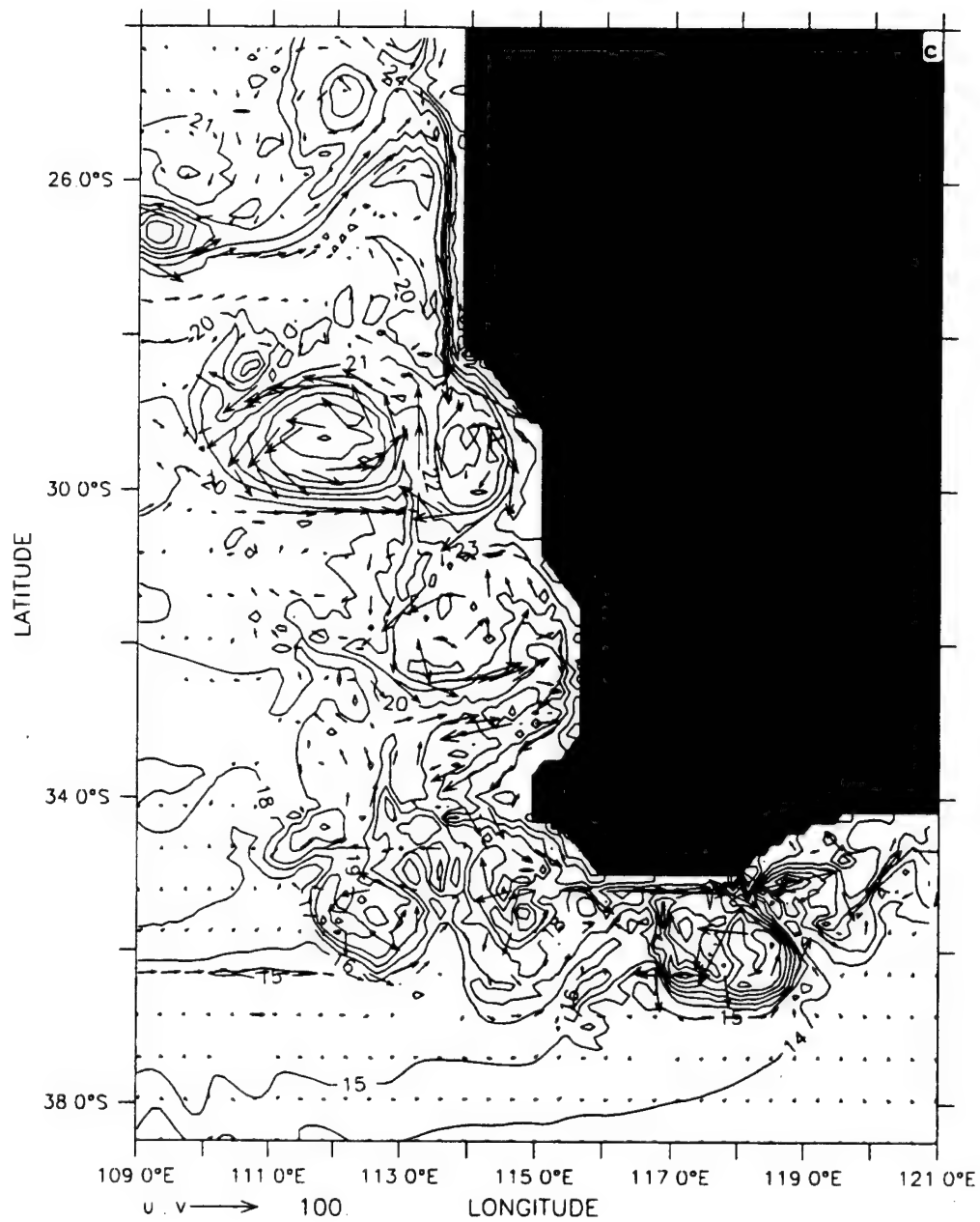
**Figure 24.** Temperature contours and velocity vectors at 10 m depth at days (a) 78, (b) 90, (c) 180, and (d) 345 of Experiment 5. The contour interval is 1°C; maximum velocity vector is 100 cm/s.

DEPTH : 10m  
T : 90



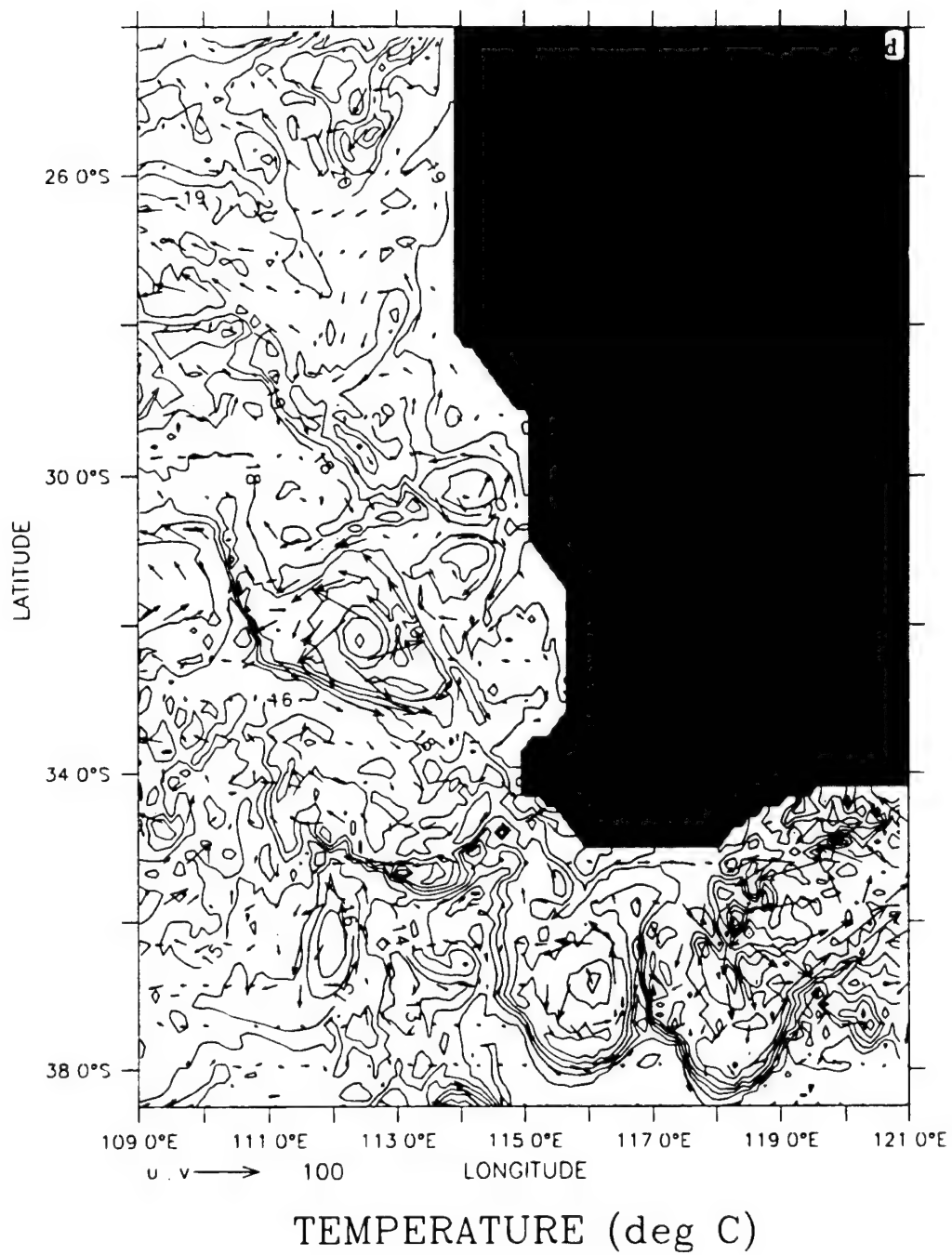
DEPTH : 10m

T : 180



TEMPERATURE (deg C)

DEPTH 10m  
T 345



LATITUDE : 28S  
T : 90

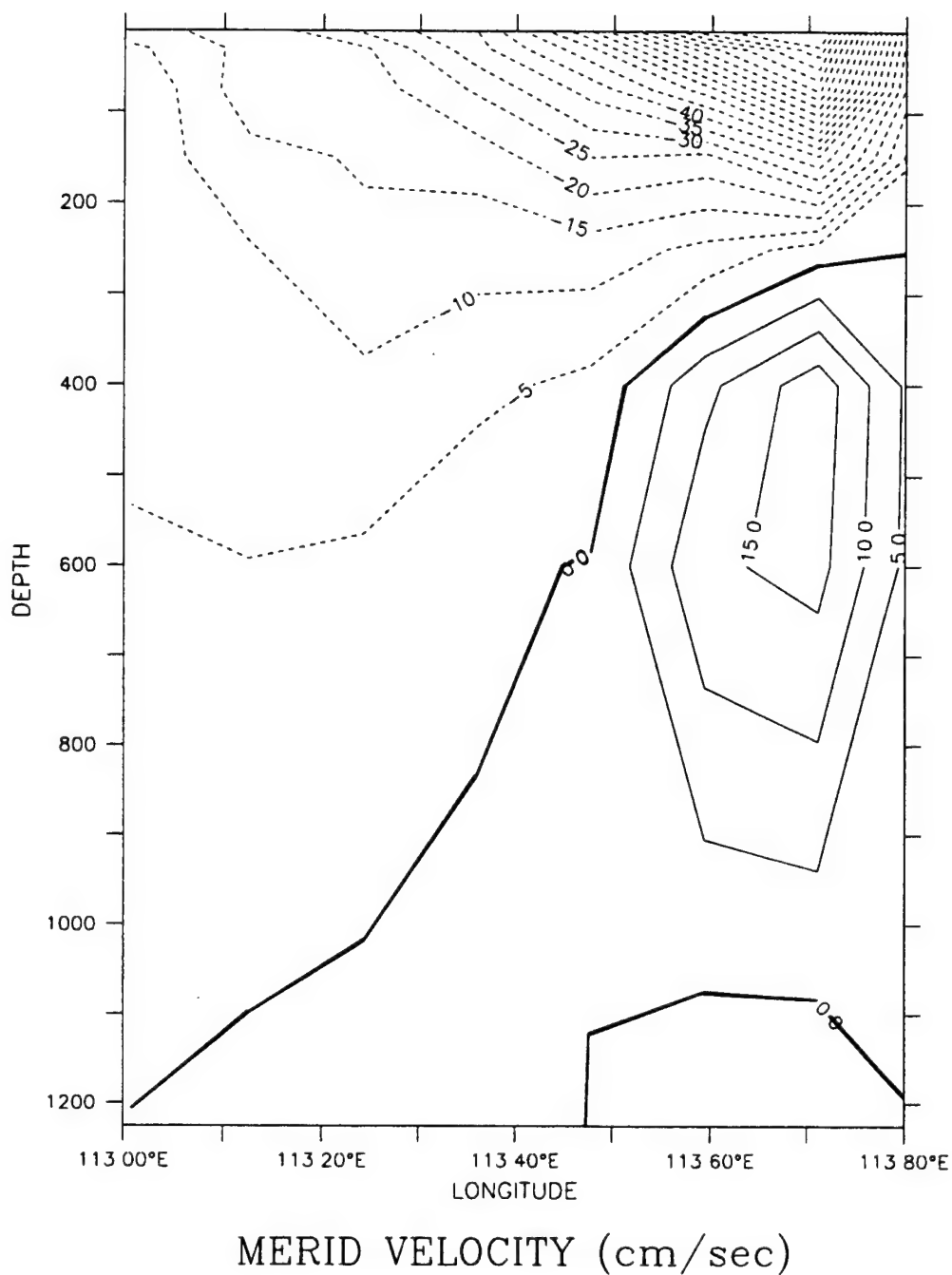


**Figure 25.** Cross-shore section of meridional velocity ( $v$ ) at 28° S (near Shark Bay), on day 90 of Experiment 5. The contour interval is 5.0 cm/s for poleward (dashed line) and equatorward (solid line) flow.

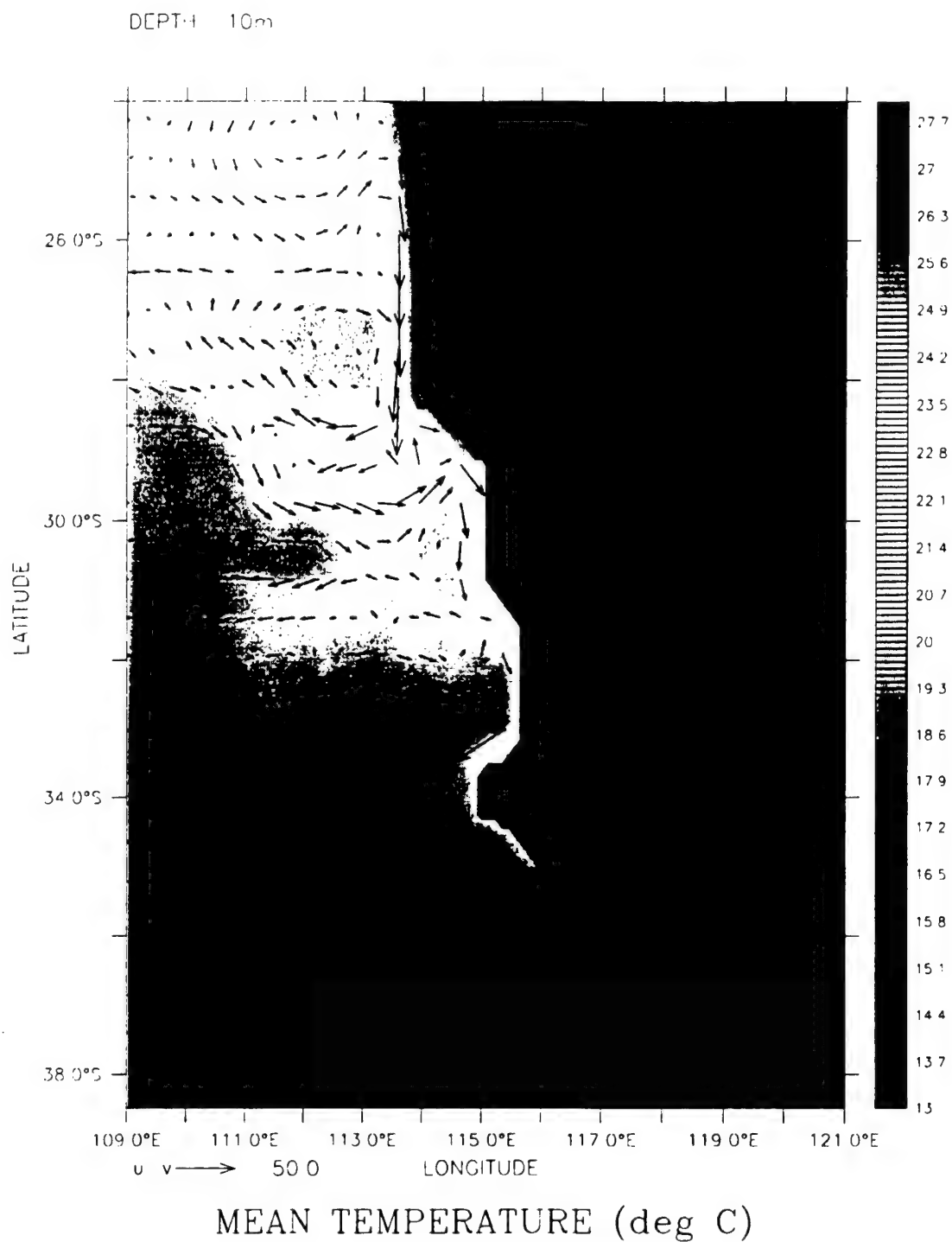


**Figure 26.** Mean temperature and velocity vectors at 10 m depth averaged for days 90 to 270 of Experiment 5. Contour interval is 0.1°C with colder waters in the south end of the model domain; maximum velocity vector is 50 cm/s.

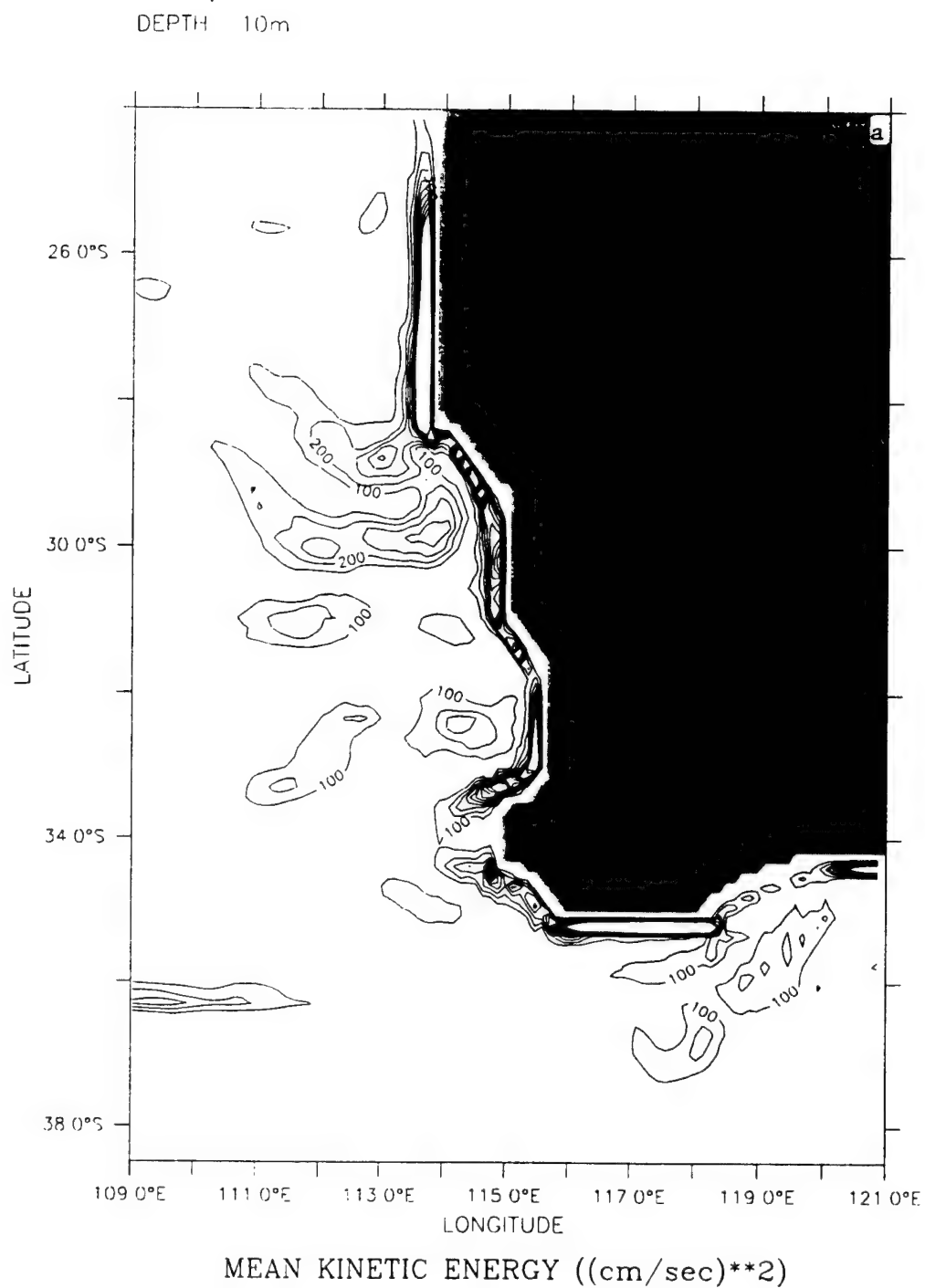
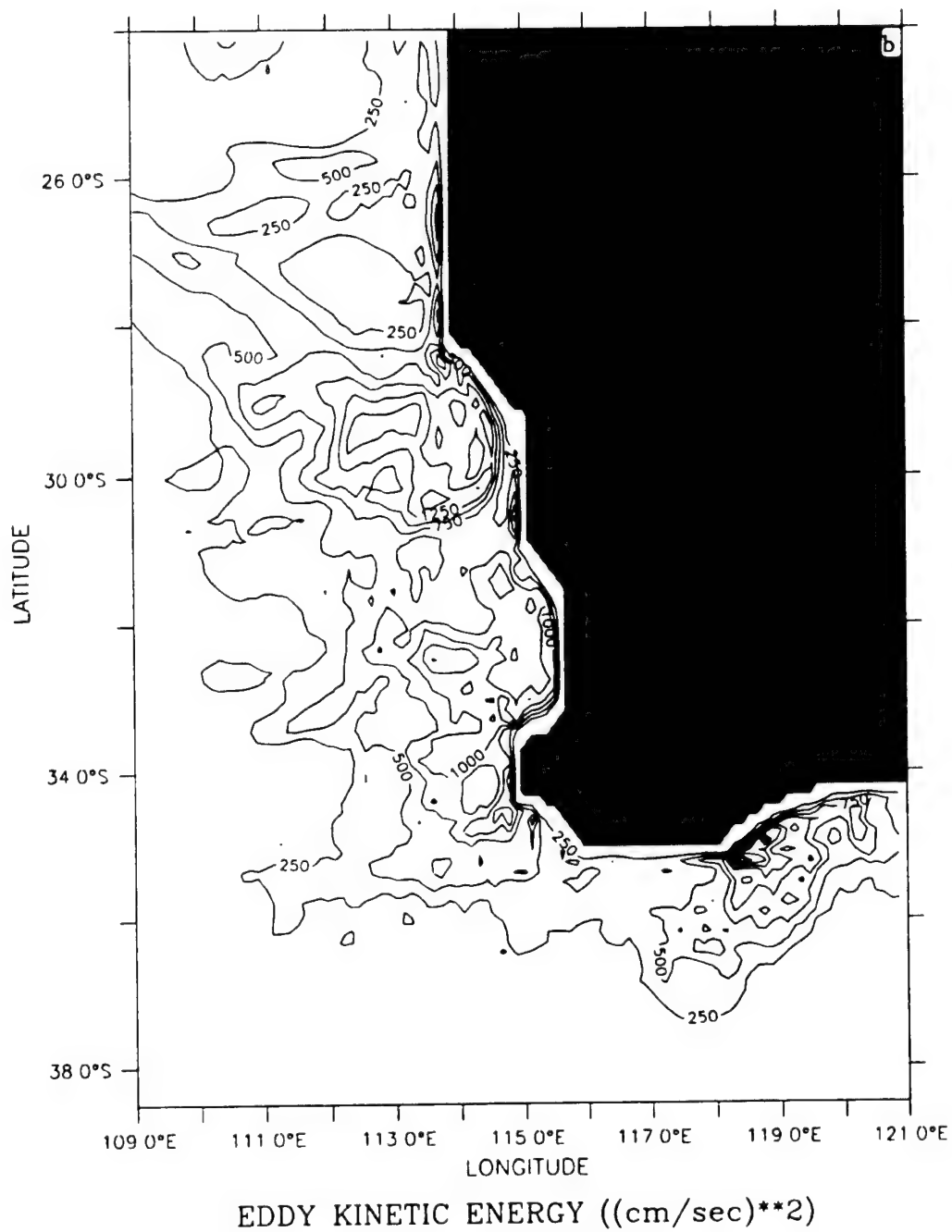


**Figure 27.** Horizontal maps at 10 m depth of (a) mean kinetic energy (MKE) and (b) eddy kinetic energy (EKE) averaged for days 90 to 270 of Experiment 5. Contour interval is  $100 \text{ cm}^2/\text{s}^2$  in (a) and  $250 \text{ cm}^2/\text{s}^2$  in (b).



DEPTH 10m



DEPTH : 600m

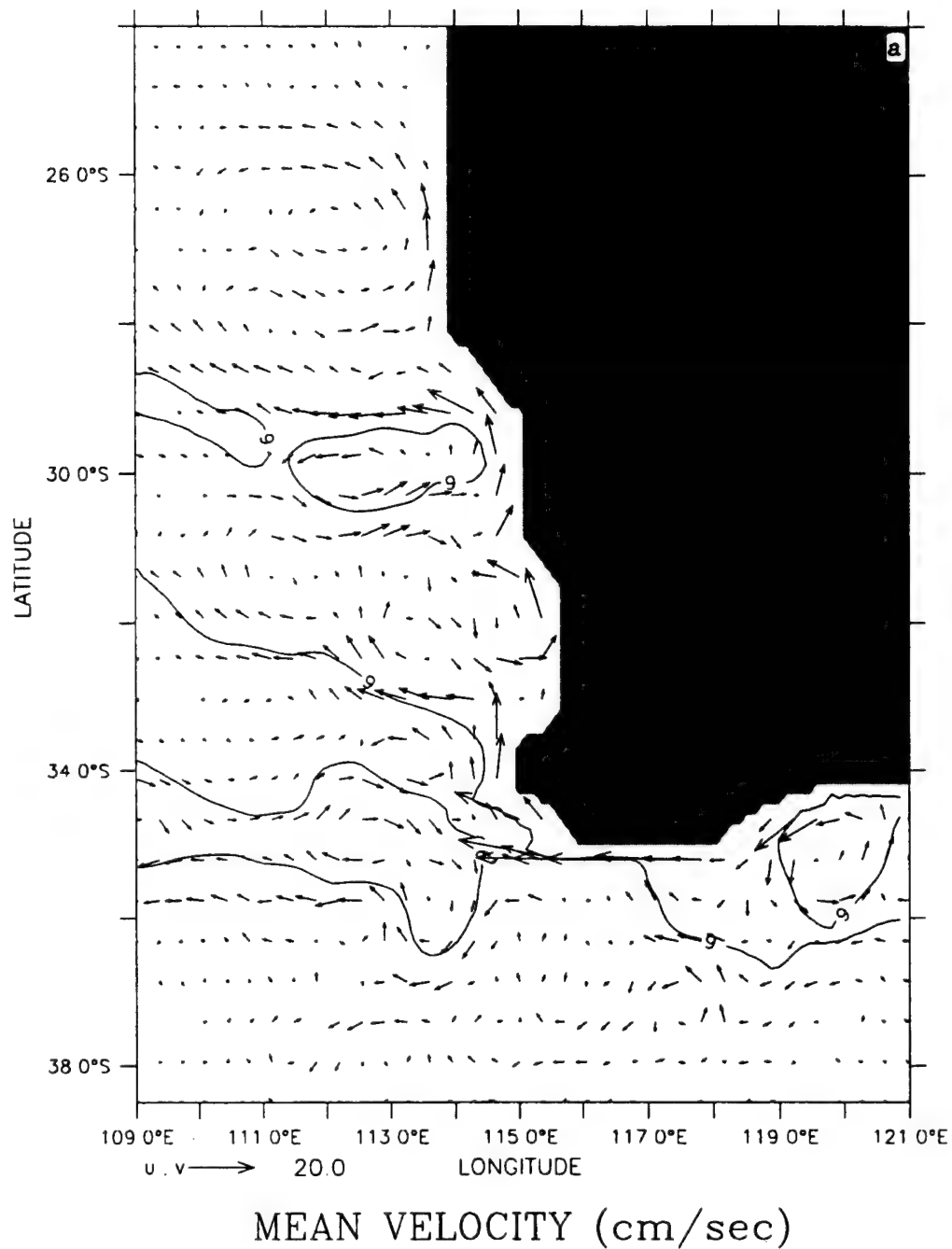
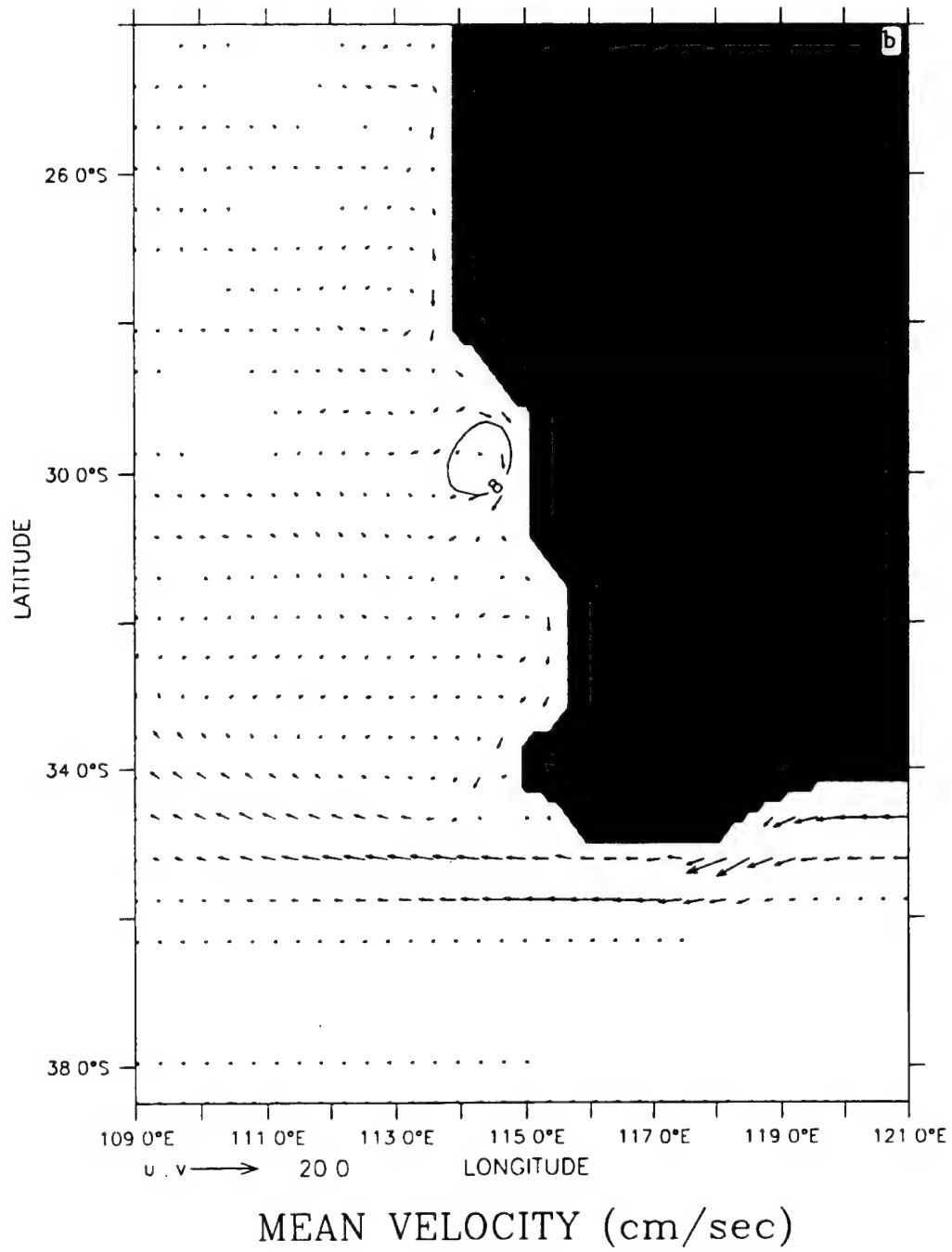
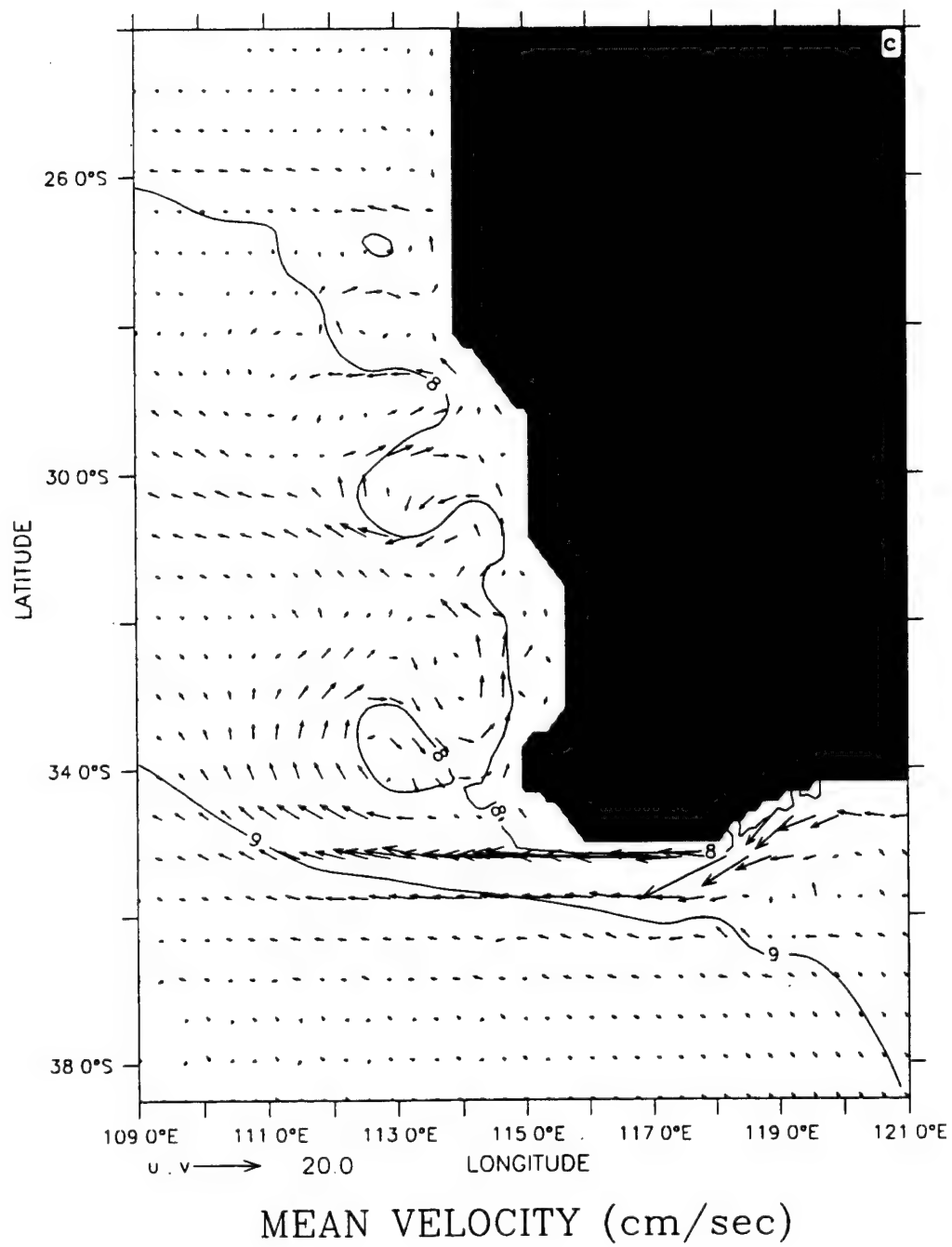


**Figure 28.** Mean temperature and velocity vectors at 600 m depth averaged for days 90 to 270 of (a) Experiment 1, (b) Experiment 2, (c) Experiment 3, (d) Experiment 4, and (e) Experiment 5. Contour interval is 1°C; maximum velocity vector is 20 cm/s.

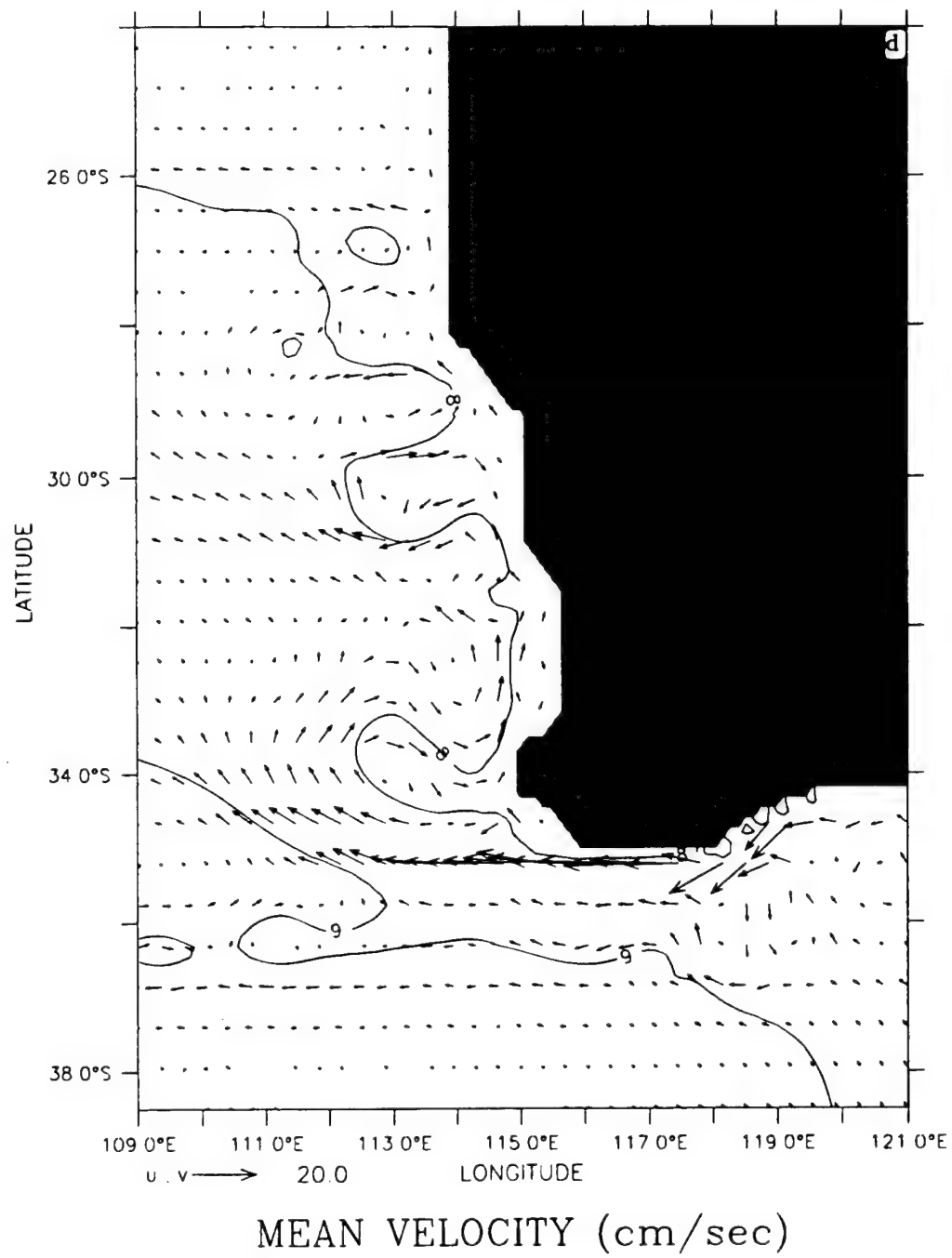
DEPTH : 600m



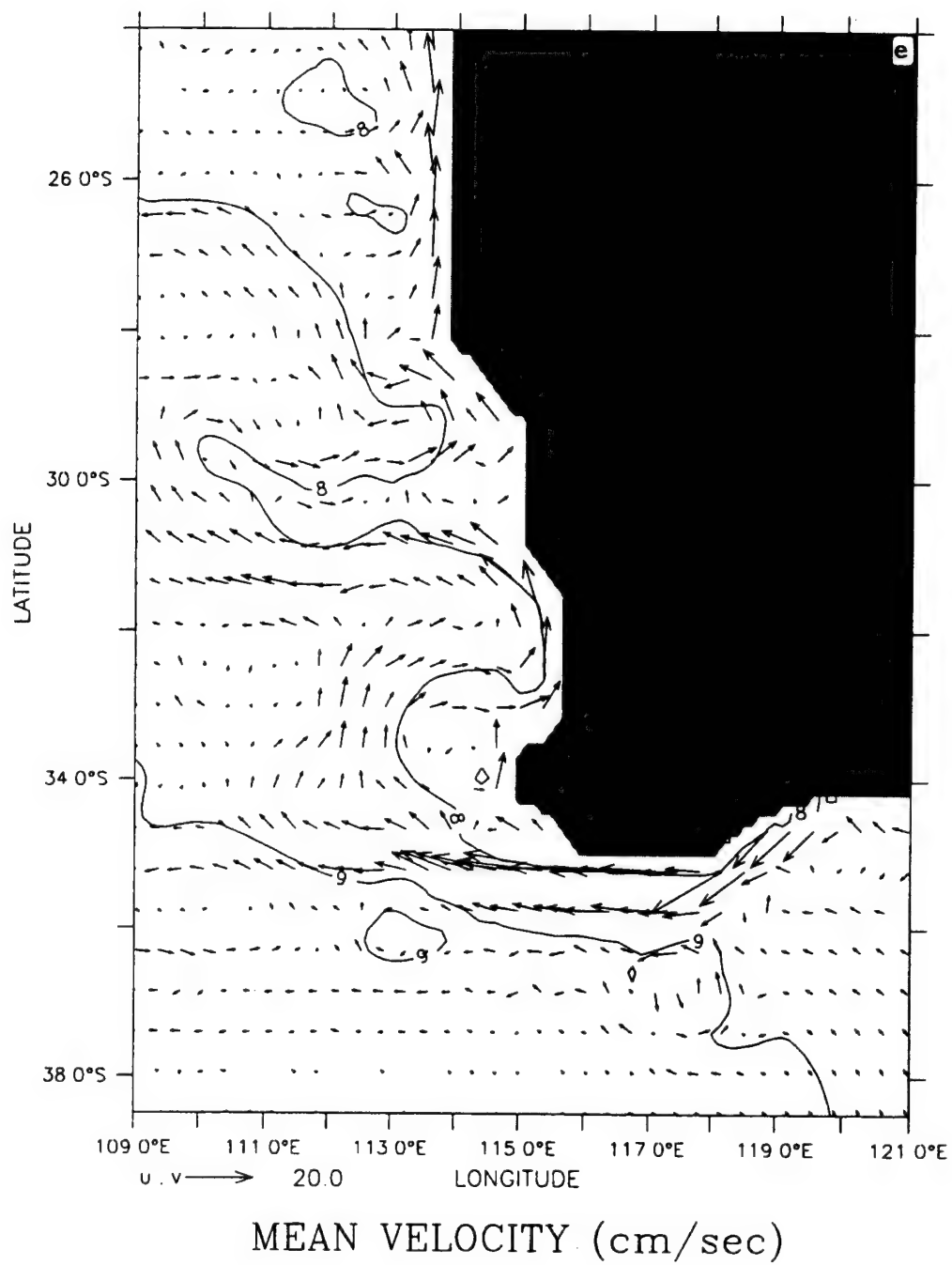
DEPTH : 600m

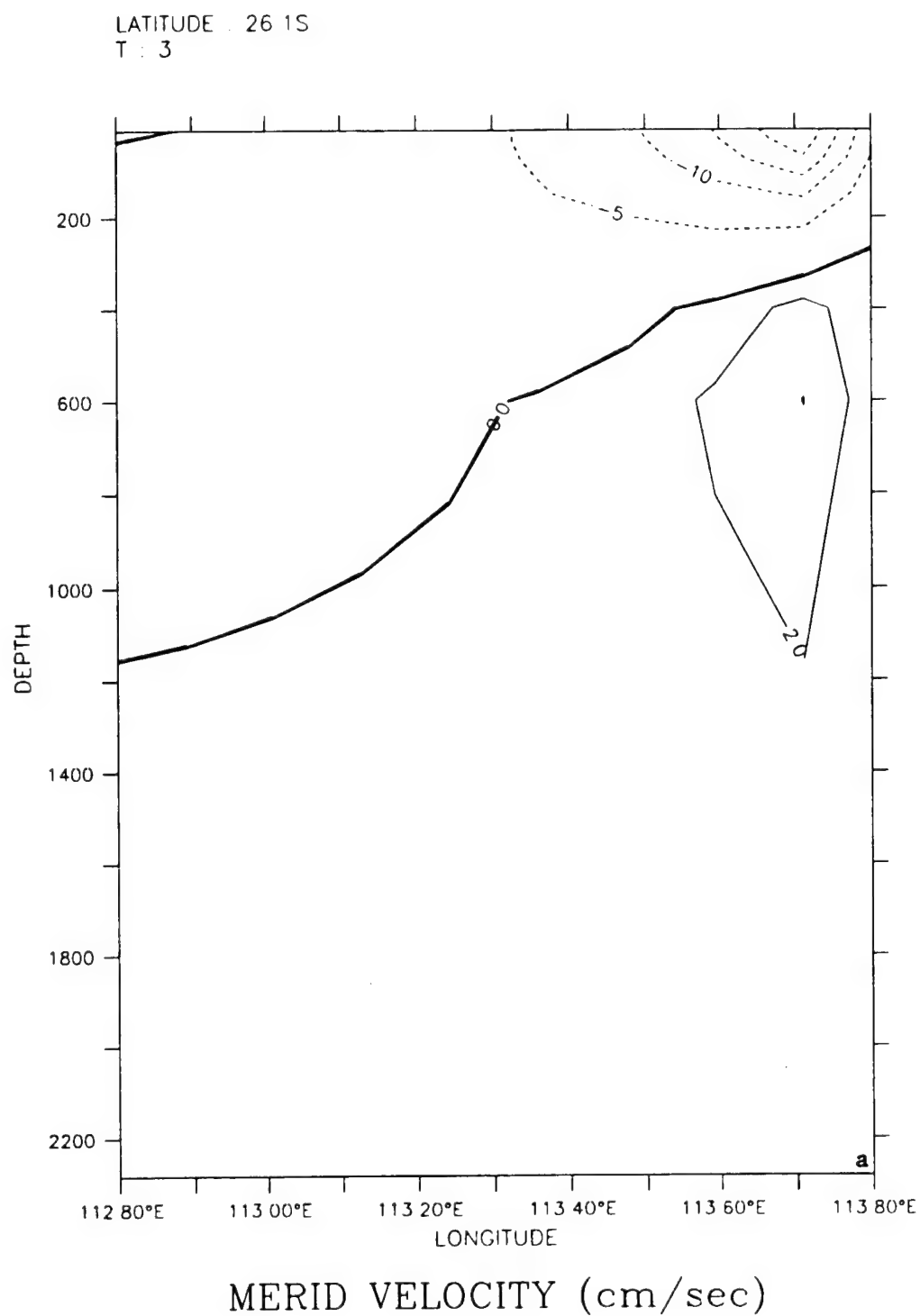


DEPTH 600m



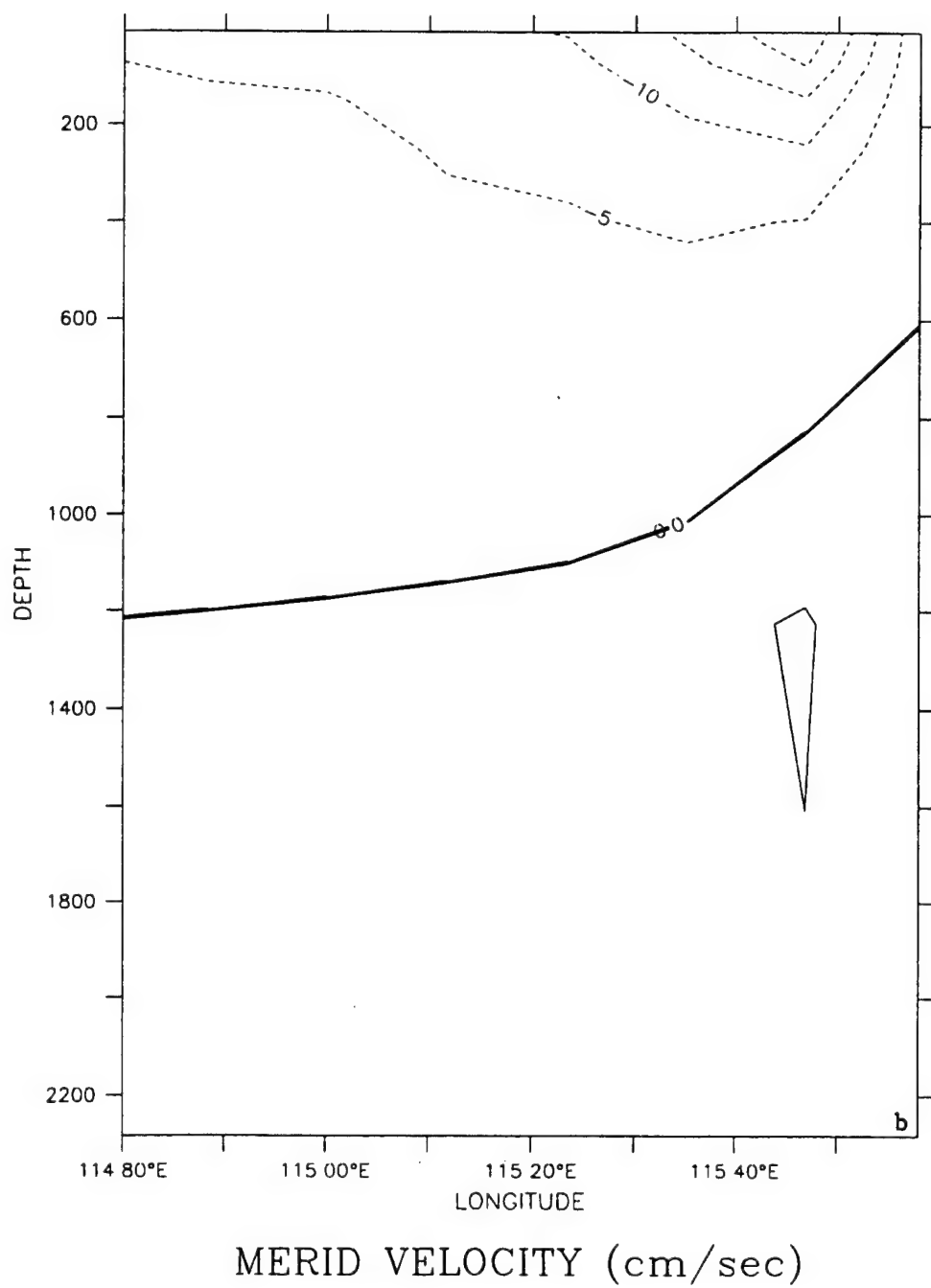
DEPTH : 600m





**Figure 29.** Cross-shore section of meridional velocity ( $v$ ) for day 3 at (a)  $\sim 26^{\circ}$  S, and (b)  $32^{\circ}$  S of Experiment 6. The contour interval is 5.0 cm/s for poleward (dashed line) flow and 2.0 cm/s for equatorward (solid line) flow.

LATITUDE : 31.9S  
T : 3





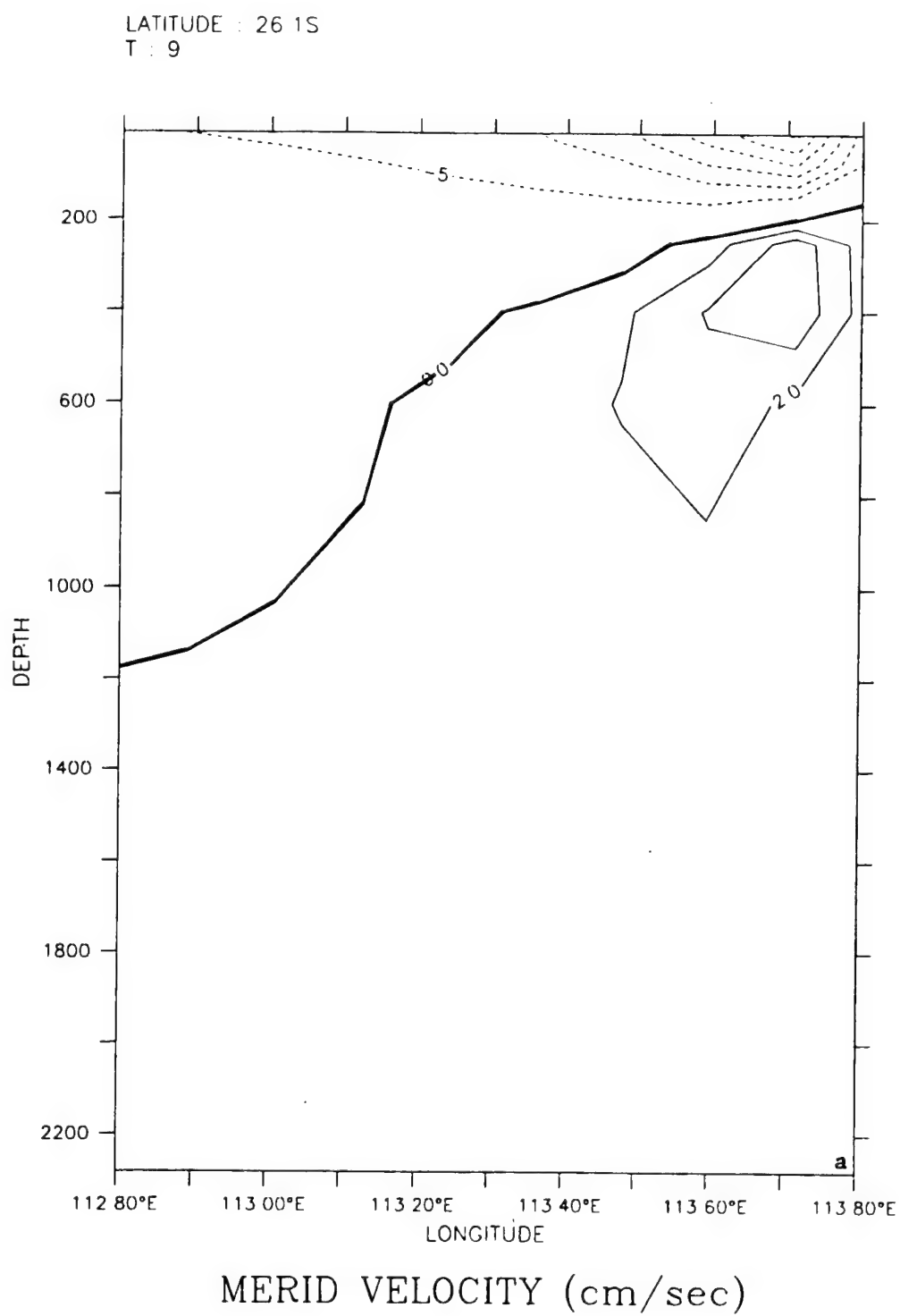
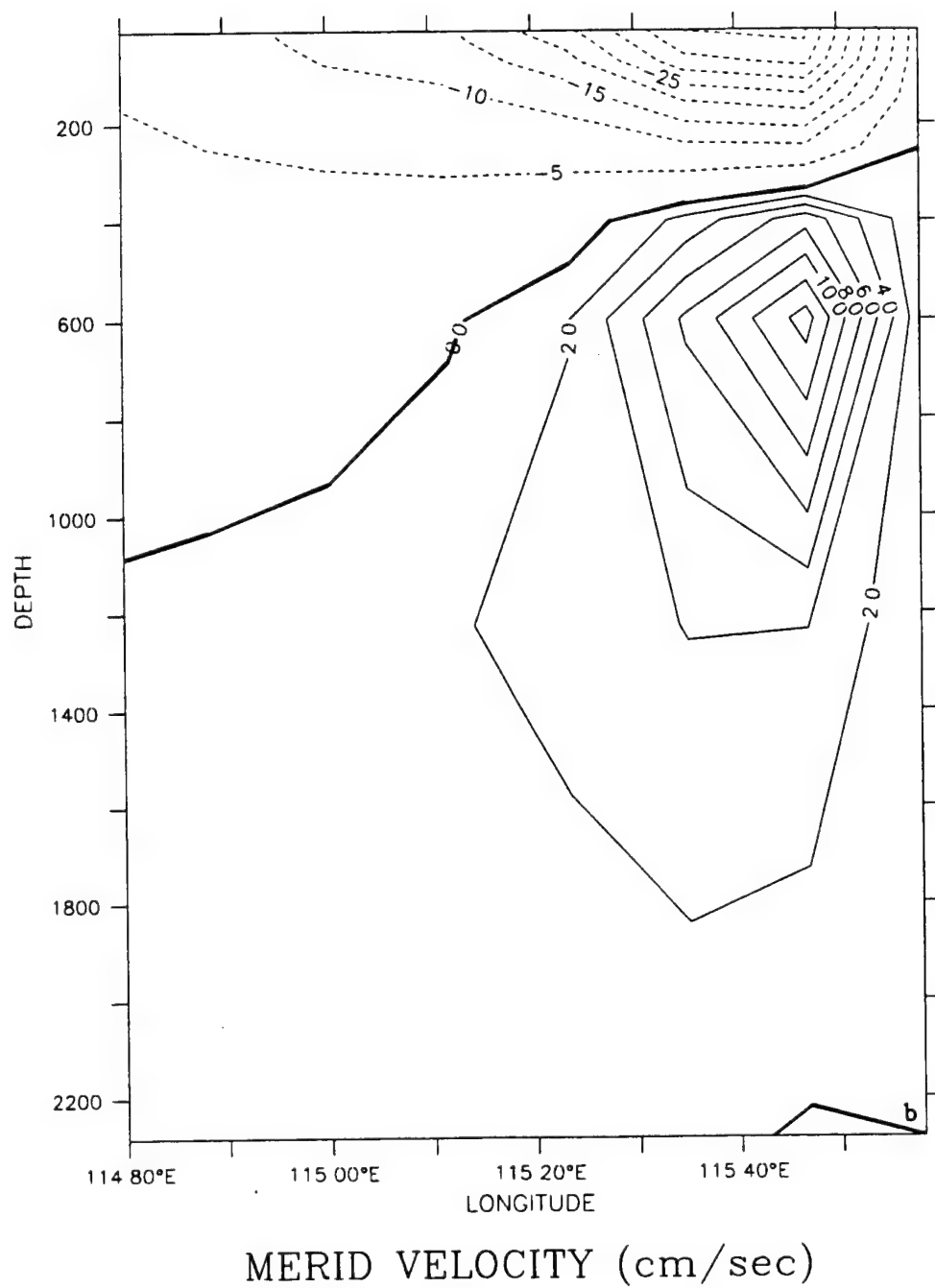


**Figure 30.** Cross-shore section of meridional velocity ( $v$ ) for day 9 at (a)  $\sim 26^\circ$  S, and (b)  $32^\circ$  S of Experiment 6. The contour interval is 5.0 cm/s for poleward (dashed line) flow and 2.0 cm/s for equatorward (solid line) flow.

LATITUDE : 31.9S  
T : 9



LONGITUDE 117E(117)  
T : 3

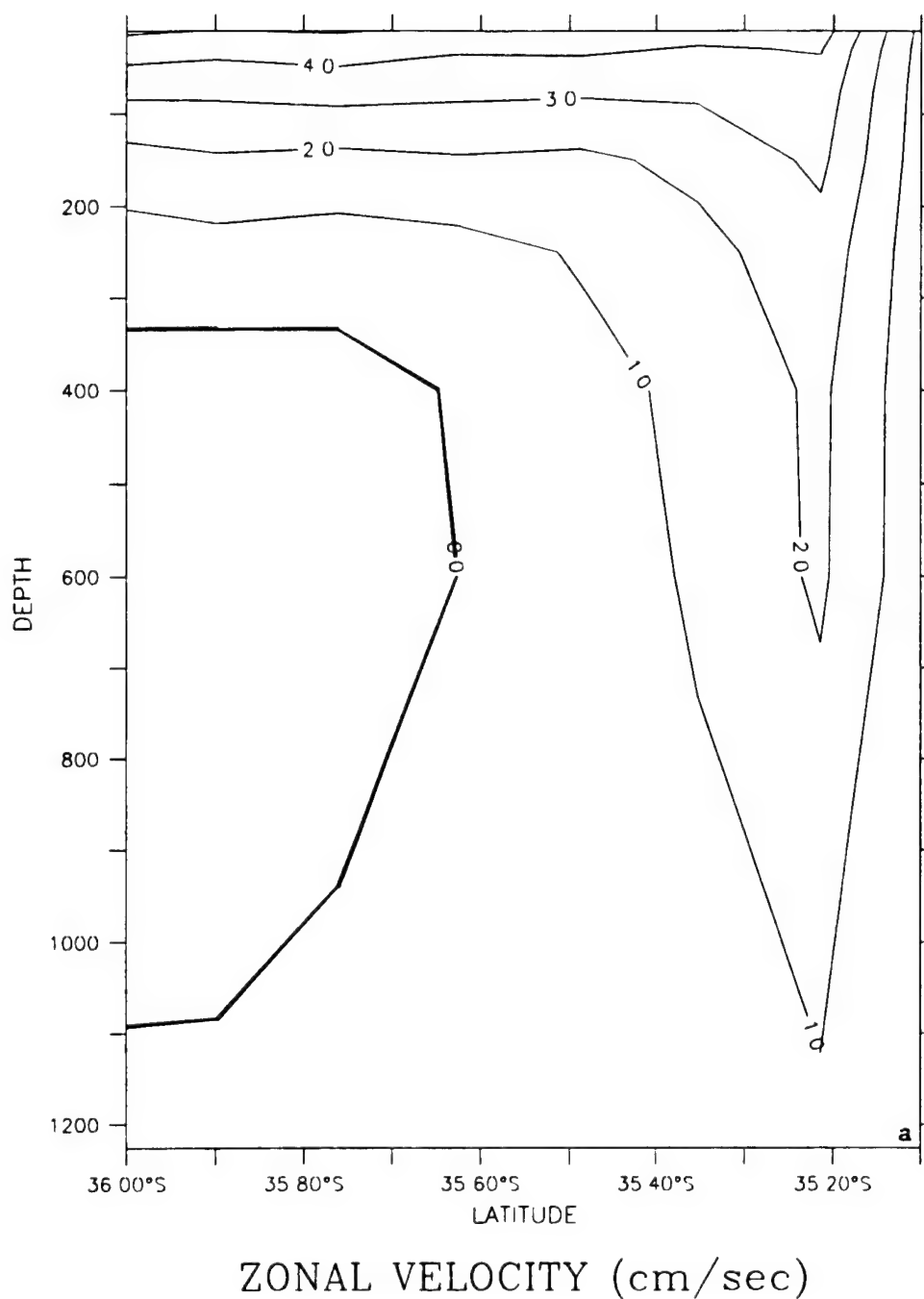
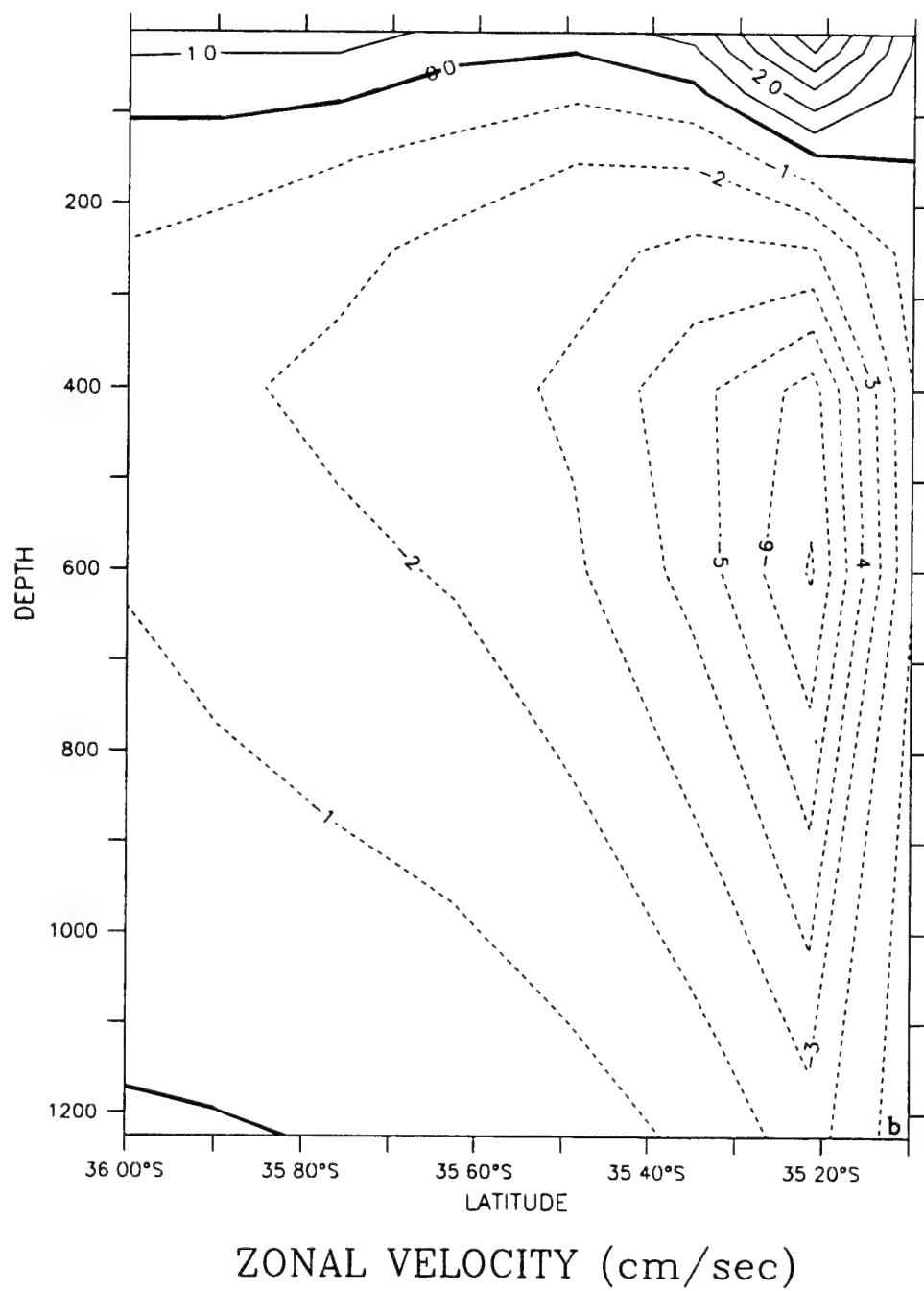
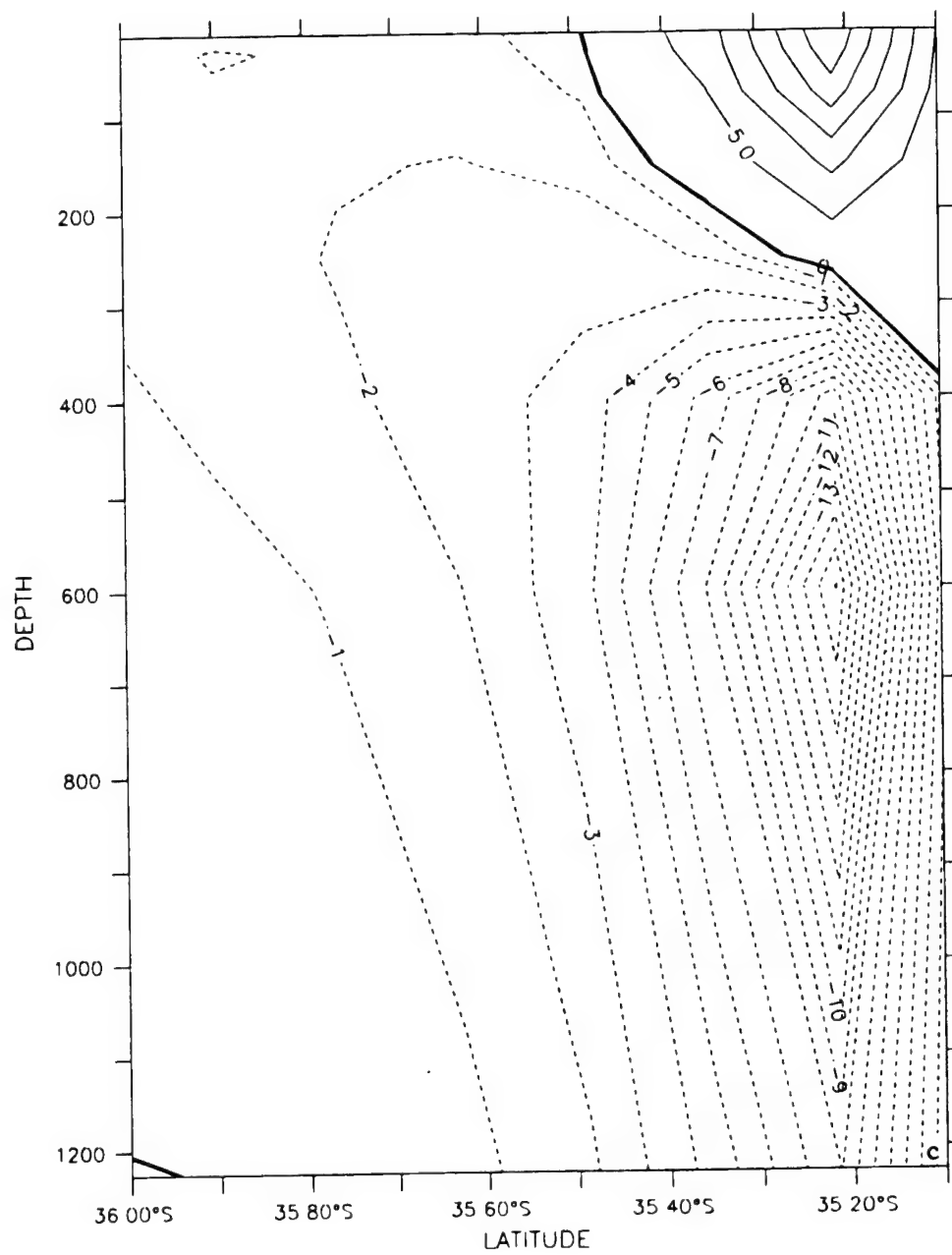


**Figure 31.** Cross-shore section of zonal velocity ( $u$ ) at  $\sim 117^\circ$  E for days (a) 3, (b) 9, and (c) 15 of Experiment 1. Contour interval is 1.0 cm/s in (a),(b) and 5.0 cm/s in (c) for eastward (solid line) flow and 1.0 cm/s for westward (dashed line) flow.

LONGITUDE . 117E(117)  
T : 9

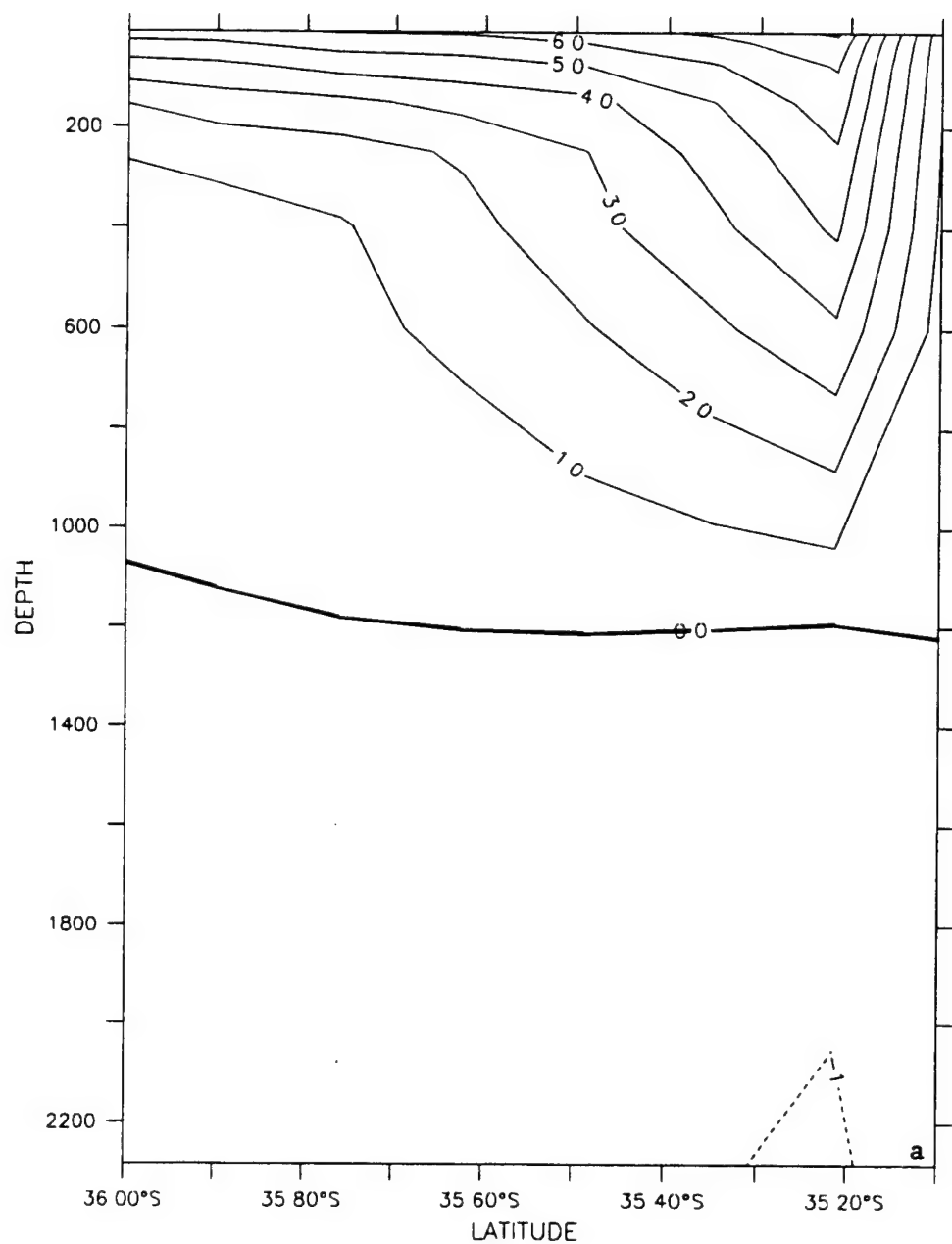


LONGITUDE 117E(117)  
T: 15



ZONAL VELOCITY (cm/sec)

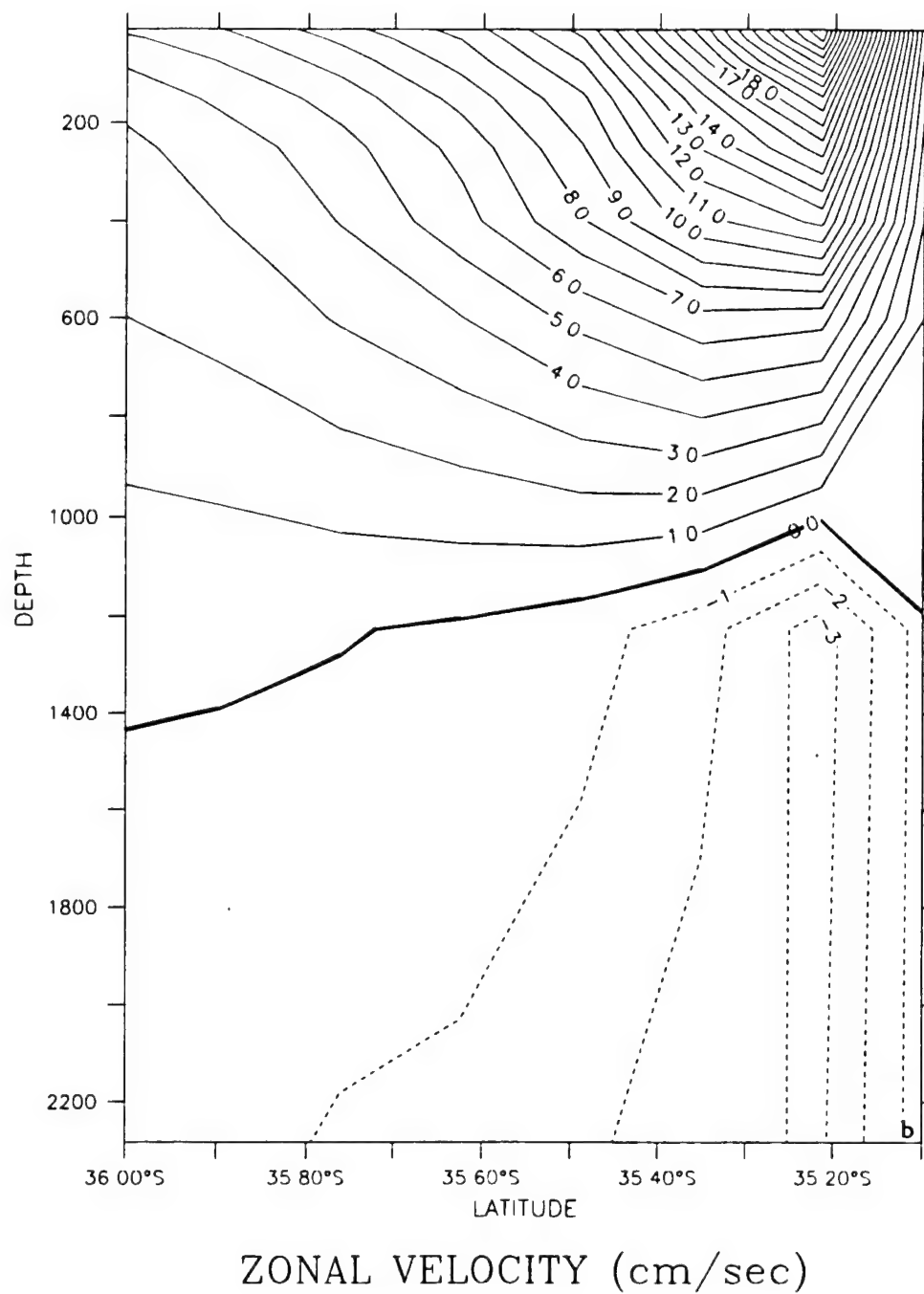
LONGITUDE 117E(117)  
T : 3



ZONAL VELOCITY (cm/sec)

**Figure 32.** Cross-shore section of zonal velocity ( $u$ ) at  $\sim 117^\circ$  E for days (a) 3, (b) 9, and (c) 15 of Experiment 6. Contour interval is 1.0 cm/s in (a),(b) and 5.0 cm/s in (c) for eastward (solid line) flow and 1.0 cm/s for westward (dashed line) flow.

LONGITUDE 117E(117)  
T : 9



LONGITUDE : 117E(117)  
T : 15

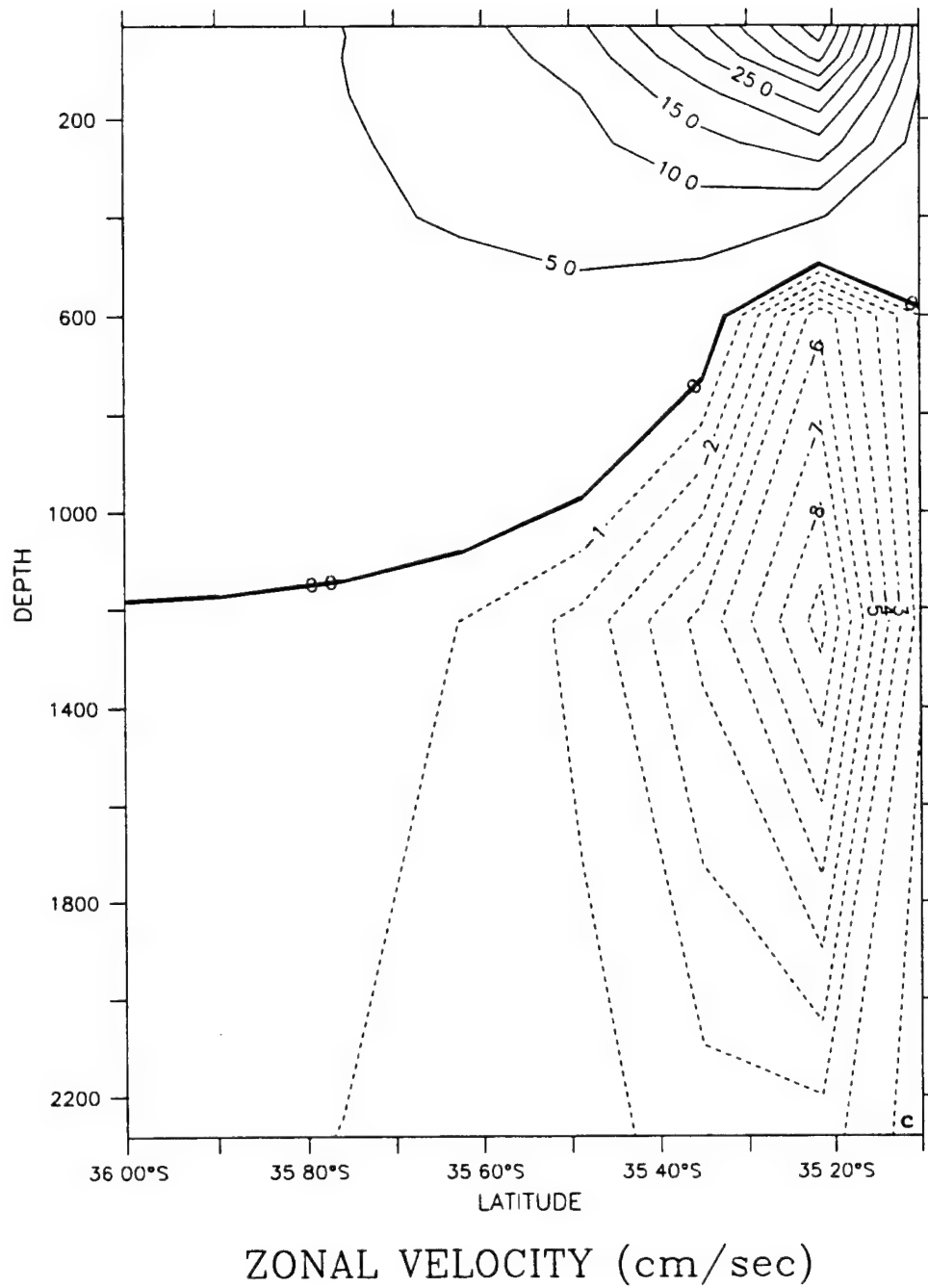




**Table 1. Values of Constants Used in the Model**

Constant	Value	Definition
$T_0$	278.2°K	Constant Reference Temperature
$S_0$	34.7	Constant Reference Salinity
$\rho_0$	1.0276 gm cm <sup>3</sup>	Density of Sea Water At $T_0$ and $S_0$
$\alpha$	$2.4 \times 10^{-4} (\text{°K})^{-1}$	Thermal Expansion Coefficient
$\beta$	$7.5 \times 10^{-4}$	Saline Expansion Coefficient
$K$	10	Number of Levels In Vertical
$\Delta x$	$1.1 \times 10^5$ cm	Cross-Shore Grid Spacing
$\Delta y$	$1.4 \times 10^6$ cm	Alongshore Grid Spacing
$H$	$4.5 \times 10^5$ cm	Total Ocean Depth
$\Delta t$	800 s	Time Step
$f_0$	$-0.76 \times 10^{-4} \text{ s}^{-1}$	Mean Coriolis Parameter
$g$	980 cm s <sup>2</sup>	Acceleration of Gravity
$A_M$	$2 \times 10^{17} \text{ cm}^4 \text{ s}^{-1}$	Biharmonic Momentum Diffusion Coefficient
$A_H$	$2 \times 10^{17} \text{ cm}^4 \text{ s}^{-1}$	Biharmonic Heat Diffusion Coefficient
$K_M$	$0.5 \text{ cm}^2 \text{ s}^{-1}$	Vertical Eddy Viscosity
$K_H$	$0.5 \text{ cm}^2 \text{ s}^{-1}$	Vertical Eddy Conductivity

**Table 2. Temperature Profile: North West Shelf Waters**

<b>Level</b>	<b>Temperature (°C)</b>
1	29.5
2	28.5
3	26.5
4	21
5	19

**Table 3. Summary of Specific Experiments and Forcing Mechanisms**

<b>Experiment</b>	<b>Initialized Thermohaline Gradients?</b>	<b>Seasonal Thermohaline Gradients?</b>	<b>Seasonal Wind Forcing?</b>	<b>North West Shelf Waters?</b>
1	NO	YES	NO	NO
2	NO	NO	YES	NO
3	YES	NO	YES	NO
4	NO	YES	YES	NO
5	NO	YES	YES	YES
6	NO	YES, but only in upper 5 levels	NO	NO

## LIST OF REFERENCES

- Arakawa, A., and V.R. Lamb (1977) Computational design of the basic dynamical processes of the UCLA general circulation model. In, *Methods in Computational Physics*, J. Chang, editor, Academic Press, 17, pp. 173-265.
- Batteen, M. L. (1997) Wind-forced modeling studies of currents, meanders, and eddies in the California Current System. *Journal of Geophysical Research*, 102, 985-1009.
- Batteen, M.L., and C.L. Butler (1998) Modeling Studies of the Leeuwin Current off Western and Southern Australia. *Journal of Physical Oceanography*, 28, 2199-2221.
- Batteen, M.L., and Y.-J. Han (1981) On the Computational noise of finite-difference schemes used in ocean models. *Tellus*, 33, 387-396.
- Batteen, M.L., M.J. Rutherford, and E.J Bayler (1992) A numerical study of wind and thermal forcing effects on the ocean circulation off Western Australia. *Journal of Physical Oceanography*, 22, 1406-1433.
- Boland, F.M., Church, A.M.G. Forbes, J.S. Godfrey, A. Huyer, R.L. Smith, and N.J. White (1988) Current-meter data from the Leeuwin Current Interdisciplinary Experiment. *CSIRO Marine Laboratories, Report 198*, 31pp.
- Camerlengo, A.L. and J.J. O'Brien (1980) Open boundary conditions in rotating fluids. *Journal of Computational Physics*, 35, 12-35.
- Church J.A., G.R. Cresswell, and J.S. GODFREY (1989) The Leeuwin Current. In: *Poleward Flows along Eastern Ocean Boundaries*, S. Neshyba, C.N.K. Moorers, R.I. Smith, and R.T. Barber, Eds, Springer-Verlag, 230-252
- Cresswell, G.R., and T.J. Golding (1980) Observations of a south-flowing current in the southeastern Indian Ocean. *Deep-Sea Research*, 27A, 449-303.
- Cresswell, G.R., and J.L. Peterson (1993) The Leeuwin Current South of Western Australia. *Australian Journal of Marine and Freshwater Research*, 44, 285-303.
- Gentili, J. (1972) Thermal anomalies in the Eastern Indian Ocean. *Nature (London) Physical Sciences*, 238, 93-95.
- Godfrey, J.S. and K.R. Ridgway (1985) The large-scale environment of the poleward-flowing Leeuwin Current, Western Australia: Longshore steric height gradients, wind stresses and geostrophic flow. *Journal of Physical Oceanography*, 15, 481-495.

Han, Y.-J., (1975) Numerical simulation of mesoscale eddies. Ph.D. thesis, University of California, Los Angeles, 154 pp.

Haney, R.L. (1974) A numerical study of the response of an idealized ocean to large-scale surface heat and momentum flux. *Journal of Physical Oceanography*, 4, 145-167.

Holland, W.R. (1978) The role of mesoscale eddies in the general circulation of ocean-numerical experiments using a wind-driven quasi-geostrophic model. *Journal of Physical Oceanography*, 8, 363-392.

Holland, W.R., and M.L. Batteen (1986) The parameterization of subgrid scale heat diffusion in eddy-resolved ocean circulation models. *Journal of Physical Oceanography*, 16, 200-206.

Holland, W.R., D.E. Harrison, and A.J. Semnter Jr. (1983) Eddy-resolving numerical models of large-scale ocean circulation. In: *Eddies in Marine Science*, Springer-Verlag, New York, pp. 379-403.

Levitus, S. R., Burgett, and T. P. Boyer (1994) World Ocean Atlas 1994, Volume 3: Salinity, *NOAA Atlas NESDI 3*, U. S. Department of Commerce, Washington D.C., 99 pp.

Levitus, S., and T. P. Boyer (1994) World Ocean Atlas 1994, Volume 4: Temperature. *NOAA Atlas NESDI 4*, U. S. Department of Commerce, Washington, D. C., 117 pp.

McCreary, J.P., Jr., S.R. Shetye, and P.K. Kundu (1986) Thermohaline forcing of eastern boundary currents: With application to the circulation off the west coast Australia. *Journal of Marine Research*, 44, 71-92.

Semtner, A.J., and Y. Mintz (1977) Numerical simulation of the Gulf Stream and midocean eddies. *Journal of Geophysical Research*, 7, 208-230.

Smith, R.L., A. Huyer, J.S. Godfrey, and J.A. Church (1991) The Leeuwin Current off Western Australia, 1986-1987. *Journal of Physical Oceanography*, 21, 323-345.

Thompson, R.O.R.Y. (1987) Continental-shelf scale model of the Leeuwin Current. *Journal of Marine Research*, 45, 813-827.

Trenberth, K.E., W.G. Large, J.G. Olsen (1990) The mean annual cycle in global ocean wind stress, *Journal of Physical Oceanography*, 20, 1742-1760.

Weatherly, G.L. (1972) A study of the bottom boundary layer of the Florida Current, *Journal of Physical Oceanography*, 2, 54-72.

Weaver, A.J., and J.H. Middleton (1988) On the Dynamics of the Leeuwin Current. *Journal of Physical Oceanography*, 19, 626-648.



## INITIAL DISTRIBUTION LIST

	No. Copies
1. Defense Technical Information Center..... 8725 John J. Kingman Rd, STE 0944 Ft. Belvoir, VA 22060-6218	2
2. Dudley Knox Library..... Naval Postgraduate School 411 Dyer Rd Monterey, CA 93943-5101	2
3. Chairman (Code OC/Bf)..... Department of Oceanography Naval Postgraduate School Monterey, CA 93943-5122	1
4. Chairman (Code MR/Wx)..... Department of Meteorology Naval Postgraduate School Monterey, CA 93943-5114	1
5. Dr. Mary L. Batteen, (Code OC/Bv)..... Department of Oceanography Naval Postgraduate School Monterey, CA 93943-5122	3
6. Dr. Curtis A. Collins, (Code OC/Co)..... Department of Oceanography Naval Postgraduate School Monterey, CA 93943-5122	1
7. Dr. Tom Curtin..... Office of Naval Research 800 N. Quincy Street Arlington, VA 22217	1
8. Dr. T. Kinder..... Physical Oceanography Division Office of Naval Research 800 N. Quincy Street Arlington, VA 22217	1



9.	LT A.W. COX .....	3
	1803 Edelweiss Cir.	
	Sandy, UT 84092	